

Design of Compliant Mechanisms for Attenuation of Unidirectional
Vibrations in Rotational Systems

by

Spencer E. Szczesny

B.S., Mechanical Engineering (2003)

University of Pennsylvania

Submitted to the Department of Mechanical Engineering
in Partial Fulfillment of the Requirements for the Degree of
Master of Science in Mechanical Engineering

at the

Massachusetts Institute of Technology

February 2005

© 2005 Massachusetts Institute of Technology
All rights reserved

Signature of Author.....
Department of Mechanical Engineering
January 14, 2005

Certified by.....
Martin L. Culpepper
Rockwell International Assistant Professor of Mechanical Engineering
Thesis Supervisor

Accepted by.....
Lallit Anand
Chairman, Department Committee on Graduate Students

Design of Compliant Mechanisms for Attenuation of Unidirectional Vibrations in Rotational Systems

by

Spencer E. Szczesny

Submitted to the Department of Mechanical Engineering on
January 14, 2005 in Partial Fulfillment of the Requirements for the
Degree of Master of Science in Mechanical Engineering

ABSTRACT

The purpose of this research was to generate the knowledge required to design compliant mechanisms that (1) attenuate undesired small-motion angular vibrations in rotational power transmission systems and (2) preserve the desired transmission of large-motion torque/angle inputs. This thesis investigates the design of vibration attenuating compliant mechanisms that are directly integrated into the load path of rotational systems. These devices enable designers to attenuate the amplitude of undesirable vibrations while simultaneously optimizing the transmission of torque inputs. The design, modeling, fabrication and experimental validation of two Compliant Vibration Attenuator (CVA) concepts will be presented. The first device, the Small Amplitude Vibration Isolator (SAVI), is a non-linear compliant device that isolates a resonating or non-resonating rotational system from vibrations by acting as a mechanical low-pass filter. The second device, the Damping Vibration Link (DVL) utilizes compliance and damping to attenuate undesired vibrations due to resonance.

A linear lumped parameter model was created in Matlab® to simulate the static and dynamic characteristics of rotational power transmission systems. This model enables one to determine the dynamic characteristics of a system for a given set of inputs, thereby making it possible to (1) understand the requirements for the CVA and (2) ascertain the effect of the CVA on the system. Finite-element simulations were conducted to verify an empirical, parametric model that describes the performance of a SAVI as a function of its stiffness parameters. Proof-of-concept prototypes were tested to verify performance predictions and to determine the practical issues related to implementation. The thesis concludes with a case study which demonstrates the effectiveness of a SAVI when integrated into the steering system of a light-duty pickup truck. The SAVI was shown to offer a 60% reduction in vibration amplitude by trading off 7 ms of delay in steering wheel-vehicle response.

Thesis Supervisor: Martin L. Culpepper

Title: Rockwell International Assistant Professor of Mechanical Engineering

BIOGRAPHICAL NOTE

Spencer E. Szczesny was born April 14, 1981, in Marlboro, NJ. From March – July 2002, he attended the University of Sydney, Sydney, AU. He graduated summa cum laude from the University of Pennsylvania with a B.S. in Mechanical Engineering and Applied Mechanics in May 2003. Starting in the summer of that year, he attended the Massachusetts Institute of Technology in pursuit of a M.S. in Mechanical Engineering, and was employed as a research assistant in the Precision Compliant Systems Laboratory. This thesis is a culmination of that research. During this time, Spencer Szczesny published two conference articles at the 2004 ASME Design Engineering Technical Conference in Salt Lake City, Utah (Design of a Compliant Revolute Mechanism for Accurate Dynamic Characterization of Automotive Steering Columns, Design of a Gimbaled Compliant Mechanism Stage for Precision Motion and Dynamic Control in z , θ_x , and θ_y Directions).

ACKNOWLEDGMENTS

There are many people who have made this work possible. First, I would like to thank the Ford-MIT Alliance, including Steven and Kristin Schondorf, Joe Saleh and Simon Pitts. They made everything run smoothly and ensured a productive collaboration between industry and academia. Still, the bulk of the credit for such a successful partnership is due to my counterparts at Ford, Rena Basch, Wei-Yi Loh and DJ Li. For their hard work, diligence and both professional and personal advice, I am grateful. I'd also like to thank Charles Wu and Isiah White for their support of the project and the resources they provided. I'd like to recognize the many professors, students, engineers and technicians who taught me the tools of the trade and got things done: Prof. Samir Nayfeh, Mark Belanger, Jerry Wentworth, Tim Mouch, John Bonnen, Kripa Varanasi, Justin Verdirame, Lorenz Hoffman, Tom Dalka, Jim Lewis, and Pat Grace. Special thanks to Chris Dibiasio, who interned with me at Ford over Summer '04, for his excellent work and friendship in a strange land. To Maggie Sullivan and Jason Pring, thank you for all your hard work making sure the lab wheels kept turning, and your abundant kindness. Most of all, I would like to give a heartfelt thanks to Prof. Martin Culpepper, who taught me, through his example, the perseverance, discipline, skills and leadership necessary to be a strong engineer.

Besides those directly related to my work, there are many who are responsible for my success. Of course, at the top of the list, are my parents, Tom and Fran, who not only gave me life but also the support and encouragement to reach my potential, and to whom I owe everything I am today. To all my family members, especially Baba and Poppy, Beano and Uncle Bob, Dzia dzia and Babcia, and all my numerous uncles, aunts and cousins, thank you for your constant love and warmth. To my closest friend Sam, thank you for your dedication and unfailing friendship – you are truly like a brother. To all my labmates, Amos Winter, Nate Landsiedel, Dariusz Golda, Shih-Chi Chen, Kartik Mangudi, Soohyung Kim, Rich Timm, Kevin Lin, and Patrick Carl, its from you guys that I learned the most and who made each and every day at the lab worth it. And finally, I'm sure she thought I forgot again, I'd like to thank my cousin, Meghan Rose, who has brought smiles to my life and who will always be with me in my heart. To all of you, and the list of friends too large to fit here, I am forever indebted and wish you all the best.

TABLE OF CONTENTS

ABSTRACT.....	2
BIOGRAPHICAL NOTE.....	3
ACKNOWLEDGMENTS.....	4
TABLE OF CONTENTS.....	5
LIST OF FIGURES	8
LIST OF TABLES	11
NOMENCLATURE.....	12
1 INTRODUCTION	14
1.1 Motivation.....	16
1.2 Research Purpose, Scope and Summary of Results.....	20
1.2.1 Selection of Vibration Attenuation Technologies.....	21
1.2.2 Generation/Optimization of Design Concepts	22
1.2.3 Modeling: Determination of CVA Performance.....	22
1.2.4 Fabrication and Testing of Devices	22
1.3 Thesis Organization	23
1.4 Background.....	23
1.4.1 Vibration Control.....	23
1.4.2 Damping Principles and Performance of Viscoelastic Material (VEM)	27
2 DESIGN OF SAVI AND DVL	32
2.1 Existing Technologies and Design Solution.....	32
2.2 Small Amplitude Vibration Isolator (SAVI) Concept Synthesis.....	36
2.3 Damping Vibration Link (DVL) Concept Synthesis	40
2.4 Summary	46
3 MODELING AND ANALYSIS.....	47
3.1 Purpose of Models	47
3.2 Small Amplitude Vibration Isolator (SAVI).....	48
3.3 Rotational Systems.....	57
3.3.1 Analysis of Rotational System Dynamics.....	57
3.4.2 Determination of Effects of SAVI.....	61

3.3.3	Determination of Effects of DVL	62
3.4	Summary of Modeling	62
4	FABRICATION.....	64
4.1	Goals	64
4.2	Small Amplitude Vibration Isolator (SAVI).....	65
4.2.1	Fabrication of Individual Components	67
4.2.2	Assembly Procedure	71
4.3	Damping Vibration Link (DVL).....	75
4.3.1	Summary of Failed Attempts	76
4.3.2	Fabrication Procedure	78
4.3.3	Assembly with Rotational System	82
4.3.3.1	Preparation	82
4.3.3.2	Connection of DVL to System Shaft	84
4.3.3.3	Alignment of System Shaft with Adapter Recess.....	86
4.3.4	Important Fabrication Issues.....	88
4.4	Summary	92
5	EXPERIMENTAL VERIFICATION.....	93
5.1	Testing of SAVI.....	93
5.1.1	MTS Testing of SAVI.....	95
5.1.2	Low-Amplitude Testing of SAVI.....	97
5.2	Verification of Lumped Parameter Model.....	100
5.3	Dynamic Testing of the DVL	104
5.4	Summary	107
6	CASE STUDY: AUTOMOTIVE NIBBLE.....	109
6.1	Background.....	109
6.2	Problem Definition.....	110
6.2.1	Kinematics	110
6.2.2	Sources.....	112
6.2.3	Factors Affecting Nibble Severity	114
6.3	Functional Requirements	116
6.4	Constraints	117

6.5	Design Selection and Optimization	118
6.5.1	Subsystem Identification.....	118
6.5.2	Characterization of Sub-System Dynamics	119
6.5.3	Choice of Design Strategy	122
6.5.4	Design Optimization.....	123
6.6	Steering System Performance Verification.....	132
6.6.1	Rig Testing.....	132
6.6.2	Vehicle Testing.....	133
6.7	Performance Review	135
6.8	Future Work.....	136
7	CONCLUSION.....	138
7.1	Research Goals and Accomplishments.....	138
7.1.1	Best Design Strategies and Associated Trade-Offs	139
7.1.2	Distribution of Load Path and its Implications.....	140
7.1.3	Practical Issues Regarding Fabrication and Implementation.....	141
7.1.4	Necessary Modeling for Design and Parameter Selection.....	142
7.2	Impact of CVA's.....	142
7.2.1	Scholarly Impact	142
7.2.2	Engineering/Practical Impact.....	143
7.3	Future Work.....	144
	REFERENCES.....	146

LIST OF FIGURES

Figure 1.1 Proposed Function of CVA Mechanism.....	15
Figure 1.2 Two CVA Designs	16
Figure 1.3 Light-Duty Truck Steering System	17
Figure 1.4 Venn Diagram of Existing Technology Limitations	19
Figure 1.5 2-DOF Model of System	24
Figure 1.6 Plot of Eq. (1.4)	25
Figure 1.7 Hystereis Loop of a VEM for a Single Loading Cycle	29
Figure 1.8 Property Variation of VEM with Temperature	30
Figure 2.1 Example of Non-Linear Stiffness Profile	35
Figure 2.2 Final Prototype of SAVI.....	36
Figure 2.3 (A) Planar Torsional Spring and (B) Engagement Stop Elements of SAVI	38
Figure 2.4 Final Prototype of DVL.....	40
Figure 2.5 Concentric Tube Design.....	41
Figure 2.6 Final Geometry of DVL	42
Figure 2.7 Torsional Load Paths of DVL	43
Figure 2.8 Plot of Relative Displacement of VEM vs Length.....	44
Figure 2.9 Adapter used to Mount DVL to Rotational System	45
Figure 3.1 FEA Simulation.....	48
Figure 3.2 Enlarged View of Radial Beam.....	49
Figure 3.3 Two Plots of Stiffness vs Ratio	52
Figure 3.4 Plot of Yield Angle vs Ratio for $t = 0.125$ "	53
Figure 3.5 Plot of Yield Angle vs Ratio for both Part Thicknesses.....	53
Figure 3.6 Geometry of Gap Spacing for Stop Assembly	56
Figure 3.7 Lumped Parameter Model of Steering Column.....	58
Figure 3.8 Frequency Response of Original System and Potential Responses of Modified Systems	60
Figure 4.1 SAVI Final Prototype.....	65
Figure 4.2 Steering Component to be Retrofitted with SAVI	66
Figure 4.3 Engagement Pin with Connection Bolt and Lock Nut	68

Figure 4.4 Flange Sub-Assembly.....	69
Figure 4.5 Exploded View of SAVI Assembly	70
Figure 4.6 Side-View of Fully Assembled SAVI Prototype.....	70
Figure 4.7 Interference Fit of Torsional Spring onto Downstream Adapter.....	73
Figure 4.8 Enlargement of Stop Engagement Sub-Assembly	74
Figure 4.9 DVL Final Prototype	75
Figure 4.10 Deep Draw of DVL	76
Figure 4.11 Bending of Round, Pre-Cut Tube.....	77
Figure 4.12 Feature Cutout from Flat Sheet	79
Figure 4.13 Bending and Welding to Form Octagonal Shaft	79
Figure 4.14 Formation of Primary Bends in Tabs	80
Figure 4.15 Pronounced Springback after Bending Process.....	81
Figure 4.16 Reversal of Springback into Preload	81
Figure 4.17 Downstream Shaft of System to be Connected to DVL.....	83
Figure 4.18 Adapter Used to Connect Reverse Section of Shaft to DVL.....	83
Figure 4.19 Support Configuration of DVL for Insertion of Roll Pin.....	84
Figure 4.20 Alignment of System Shaft for Roll Pin Insertion	85
Figure 4.21 Final Position of Roll Pin*	86
Figure 4.22 Alignment of Shaft and DVL with Adapter	87
Figure 4.23 Comparison of Final Assembly of Shaft and DVL with Original Shaft	88
Figure 4.24 Stack-up of Errors in Bending Angles for Inner Shaft.....	89
Figure 4.25 Warping Damage to Inner Shaft from Hammering.....	90
Figure 5.1 Testing Setup for MTS Experiments.....	95
Figure 5.2 Plot of Reversed Loading Curve for SAVI	96
Figure 5.3 Plot of Torque Ramp	96
Figure 5.4 Test Setup for Rheometer Testing.....	98
Figure 5.5 Results from Rheometer Testing.....	99
Figure 5.6 Experimental Fixture for Characterization of Steering Column	100
Figure 5.7 Measured Transfer Function of Steering Column	102
Figure 5.8 Measured and Predicted Mode Shape of Column	103
Figure 5.9 Experimental Setup for Testing of DVL	105

Figure 5.10 Measured Transfer Function of Accelerometer Response	106
Figure 6.1 Transmission of Nibble	111
Figure 6.2 Kinematics of Turning Motion Caused by Longitudinal Translation	112
Figure 6.3 Schematic of McPherson Strut Suspension with Rack-and-Pinion Steering	115
Figure 6.4 Potential Working Space for Design	119
Figure 6.5 Lumped Parameter Model of Steering System.....	120
Figure 6.6 One DOF Translational Model of Steering System	121
Figure 6.7 Frequency Response of One DOF Model of Steering Column.....	122
Figure 6.8 Full Steering System Test Setup.....	123
Figure 6.9 Frequency Response of Steering System Before and After Rig Modifications	125
Figure 6.10 One-DOF Rotational Model in ADAMS	127
Figure 6.11 ADAMS Model for Calculating Angular Delay	129
Figure 6.12 Plot of Angular Delay vs SAVI Stiffness for Transitions at 1 and 2 deg.....	130
Figure 6.13 Surface Plot of Percent Reduction vs Delay and SW Inertia for Stops at 2 deg	131
Figure 6.14 Comparison of Frequency Response between Control Average and SAVI.....	133
Figure 6.15 Peak Value of Linear Acceleration of SW Accels vs Measured Excitation Frequency for Imbalance Testing	134

LIST OF TABLES

Table 2.1	Vibration Attenuation Technology Selection Matrix	34
Table 3.1	Dimension Ranges for FEA Simulation of Planar Torsional Spring.....	52
Table 3.2	Calculated Values for C from Simulation.....	54
Table 5.1	Selected Values for Design Parameters and Dimensions of SAVI	94
Table 5.2	Measured and Predicted Results of DVL Experiment.....	106
Table 5.3	Potential Damping Ratios for DVL and Conventional Damping Methods.....	108
Table 6.1	Factors Affecting Nibble Severity in System Shown in Figure 5.3.....	114
Table 6.2	Calculated Natural Frequencies and Normal Modes	121
Table 6.3	Labeling of Steering System Elements.....	124
Table 6.4	Parameters Varied in Optimization.....	126
Table 6.5	Percent Reduction (%) of Various Combinations of Stiffness and Inertia	128
Table 6.6	Selected Values for Design Parameters of SAVI and Column.....	132
Table 6.7	Predicted Performance of Steering System with SAVI.....	132
Table 6.8	Performance of SAVI Prototype.....	135

NOMENCLATURE

UPPER CASE:

C	Proportionality between length of radial beam elements and packaging diameter of torsional spring of SAVI [---]
D	Packaging diameter of SAVI [m, inches]
E	Young's modulus of material used for torsional spring of SAVI [Pa, psi]
F	Transverse force applied to radial beam elements as result of angular deflection of SAVI [N, lbf]
I	Second moment of area of radial beam elements [m^4 , inches ⁴]
L	Length of radial beam elements [m, inches]
R	Radius of stop engagement assembly [m, inches]
U	Strain energy of spring element [Nm, in-lbf]
X	Amplitude of displacement of body at which control input is applied [m, inches or radians, degrees]
Y	Amplitude of displacement of body at which upstream vibration is applied [m, inches or radians, degrees]

LOWER CASE:

c	Coefficient of viscous damping [N-s/m, lbf-s/in or Nm-s/rad, in-lbf-s/rad]
d	Linear deflection of radial beam element [m, inches]
g	Gap spacing of stop engagement assembly [m, inches]
h	Beam width of radial beam elements [m, inches]
k	Spring constant [N/m, lbf/in or Nm/rad, in-lbf/rad]
t	Part thickness of torsional spring of SAVI [m, inches]
x	Displacement of body at which control input is applied [m, inches or radians, degrees]
y	Displacement of body at which upstream vibration is applied [m, inches or radians, degrees]

GREEK:

α	Pivot angle of wheel-strut assembly due to longitudinal translation [radians]
γ	Shear strain of VEM [radians]
δ	Phase difference between stress and strain in VEM [radians]
ζ	Damping ratio [---]
ζ^o	Damping ratio of original rotational system [---]
η	Loss factor [---]
θ_i	Angular rotation of discrete inertial element [radians, degrees]
θ_s	Angular deflection of SAVI at which stops engage [radians, degrees]
σ_{MAX}	Maximum axial stress in radial beam elements due to bending [Pa, psi]

σ_Y	Yield stress of material used for torsional spring of SAVI [Pa, psi]
τ	Shear stress of VEM [Pa, psi]
ϕ	Phase difference between displacement of output and input of lumped parameter model [radians]
ω	Excitation frequency applied to rotational system [rad/s, Hz]
ω_n	Natural frequency [rad/s, Hz]
ω_n^o	Natural frequency of original rotational system [rad/s, Hz]

SUBSCRIPTS:

F_1	Force/torque of upstream vibration [N, lbf or Nm, in-lbf]
F_2	Force/torque of control input [N, lbf or Nm, in-lbf]
I_i	Moment of inertia of i^{th} discrete inertial element [$\text{kg}\cdot\text{m}^2$, $\text{slugs}\cdot\text{in}^2$]
I_{si}	Moment of inertia of i^{th} steering column component [$\text{kg}\cdot\text{m}^2$, $\text{slugs}\cdot\text{in}^2$]
K_i	Torsional spring constant of i^{th} steering column component [Nm/rad, in-lbf/rad]
K_L	Linear stiffness of radial beam elements [N/m, lbf/in]
W_d	Energy loss due to damping [Nm, in-lbf]
c_{eff}	Effective viscous damping coefficient for steering system [Nm-s/rad, in-lbf-s/rad]
d_Y	Linear deflection of radial beam element at yield [m, inches]
k_{eff}	Effective spring constant for steering system [Nm/rad, in-lbf/rad]
m_1	Mass of body at which upstream vibration is applied [kg, slugs]
m_2	Mass of body at which control input is applied [kg, slugs]

SUPERSCRIPTS:

G'	Storage modulus of VEM [Pa, psi]
G''	Loss modulus of VEM [Pa, psi]
G^*	Complex modulus of VEM [Pa, psi]

CHAPTER

1 INTRODUCTION

The purpose of this research was to generate the knowledge required to design compliant mechanisms that (1) attenuate undesired small-motion angular vibrations in rotational power transmission systems and (2) preserve the desired transmission of large-motion torque/angle inputs. Traditional vibration isolation devices attenuate the desired inputs traveling in the direction of primary power transmission (e.g. the downstream direction) as well as the unwanted vibrations traveling in the reverse direction (e.g. the upstream direction). As a result, designers face trade-offs between obtaining a desired level of system performance and reduction of unwanted vibrations. Alternate techniques, such as damping and inertia-spring elements, may be applied external to the load path of the system in ways which reduce small-amplitude vibrations without significantly affecting desired torque transmission of the system [1,2]. Even so, the effect of most damping technologies is limited as they are not incorporated into the system load path, and therefore they only damp a fraction of the small-amplitude strain energy. Likewise, inertia-spring devices require addition of inertia to a system that may alter performance in unacceptable ways (e.g. torque requirements).

The central thesis of this research is that a modular Compliant Vibration Attenuator (CVA) may be integrated into the system to modify its structural characteristics so that low-amplitude, high-frequency rotations are reduced while large-amplitude, low-frequency rotations are transmitted. For instance, in vehicle steering systems, it is desirable to maintain a given level of steering performance (large-motion inputs sent downstream) while simultaneously reducing small-amplitude vibrations which travel up the column. In this work, we consider only situations where the upstream vibration travels in the reverse direction and occurs at a higher frequency, at least 5x larger, than the control inputs. Therefore, a CVA may be represented as the unidirectional mechanical low-pass filter shown in Figure 1.1. Here, unidirectional refers to the CVA's performance differentiation between the vibration and control inputs, which travel through the system in opposite directions.

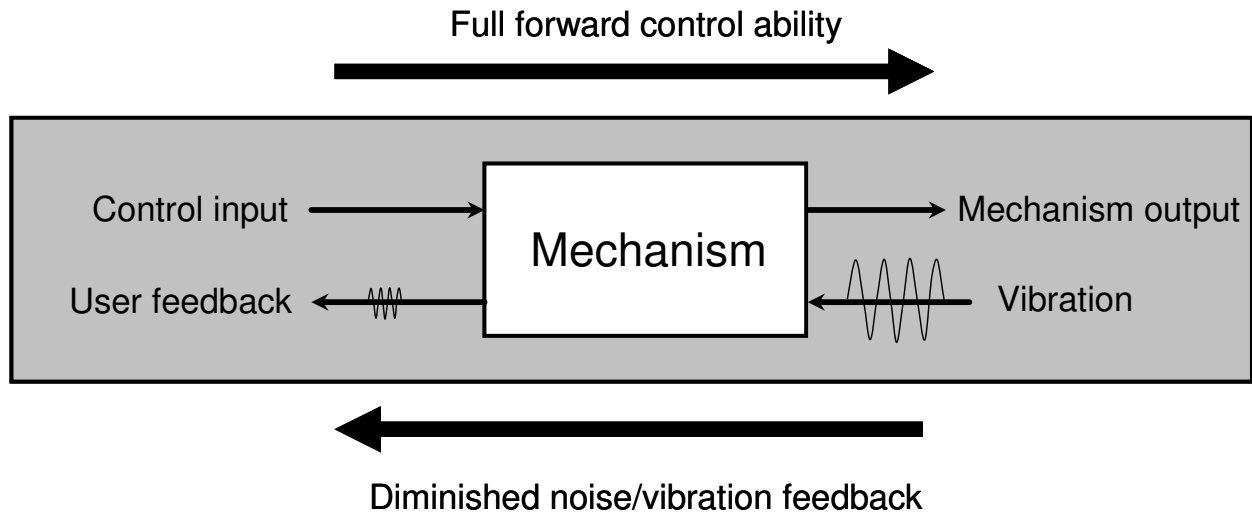


Figure 1.1 Proposed Function of CVA Mechanism

As a result of this research, the two designs, shown in Figure 1.2 were created, modeled and tested. The first concept, the Small Amplitude Vibration Isolator (SAVI), attenuates small-amplitude vibrations in resonating and non-resonating systems via non-linear stiffness characteristics. The SAVI is engineered to possess a low torsional stiffness below a given transition angle and comparatively high stiffness above that angle. The transition angle defines the limit on the amplitude of vibrations which may pass through the system. When a rotation exceeds the transition angle, the rotation may be transmitted through the system. The second concept, the Damping Vibration Link (DVL), may be used to attenuate vibrations in resonating systems. The DVL may be engineered to possess specific stiffness and damping properties. When integrated into the structural load path of the rotational system, the DVL may add damping to the system without affecting its stiffness characteristics, and attenuate resonant vibrations of any amplitude within a specific frequency range.

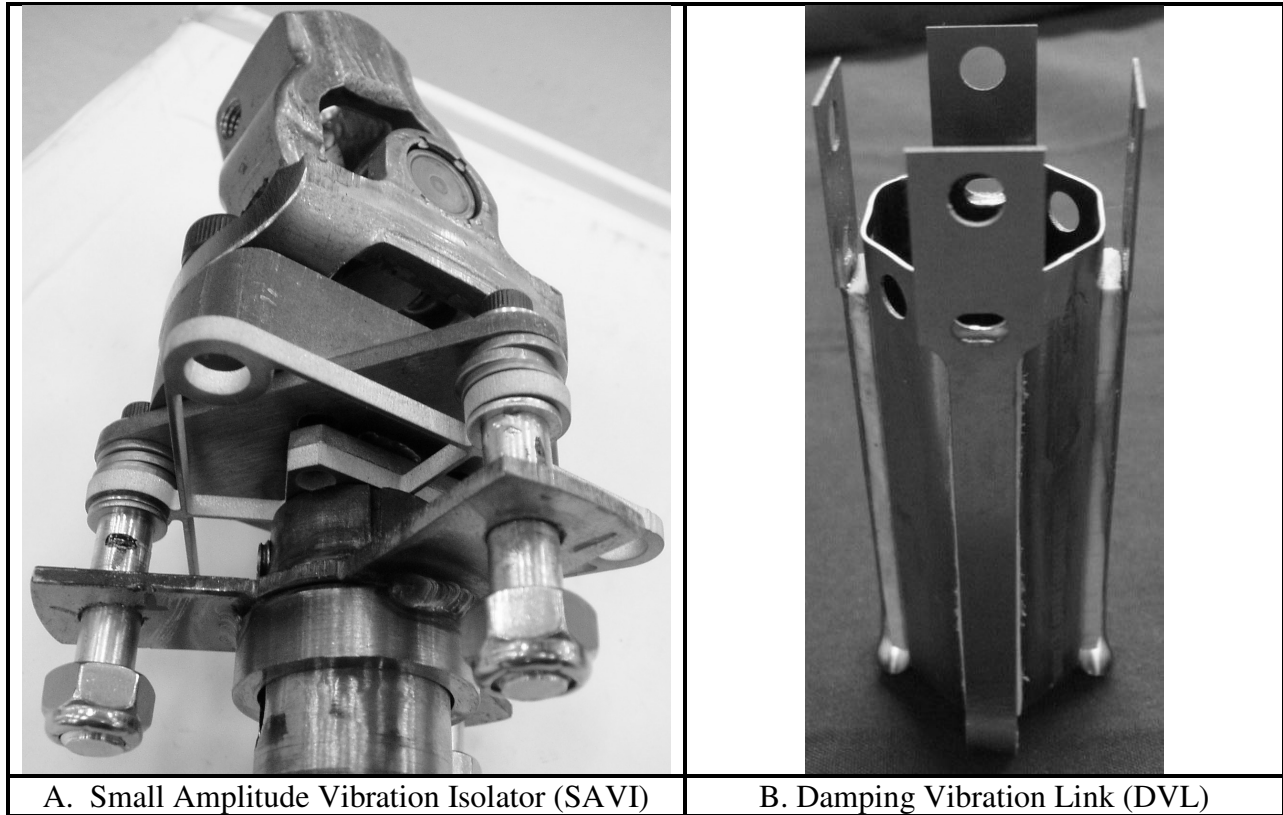


Figure 1.2 Two CVA Designs

1.1 Motivation

In general, rotational power transmission systems are used to transmit an input applied on one component through to a second component. For a linear system, reciprocity dictates that the reverse action is also true – an input applied to the second component will be transmitted back to the first. For example, consider the steering system shown in Figure 1.3. The control input is the angular displacement of the steering wheel and the desired output is the steering angle of the front tires. Since these two objects are directly connected through mechanical linkages, the angular position of the steering wheel may also be dictated by the position of the suspension system components and the tires. Under certain conditions, movement in these components cause vibrations to travel upstream toward the steering wheel, causing unwanted rotational steering wheel vibrations (nibble).

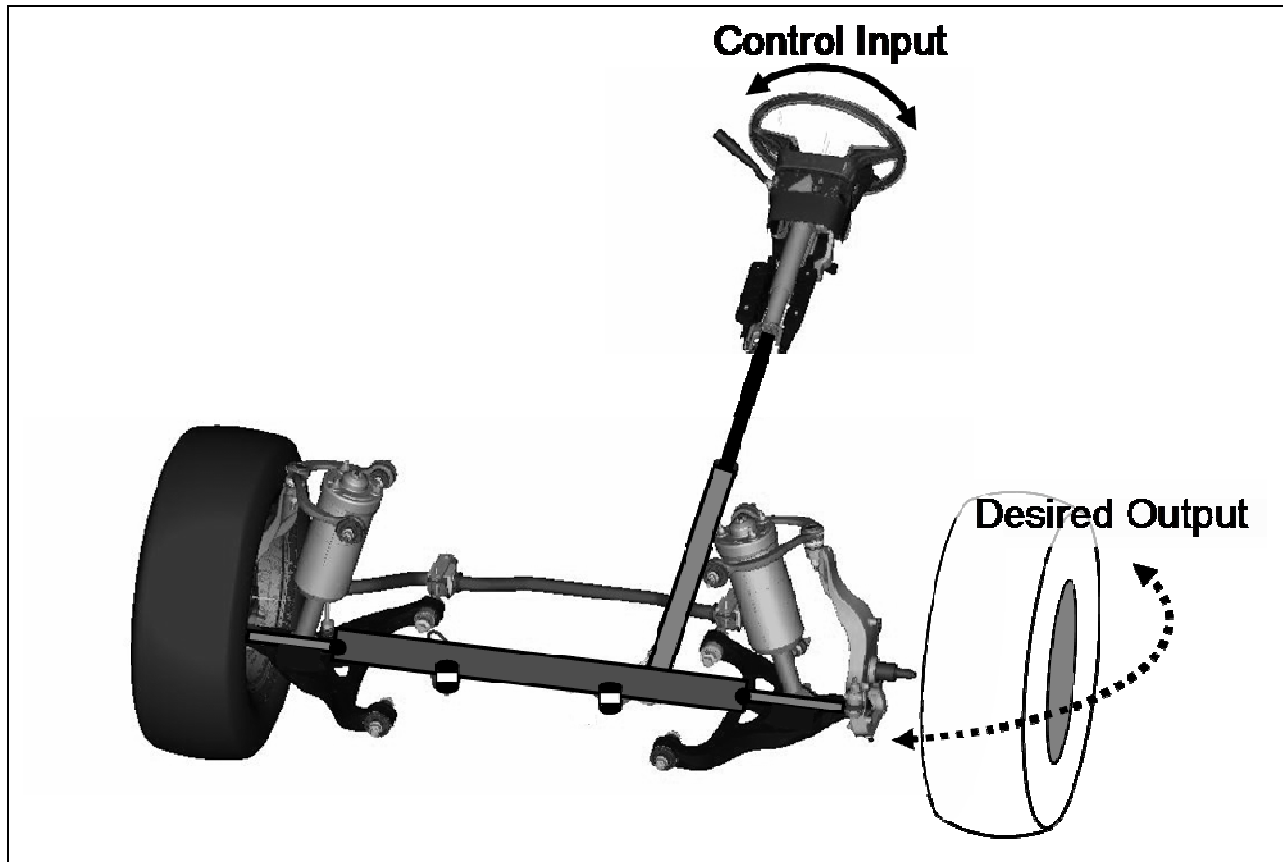


Figure 1.3 Light-Duty Truck Steering System

Several attempts have been made to use low-cost conventional vibration treatments to solve this problem [25, 26, 27, 28, 29, 30, 31 32]. If applied without concern for the system requirements, these methods may be able to solve the problem. However, the limitations on system performance place constraints on the design of potential solutions and thereby reduce their effectiveness. Mead [1] gives a comprehensive study of the various techniques that are available to reduce vibrations in a general system. A brief description of the effectiveness of these methods is provided below:

- Redesign of the system: Vibrations may be reduced by modifications of existing system components. This is often not possible due to performance, packaging and cost constraints.

- **Vibration isolation mounts:** By placing a low-stiffness spring element in series with a structure and its support foundations, the structure may be isolated from vibrations that occur within its supporting foundation. However, since the control input and upstream vibrations in a system pass through this low-stiffness element, vibration isolators attenuate both desired and undesired rotations.
- **Damping:** Constrained layer viscoelastic damping (CLD) introduces damping in a system by bonding viscoelastic material to the system components. This approach only works to reduce vibrations in resonating systems.
- **Tuned mass dampers and inertial absorbers:** These devices can remove vibrations over a narrow range of frequencies. This narrow performance window and the need to add inertia may preclude the use of such devices in many systems.

Although each of these techniques has different performance limitations and advantages, they share one similarity; they are all limited by their inability to separate performance from the constraints imposed on the system to which they should be applied. This is demonstrated by the Venn diagram shown in Figure 1.4.

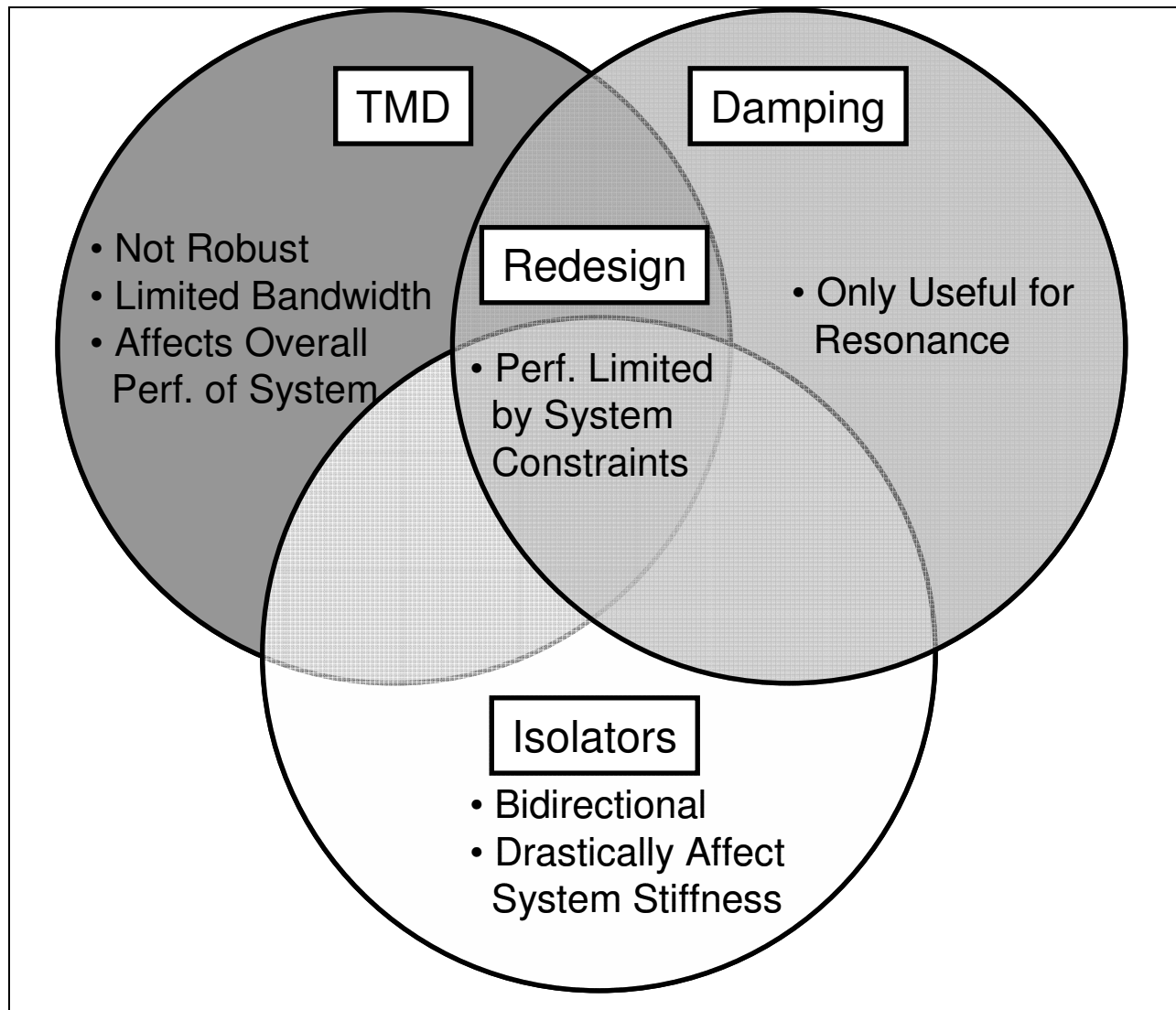


Figure 1.4 Venn Diagram of Existing Technology Limitations

As a CVA is coupled with the load path of the system and preserves the transmission of desired inputs, the limitations of conventional methods may be avoided. Furthermore, the full load of a rotational system, rather than a fractional amount, is applied to a CVA. This allows for a greater potential vibration attenuation compared to conventional damping treatments. Of course, this requires that the dual functions of a CVA, i.e. power transmission and vibration attenuation, be uncoupled. The concepts in Figure 1.2 satisfy this requirement. For instance, the SAVI physically decouples the load paths of the undesired small-amplitude vibrations and the desired large-amplitude inputs through its non-linear stiffness characteristics. Likewise, the DVL can be

designed to have a particular stiffness, which will properly transmit the desired torque/angle inputs, and attenuate resonant vibrations via added damping.

1.2 Research Purpose, Scope and Summary of Results

The questions that will be answered as a result of this research are:

1. What designs are well-suited to create a low-cost CVA that can transmit a desired torque input and reduce an undesirable vibration input? What are the associated trade-offs or relationships between these two functions?
2. How will the load path of the system interact with these designs, and what are the implications of the changes on the kinematics and dynamics of the system?
3. What are the practical issues regarding the design process, fabrication and implementation of these devices?
4. How will a CVA be chosen for a particular vibration problem? What modeling techniques are necessary to select a CVA design, determine its dimensions and predict its performance in a rotational system?

These questions were answered through the following research tasks:

1. Select the most suitable vibration attenuation technologies to be integrated in a CVA.
2. Generate and optimize design concepts that can satisfy a range of mechanical vibration problems.
3. Develop models to determine the performance benefits for a given application.
4. Build and test prototypes of the designs to validate the models and confirm performance.

After considering many technologies, a low-stiffness non-linear spring (SAVI) and viscoelastically damped device (DVL) were chosen for use in the design of two CVA's. Four metrics were considered when choosing the vibration technology:

- Frequency response of system to upstream vibration.
- Delay, either time or displacement, in response of forward input
- Simplicity - The simplicity of the design refers to the manufacturability and ease of implementing the device into the existing system, along with its associated maintenance and cost.
- Robustness - The robustness considers the frequency bandwidth of vibrations that the device can attenuate in addition to the effects on its performance as a result of environmental changes and manufacturing variations.

The SAVI would serve as a vibration isolator for resonating and non-resonating systems experiencing low-amplitude upstream vibrations. The DVL would serve as a back-up device for a resonating system that violated the constraints on the SAVI. A lumped parameter model for an arbitrary rotational system was created in Matlab®, and an analysis procedure was developed to accurately characterize the dynamics of moderately simple rotational systems and predict the performance of the device on the system. Both devices were then fabricated and tested. The application of the SAVI technology was demonstrated in the steering column of a light-duty truck.

1.2.1 Selection of Vibration Attenuation Technologies

The most important decision for designing a CVA was choosing which attenuation technologies to incorporate into the design. As will be explained later, the primary chosen method was to create vibration isolation in the system through the use of a low-stiffness, non-linear torsional spring. As this method requires the system stiffness to be tunable, another method was needed to account for situations in which a stiffness change was not acceptable. Therefore, damping was chosen as an alternative due to its negligible effect on the functional performance of a system.

1.2.2 Generation/Optimization of Design Concepts

The SAVI concept, shown in Figure 1.2A, is composed of a planar torsional stiffness element and an interlocking angular displacement stop. These components can be tuned to create non-linear stiffness characteristics, where for small angles the torsional stiffness element causes vibration isolation in the rotational system, and for large angles the stops transmit the control torque input. The DVL, shown in Figure 1.2B, adds viscoelastic damping to a rotational system. The energy transferred through the DVL is partially dissipated by the viscoelastic material which is located between the metal constraining layers. The decisions that lead to both of these final designs will be explained in Chapter 2.

1.2.3 Modeling: Determination of CVA Performance

A lumped parameter model of a general rotational system was created to characterize the dynamics of a rotational system and predict the performance of the system when augmented by either device. This model aids in selecting which device to use for a given vibration problem.

Design guidelines were generated that:

- Describe under what conditions either the DVL or SAVI should be chosen as the appropriate design solution.
- Provide a method for determining an accurate prediction of the performance and trade-offs for either device in many applications.
- Allow for the selection of the design parameters for optimized performance.

Finite-element simulations were used to ascertain SAVI dimensions which achieve the chosen design parameters.

1.2.4 Fabrication and Testing of Devices

Proof-of-concept prototypes for each device were fabricated and tested. The SAVI prototype provided a 60% reduction of upstream vibration amplitudes while introducing 7 ms of delay.

The DVL prototype tested had a damping ratio of 0.084 and was capable of matching the stiffness of the other components in a vehicle steering system.

1.3 Thesis Organization

The remainder of the first chapter presents a brief background of the nature of vibrations in rotational systems and the material properties of viscoelastic materials. This information is necessary to understand the fundamental principles of each design and their importance. The second chapter describes the selection of the vibration attenuation technologies, the design process, and the important design parameters. Modeling and analysis of the SAVI are covered in the third chapter. The fourth chapter deals with the fabrication of the devices. In the fifth chapter, the experimental validations of each design are covered. This is followed by a case study which describes an application in a light-duty truck steering system. The thesis closes with a summary of results and discussion of future research.

1.4 Background

1.4.1 Vibration Control

The simplest way to describe upstream vibrations is with a two degree-of-freedom (DOF) lumped parameter model, shown in Figure 1.5. The two masses represent objects that are subjected to the given input, be it force or displacement, and whose position is of importance. Here, m_1 signifies the point of application of the upstream vibration and m_2 is that of the desired input. These bodies are then connected by an equivalent spring and dashpot that represent the rest of the system. The effect of the upstream vibration is measured through the displacement of m_2 as a result of the motion of m_1 .

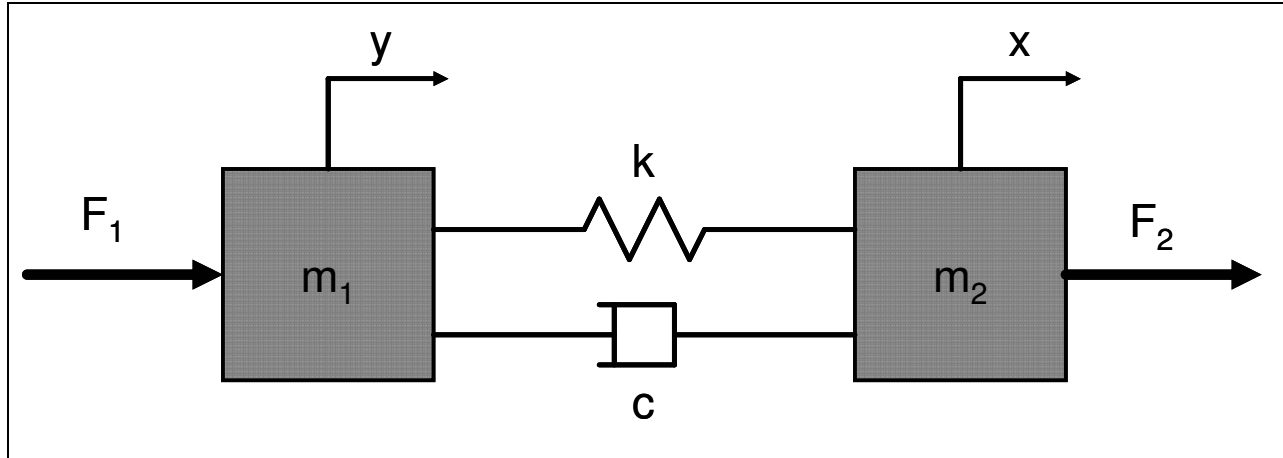


Figure 1.5 2-DOF Model of System

Assuming that the source upstream vibration may be measured and described by a harmonic displacement of m_1 with the form:

$$y = Y \sin(\omega t) \quad (1.1)$$

The equation of motion describing the remaining single DOF may be written as:

$$m_2 \ddot{x} + c(\dot{x} - \dot{y}) + k(x - y) = 0 \quad (1.2)$$

If we assume that the system is linear, then the position of m_2 can also be described as a harmonic function of time with the same frequency as follows:

$$x = X \sin(\omega t - \phi) \quad (1.3)$$

Combining Eqs. 1-3, we can solve for the ratio of the amplitudes of x and y and for the phase difference ϕ :

$$\left| \frac{X}{Y} \right| = \sqrt{\frac{k^2 + (\omega c)^2}{(k - m_2 \omega^2)^2 + (\omega c)^2}} \quad (1.4)$$

$$\tan \varphi = \frac{m_2 c \omega^3}{k(k - m_2 \omega^2) + (\omega c)^2} \quad (1.5)$$

In Figure 1.6, Eq. 1.4 is plotted as a function of the excitation frequency, ω , natural frequency, ω_n , and damping ratio, ζ where:

$$\omega_n = \sqrt{\frac{k}{m_2}} \quad (1.6)$$

$$\zeta = \frac{c}{2\sqrt{m_2 k}} \quad (1.7)$$

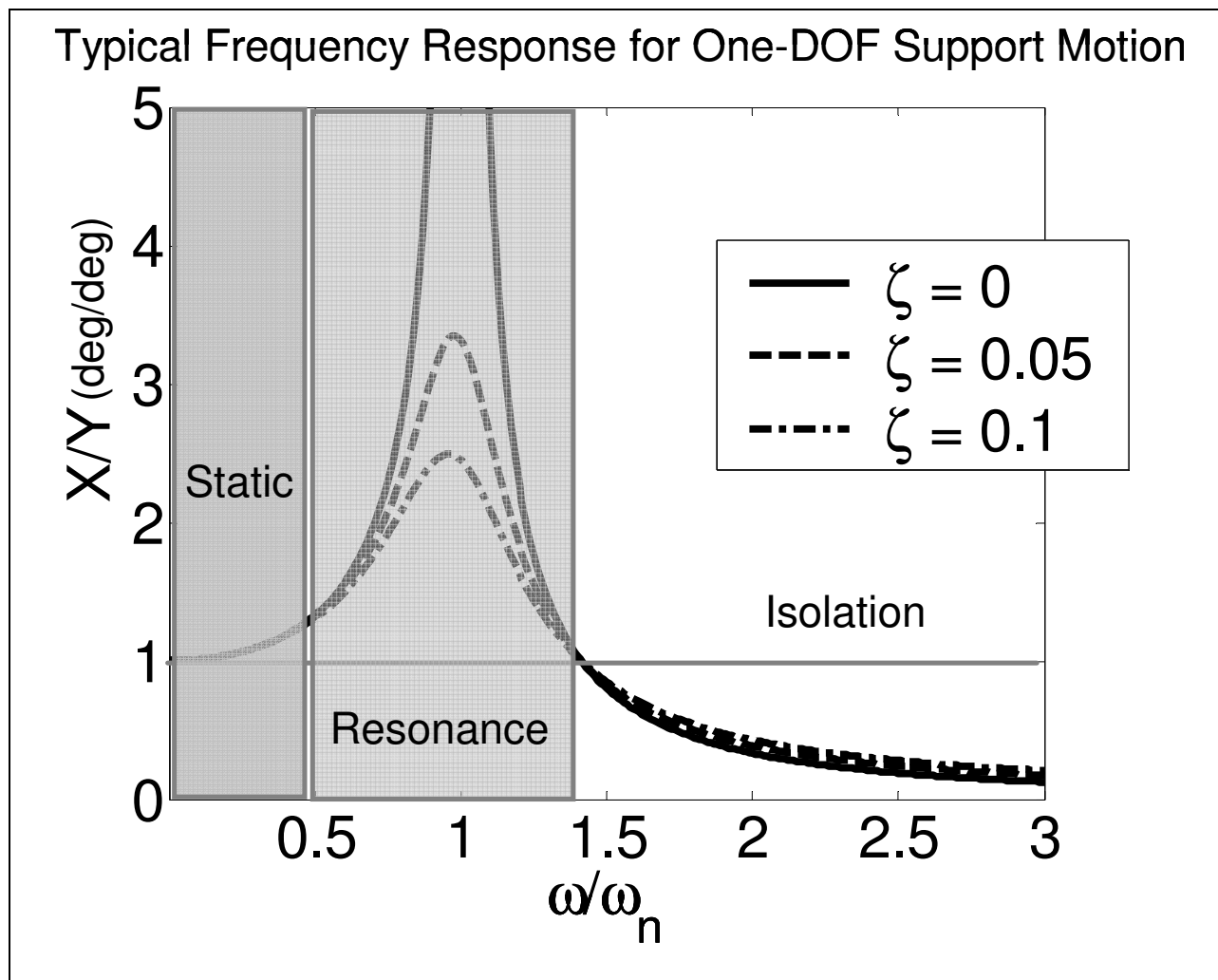


Figure 1.6 Plot of Eq. (1.4)

Looking at the plot, it is clear that there are three distinct regions of the response of x . When m_1 is moving near the natural frequency of the system, the displacement of m_2 increases dramatically. This magnification of x is called resonance and is commonly the cause of large undesirable upstream vibrations. Below about one-quarter of the natural frequency, the amplitude of x is nearly the same as that of y . Here the spring-dashpot system acts like a rigid connection between m_1 and m_2 , and the response is similar to static loading. Finally, for frequencies above $\sqrt{2}\omega_n$, the amplitude of x drops below the amplitude of y and asymptotically approaches zero. It is usually preferred for the system to lie within this regime of vibration isolation, however, competing constraints do not always allow for this.

The methods available for reducing the effects of the vibration are varied and depend on which regime the system is in for a given input. If the problem is due to resonant amplification, the best solution is to move the natural frequency of the system away from the forcing frequency. From Eq. 1.6, this may be accomplished by altering the mass or stiffness properties of the system. The level of vibration that is acceptable and other constraints on these alterations determine whether to increase or decrease the natural frequency and by how much. If this is not possible, the next best method is to increase the damping in the system. As seen in Figure 1.6, the best possible situation is to reduce the output vibration to a level equal to that of the input. One should also note that the more damping that originally exists in the system, the less effect the added damping will have, and that adding damping only works for resonance. If the system is in isolation, increased damping makes the vibration worse.

Sometimes the problem is not resonance but rather the amplitude of the input vibration itself is above acceptable levels. In this situation, there seems to be no solution other than moving the system to a state of vibration isolation, where the output response amplitude is lower than that of the input. This may require large changes in stiffness or inertia, which is typically not practical. It is important to recognize an assumption in the equations above, namely that the input is a displacement input and its nature is independent of the system. In practice, the input is more typically a force and the actual displacement caused by its application is heavily dependent on the system properties. Thinking of the problem in this way forces the designer to determine the

effect of parameter changes through iteration, but also highlights another possible solution to large input amplitudes. For a given force, the acceleration of the system, and thereby its displacement, is reduced proportionally by an increase of its inertia. Therefore, an increase of the system's total inertia can have a larger effect on its dynamics than simply reducing its effective stiffness.

Still, gross mass or stiffness changes often cannot be made. Typically, these parameters are determined by other more critical performance or safety criteria. For example, in the case of a vehicle steering system, the steering wheel accounts for nearly all of the inertia in the steering column, and if increased, may create a safety hazard to the driver during an accident. The effective stiffness of the system cannot be drastically changed because of the negative implications for handling performance and customer perceptions of quality. For these reasons, it is more desirable to make local or unidirectional stiffness alterations to manipulate the dynamic performance of a system. Additionally, if the vibration problem is due to resonance, adding damping may cause a large reduction in output amplitude while leaving the overall system dynamics unchanged. These topics have been studied for decades in vibration research and several methods have been developed to achieve both of these design goals [1]. As will be demonstrated, the traditional approaches to solving such problems do not provide optimized solutions for the unidirectional problem.

1.4.2 Damping Principles and Performance of Viscoelastic Material (VEM)

In order to properly understand how to design a damper using VEM, it is necessary to understand the fundamental principles of the materials themselves. Viscoelastic materials are typically polymers that exhibit both the behavior of an elastic solid and the behavior of a viscous fluid. The strain of a purely elastic material for small deformations, according to Hooke's law, is directly proportional to the stresses imposed on it. In contrast, a Newtonian fluid develops shear stresses that are directly proportional with the rate of strain of the fluid. Furthermore, in purely elastic materials, the work done on the material is stored in the form of strain energy, whereas in purely viscous fluids, this work is dissipated in the form of heat. The strain generated in a

viscoelastic material is partly due to the storage of strain energy characteristic of elastic solids and partly due to the tendency to flow under loads characteristic of viscous fluids.

Consequently, if a VEM is subjected to a sinusoidal shear stress, a portion of the energy input is recovered and a portion is dissipated after each cycle. The strains created by each process would either be in-phase (elastic) or 90° out-of-phase (viscous) with the stress, and are represented by a storage and loss modulus. The storage modulus, G' , is the ratio of the stress in-phase with the strain to the total strain, and the loss modulus, G'' , is the ratio of the stress 90° out-of-phase with the strain to the total strain. Typically, these constants are written in a compact form called the complex stiffness of the material:

$$\frac{\tau}{\gamma} = G^* = G' + iG'' \quad (1.8)$$

$$G^* = G'(1 + i\eta) \quad (1.9)$$

Here, η is the ratio of the loss modulus to the storage modulus due to shear, and is called the loss factor of the material. This quantity can also be related to the actual phase difference, δ , between the stress and strain by [2]:

$$\eta = \tan \delta \quad (1.10)$$

The amount of work dissipated per unit volume by the material, W_d , may be calculated and visualized by the area enclosed within a plot of the shear stress vs strain, or hysteresis loop, of the VEM, shown in Figure 1.7.

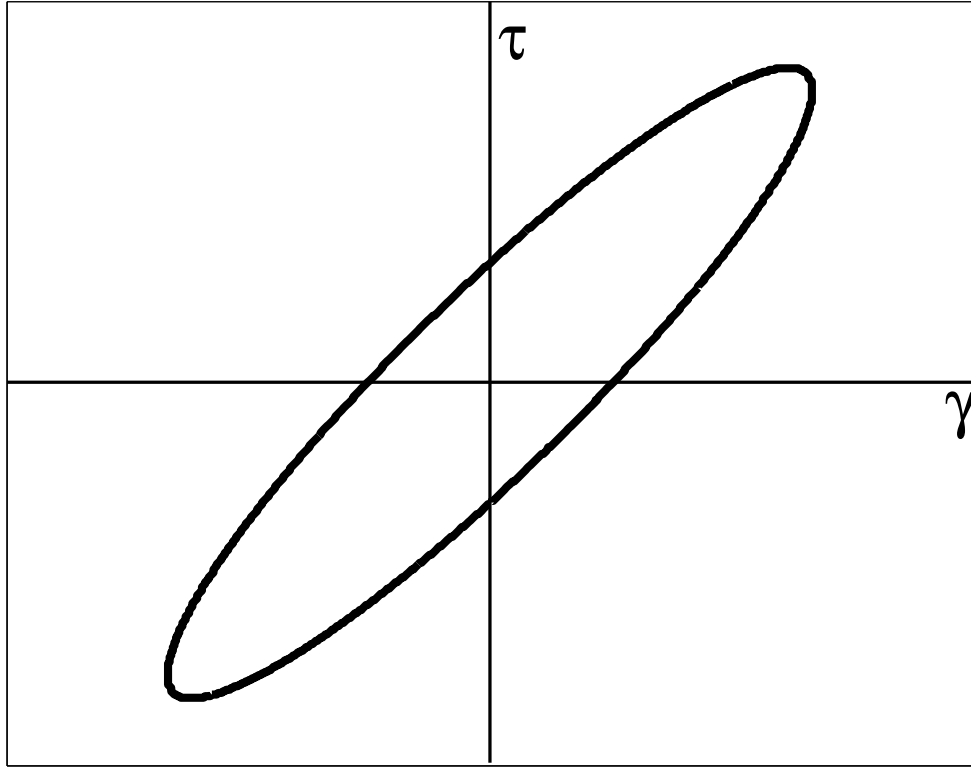


Figure 1.7 Hysteresis Loop of a VEM for a Single Loading Cycle

Since the loss factor is a measure of the amount of energy dissipated compared to the amount of energy stored within a material, it follows that:

$$\eta = \frac{W_d}{2\pi U} \quad (1.11)$$

Here, U is the maximum energy stored by the material during the loading cycle. Clearly, the larger the value of η , the larger the value of W_d and the thicker the hysteresis loop [3].

It is also important to note the environmental effects on VEM and how these effects can alter the performance of a design. Like most polymers, the properties of viscoelastic materials are highly dependent on temperature and, to a lesser but still significant degree, frequency. As the temperature of a VEM is varied, the material passes through three distinct mechanical regimes as shown in Figure 1.8.

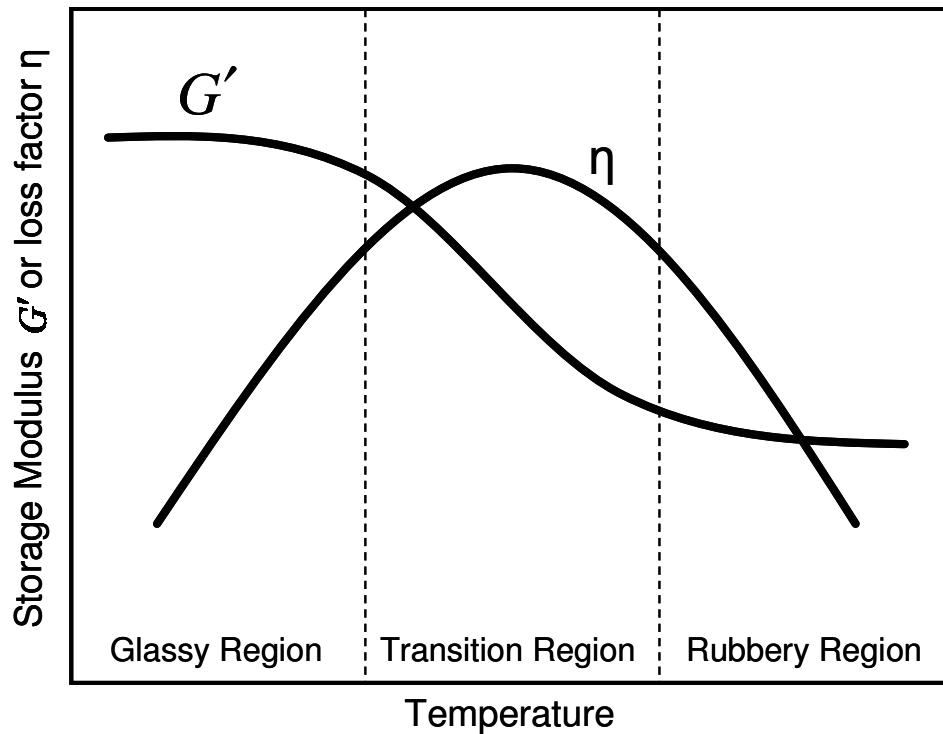


Figure 1.8 Property Variation of VEM with Temperature

At low temperatures, or the glassy region, the storage modulus of a VEM is large while the loss factor is low. As the temperature is increased, the storage modulus decreases rapidly and the loss factor rises to a maximum. If the temperature is raised further, the VEM enters a rubbery stage where the storage modulus is a minimum and the loss factor decreases again. The total change of the storage modulus may be as great as eight decades over only a few decades of temperature change. The zone between the glassy and rubbery regions is called the transition region, and is typically where the operating temperature of the device should lie for the maximum damping effect. For variations in frequency, qualitatively the parameter trends are the inverse of those for temperature. However, the changes occur over a much larger scale; at high frequencies the storage modulus is at a maximum, at low frequencies the storage modulus is at a minimum, and in between the modulus exhibits its greatest rate of change while the loss factor reaches a maximum [2].

From a design perspective, these variations highlight an important concept. In order to achieve a maximum level of damping, the stiffness of the material must not be so large as to limit the strain, and hence the strain energy, yet it must not be so low that the stress is absorbed by other stiffer elements. In other words, at high frequencies the large velocity of the deformation causes the viscous portion of the VEM to be very stiff, limiting the amount of energy dissipated by the material. At low frequencies, the stress absorbed by the viscous elements of the VEM compared to the elastic elements is low, again limiting the amount of damping achievable. This same concept will also apply when optimizing the geometry of the damper design itself.

CHAPTER

2 DESIGN OF SAVI AND DVL

The design of the SAVI and DVL first required a selection of vibration attenuation technologies to be implemented in the devices. This was accomplished by evaluating the multitude of existing methods based on a reasonable comparison of the performance metrics listed in Chapter 1: (1) potential vibration amplitude reduction, (2) delay, either time or displacement, in transmission of control input, (3) simplicity and (4) robustness. Design concepts were then generated that made most efficient use of these technologies, balanced the inherent associated trade-offs and allowed for the most flexible choice of design parameters.

2.1 Existing Technologies and Design Solution

Although a Compliant Vibration Attenuator is conceptually a very different type of device compared to conventional modular treatments, they must utilize the same fundamental technologies to reduce vibrations. A widely accepted and popular method for reducing vibrations in machine tools to laptops is through the use of vibration isolators [1]. With a low-stiffness element placed directly in the load path between the structure and the foundation, the structure system is placed within the vibration regime, shown in Figure 1.6, of vibration isolation. Looking at this figure, it is clear that this may be an extremely effective method for eliminating vibrations in a system.

However, this isolation occurs in both directions – that is, any vibrations in the structure system will not be passed to the foundation. For machine tools, this is not a concern, however, a requirement for both the SAVI and DVL is that they must transmit control torque inputs. Therefore, conventional vibration isolation techniques are not suitable choices for CVA's.

At the other end of the spectrum are damping technologies. As damping has the advantage of minimizing vibrations in a structure without altering other performance parameters, much

research work has been invested in its development. There is a large body of literature devoted to damping treatments [1 - 4].

Damping may be added to a system in many ways. Friction, normally an unwanted source of inefficiency, may be utilized to dissipate energy in the form of heat. The same principle applies for viscous fluidic and squeeze film dampers. Electro and magnetorheological fluids may be used to create variable viscosity dampers whose dampening effects may be changed at will [5]. Certain elastic solids also exhibit viscous losses like a fluid and are aptly named viscoelastic materials (VEM) [3]. Nakra reviews much of the past and current work on VEM including its most prevalent use, constrained layer damping (CLD) [6]. CLD techniques have been extended to machine structures [7], and have already been used to reduce torsional vibrations [8 - 12]. Passive damping is also achieved through shunted piezoelectric actuators [13], magnetic eddy currents [14], and most recently granular or low-wave speed media [15].

Vibration control has been accomplished through means other than introducing losses or a low stiffness element into the system. In cases where expense is not a constraint, vibrations may be reduced or eliminated actively through the use of actuators. As described in Chapter 1, tuned mass dampers can effectively cancel a single vibration mode without drastically altering the total system inertia [16]. In order to choose the most appropriate technology for use in a CVA, a selection matrix, shown in Table 2.1, was used. Each technology was rated for its general performance in the various performance areas listed in the left-hand column.

Table 2.1 Vibration Attenuation Technology Selection Matrix

Metric	Resonance				Non-Resonance		
	VEM	Viscous Damper	Shunted Piezos	Eddy Currents	Non-Lin. Spring	Tuned Mass	Active Control
Amplitude Reduction	0	+	+	-	0	0	+
Neg. Effect on System Perf.	0	0	0	0	0	0	+
Bandwidth	0	0	0	0	0	-	0
Environmental Sensitivity	0	+	+	+	0	0	0
Installation	0	-	-	0	0	0	-
Cost	0	0	-	-	0	0	-

From this matrix, it was determined that the best technology that would allow for the broadest application and best performance of a CVA was a non-linear spring. Like a normal low-stiffness spring element described above, a non-linear spring can effectively isolate a resonating or non-resonating system from a wide range of small amplitude frequency inputs. However, a non-linear spring does not perform the same way under all conditions. For large amplitude inputs, the non-linear spring may become very stiff and, therefore, also effectively transmit torques or displacements. An example of a stiffness profile for a non-linear spring is shown in Figure 2.1. Hence, if the unwanted upstream vibrations in a system have smaller amplitudes than that of the desired torque inputs, a non-linear spring can act as a very good CVA. Of course, there will be a certain amount of angular or time delay in the response of the system to the larger amplitude torque inputs. Nevertheless, as long as the difference in the amplitudes of the upstream vibration and the control inputs is not too small, and the low-amplitude stiffness of the system is not critical, a non-linear spring is the best choice for providing vibration attenuation in a CVA.

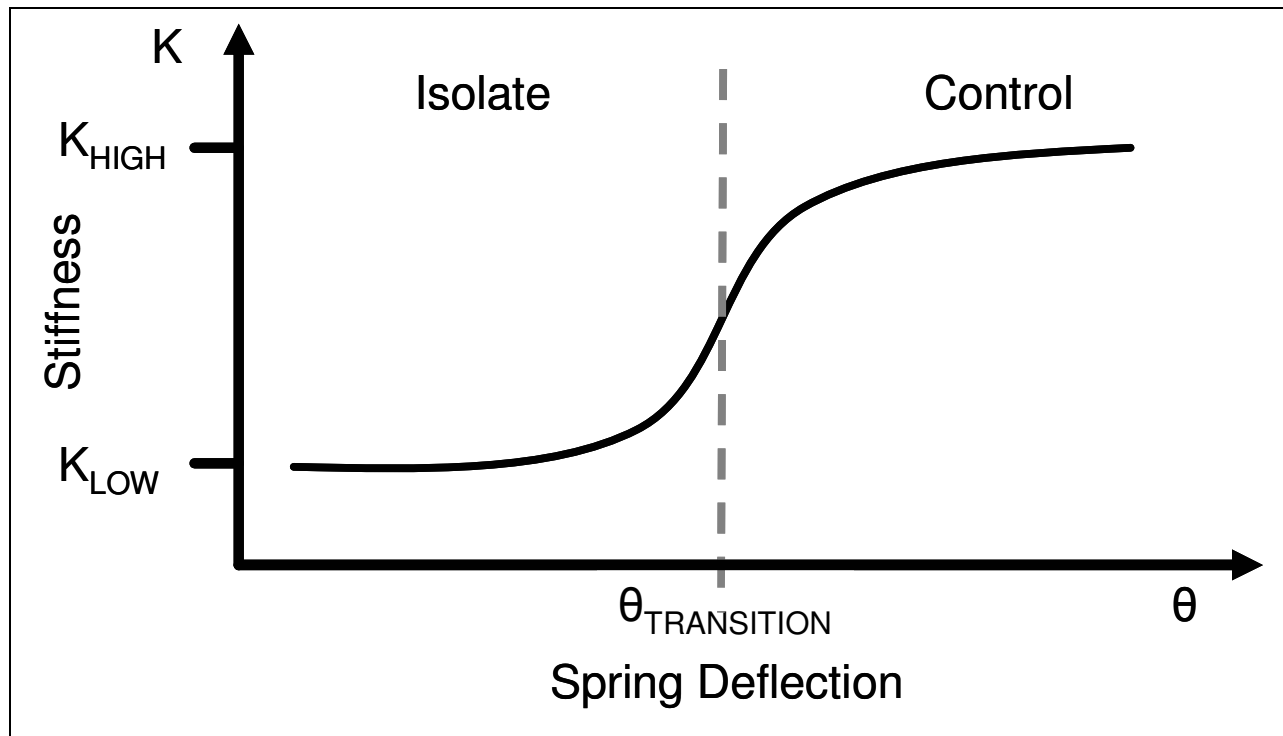


Figure 2.1 Example of Non-Linear Stiffness Profile

In order to account for systems in which the conditions necessary to use a non-linear spring do not hold, damping from VEM was chosen as the second most effective technology for use in a CVA. VEM is a very convenient and relatively cheap way to add damping to a system to reduce the vibration of a resonance at a large range of frequencies, and may be designed to have a minimal effect on the overall system performance. Although this solution is limited to a resonating system, most vibration problems are a result of some type of resonance in the structure. Therefore, if the natural frequency of the system cannot be moved by changing the system's stiffness with a non-linear spring, it is likely that adding damping could be a good alternative. Again, these technologies were chosen as a starting point for the preliminary designs of a CVA, and others could also be investigated in the future.

Solutions involving friction were omitted because the related wear and resistance caused by their use is generally not desirable. Furthermore, granular materials are still not well understood and are shown to work only for higher order modes. Active control and the use of piezoelectrics was not considered because their costs are prohibitive for most applications. Viscous dampers, while offering large damping levels, may be difficult to integrate into an existing system, and limits the

variety of design concepts. Again, tuned mass dampers may be very effective in removing problematic vibrations. However, they may be tuned for a single frequency only and can not affect other frequencies without additional dampers, adding more inertia and complexity to the system. Finally, the losses due to magnetic eddy currents are typically not great enough to significantly affect vibrations, and the equipment may be expensive. Therefore, the best combination of design strategies for vibration attenuation with the broadest spectrum of applications was determined to be non-linear springs and VEM. It is important to note the metrics are not weighted equally, and that in certain situations there may be other good design solutions.

Several concepts were generated for both of these strategies culminating in the two designs shown in Figure 2.2 and Figure 2.4. In the following sections, the process of creating these designs will be explained.

2.2 Small Amplitude Vibration Isolator (SAVI) Concept Synthesis

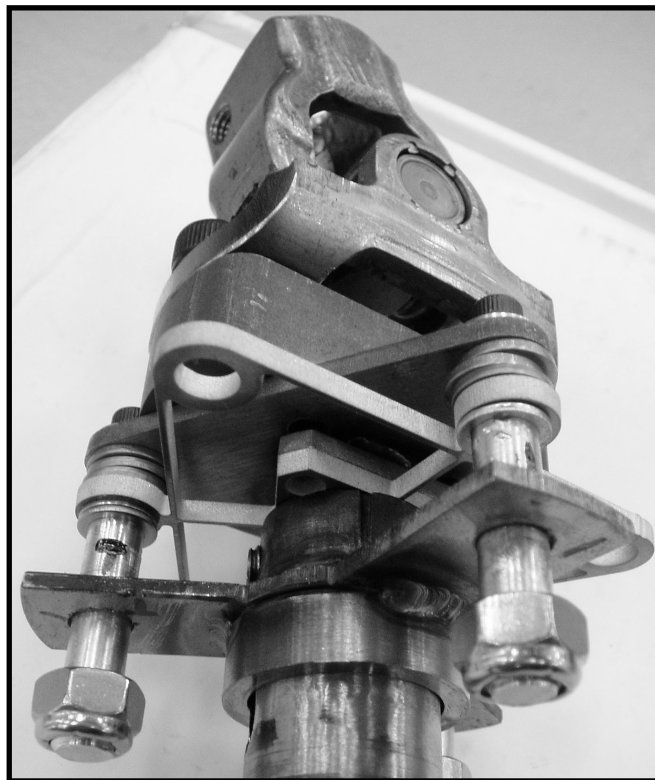


Figure 2.2 Final Prototype of SAVI

In review, the basic function of the SAVI is to reduce the effective stiffness of the rotational system so that, for small amplitudes, it will be in the vibration isolation regime shown in Figure 1.6. However, for larger amplitudes the SAVI should have a minimal effect on the total stiffness of the system so that all motion and torques are properly transmitted. This necessitates a non-linear stiffness for the device, similar to one shown in Figure 2.1, where at a certain angular deflection the stiffness increases significantly. This stiffness profile restricts the SAVI's use to systems that do not have tight constraints on their low-amplitude stiffness, and in which upstream vibrations occur at lower amplitudes than the intended input. How much separation must exist between these two input amplitudes and the maximum amplitude for the upstream vibrations depends on the system under consideration. Nevertheless, in practice there are many systems for which the SAVI is applicable, including automotive steering systems.

The two major components of the SAVI, shown in Figure 2.2, are a planar torsional spring and an interlocking angular displacement stop, individually shown in Figure 2.3. The planar spring, developed by Professor Martin Culpepper, provides the low stiffness for attenuating the upstream vibrations and may be designed to have a specific stiffness by varying the dimensions of the beam elements in the design. It is also easily and rapidly fabricated using waterjet or stamping processes. This was important in the development of an initial prototype, and will also be valuable later for large-scale manufacturing. The center of the spring is attached to the downstream portion of the system and the three holes highlighted in Figure 2.3 are connected to the reverse portion via bolts. These bolts are threaded into pins that descend past the planar torsional spring and lie within holes cut into a flange. The sizes of these pins and the holes they are in are specifically designed so that at a particular angular deflection of the torsional spring, the sides of the pins engage with the flange. This engagement creates the transition point in the stiffness profile of the SAVI, and directly transmits any large amplitude torque through to the opposite portion of the system. As long as the resulting deflection of the SAVI to any upstream vibration is less than the angular deflection at which the engagement occurs, the rotational system is in vibration isolation.

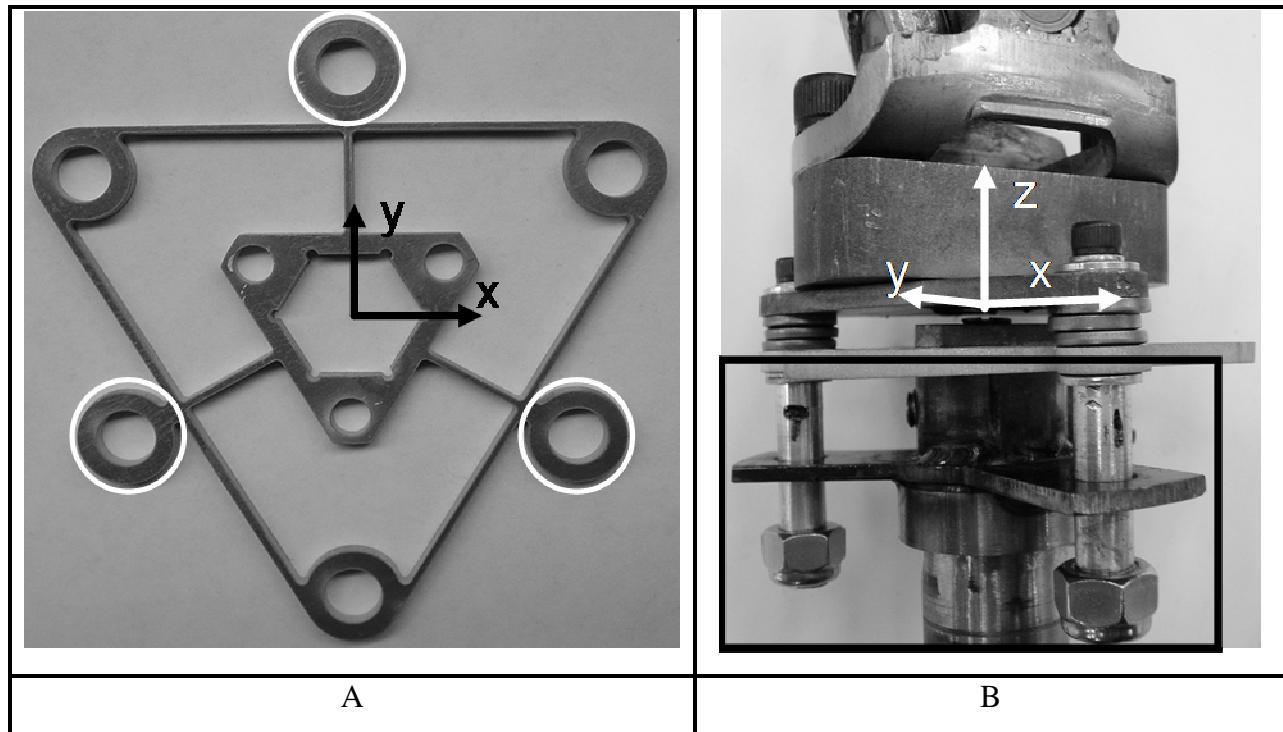


Figure 2.3 (A) Planar Torsional Spring and (B) Engagement Stop Elements of SAVI

The pins and flange that form the engagement stop also provide three other important functions: (1) provide a safety to protect the compliant torsional spring from high torque loads, (2) hold the assembly together in case the torsional spring does fail, and (3) protect the torsional spring from any moment loads created when the device is installed in the system. The pins themselves provided the dual functions of absorbing the high shear loads experienced when they engage the flange, and also protect the bolts used to connect the planar torsional spring to the upstream adapter from any bending moments experienced in the process. To aid the latter function, the flange was placed as close as possible to the upstream adapter, minimizing the bending moment caused by the stop engagement. Another element, called a lock plate, was also used to ensure that the torsional spring stayed attached to the downstream portion of the system. Most of these functions of the engagement system and lock plate were discovered as a result of fabrication and testing of the SAVI, and will be discussed further in Chapter 4. All other components of the assembly were used simply to allow for convenient integration of the device with a pre-designed rotational system.

Besides offering a high performance potential, the selection of a non-linear spring in section 2.1 also offers the large advantages of simplicity and flexibility, as evident in the design of the SAVI. Since few components are actually necessary in the design, the part count is small, thereby reducing manufacturing complexities and cost. With fewer parts, there is also a lower probability of failure. Furthermore, there are many other configurations for both the planar torsional spring and the engagement stops that could be used to either improve the performance of the device or provide a more suitable installation in another rotational system. The one shown in Figure 2.3 was developed simply as a proof-of-concept and is not the best topology or assembly of the device. In fact future designs are already in the process of being developed that could allow for simpler manufacturing, less sensitivity to tolerances and a smaller part count.

Nevertheless, there are important design parameters associated with the SAVI, the most significant of which are the manufacturing tolerances of the stop engagement. Depending on the desired angular deflection at engagement and the dimensions of the SAVI, the gap between the pins and the flange holes could be as small as 0.76 mm (0.030"). This is a very tight tolerance for not only the manufacturing processes but also for the assembly of the device. If this tolerance were relaxed by increasing the angular deflection at the stop engagement, then there may be two other problems. First, the delay in the system response to the desired torque inputs could grow too large. Second, depending on the torque loads and stiffness of the SAVI, the planar torsional spring could yield before the stops engage, thereby causing short-cycle fatigue failure. As long as these considerations do not become limiting issues, the rest of the design and subsequent fabrication of the SAVI is relatively straightforward.

Also, as will be seen in the following chapters, the fabrication of the torsional spring element will cause dimensional variations that could significantly affect the performance of the SAVI. For this thesis, an abrasive waterjet machine was used to cut the planar spring from a sheet of 7075-T651 aluminum. As will be discussed in the modeling and fabrication sections of this paper, the taper created in the part by the abrasive waterjet must be carefully measured and considered in the design and fabrication processes.

In the next section, the design of the DVL will be discussed. Besides the obvious functional differences between the two designs, note the added complexities and possible manufacturing difficulties inherent in the DVL. These issues and how they affect the design of the DVL will be focused on in Chapter 4.

2.3 Damping Vibration Link (DVL) Concept Synthesis

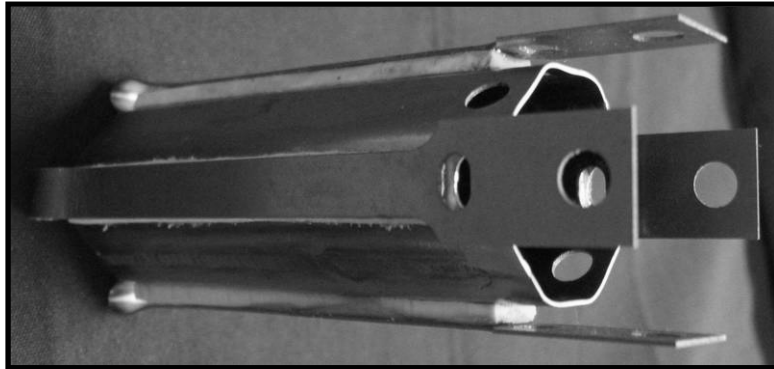


Figure 2.4 Final Prototype of DVL

Recall that the fundamental goal is to create a device that will introduce damping into a rotational system. Therefore, the final design need to fulfill at least two requirements: to provide damping, and to transmit torque from the upstream to the downstream of the system and vice versa. With this in mind, we shall take a look at previous attempts at this goal using conventional treatments.

As noted earlier, VEM has been applied to damp torsional vibrations before [8 – 12]. In all of these studies, VEM has either been sandwiched between two elastic concentric tubes or applied externally. For our purposes, if a concentric tube design were to be used, the boundary conditions imposed by the rotational system would be such that the outer tube is connected to the upstream portion of the system and the inner tube is connected to the downstream portion, or vice versa, as shown in Figure 2.5A. Another way to consider the situation is to imagine that the inner shaft is grounded on the downstream end and the outer tube is free with a torque applied to the upstream side. Therefore, the two tubes are coupled only through the VEM with the torsional

rigidity of the inner tube acting as a constraining layer and providing some damping to sinusoidal loadings.

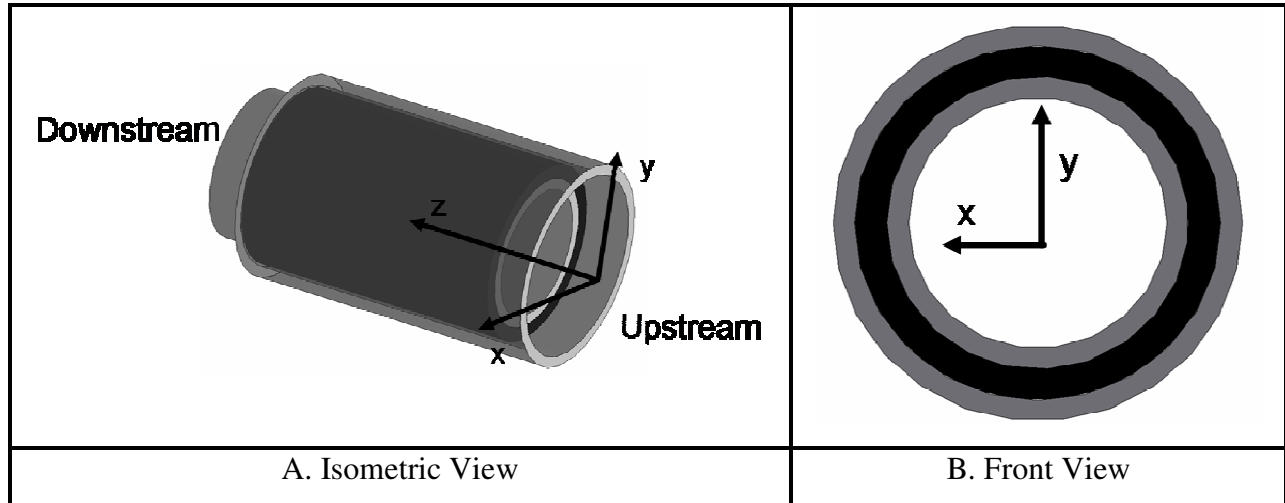


Figure 2.5 Concentric Tube Design

Being somewhat different than the boundary conditions previously studied, our situation will no doubt create a large shear stress in the VEM since the entire torque load must pass through it. This will generate a large amount of damping, but it also will create a problem of plane strain. As a small differential volume of the VEM is sheared, it naturally tends to shrink in the radial direction of the device. However, since an equivalent volume of the VEM 180 degrees around the circumference of the tubes undergoes the same deformation, the two radial strains will cancel. This constraint greatly increases the stiffness of the VEM, which reduces the strain energy it absorbs and significantly lowers the amount of damping. This effect was studied by Vinogradov [17], who determined that higher damping levels were possible if the VEM was separated by cuts along the longitudinal axis of the assembly. Furthermore, a concentric tube design, as shown in Figure 2.5, would be difficult to manufacture.

As an alternative, the VEM may be applied as segmented Constrained Layer Damping (CLD) treatments to the exterior of a single tube. As the entire tube is not covered, it eliminates the problem of plane strain. Nevertheless, the only way to develop strain in the VEM is now through axial warping of the tube. This is a less effective use of the VEM, and for reasonable dimension and constraining materials, damping ratios are limited to about 0.055 [8]. For these

reasons, a new design was created to combine the high damping potential of the concentric tubes with the elimination of plane strain through external CLD application. The geometry of this concept is shown below in Figure 2.6.

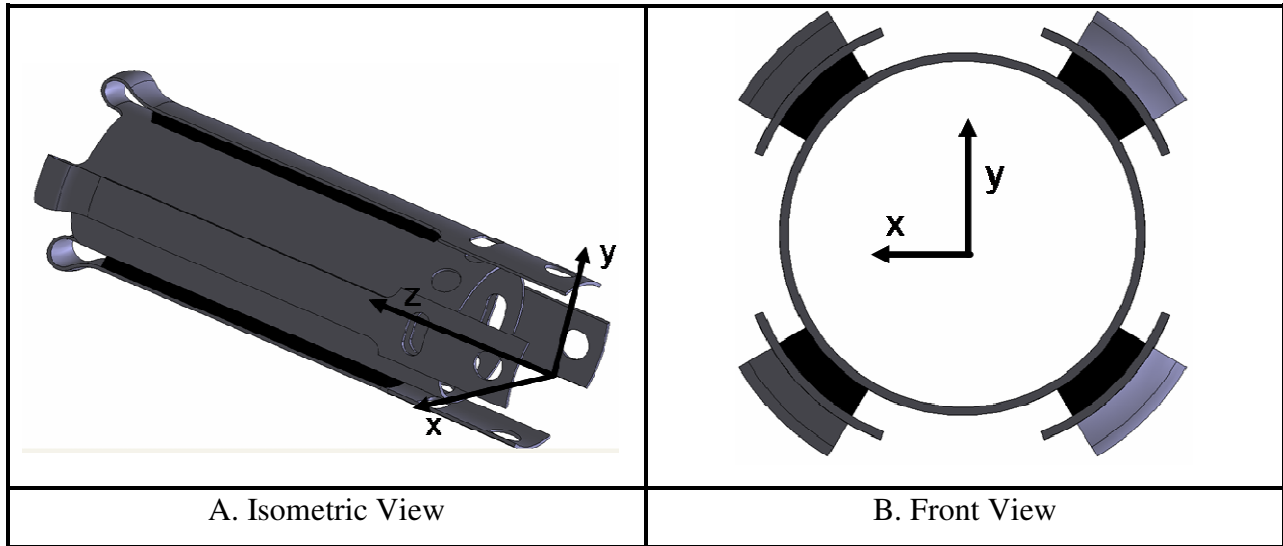


Figure 2.6 Final Geometry of DVL

Comparing this to the concentric tube design, the major differences are that the outer tube has become separated into narrow tabs and the two elastic layers have been connected on one side. Separating the tabs allows for the VEM bonded between them and the inner shaft to contract radially as it is sheared. Connecting the tabs to the inner shaft at one end helps to secure the tabs and also enables more design variability. Depending on the selection of dimensions and materials, the torque load applied to the DVL may be shared between the VEM and the constraining layers. The applied torque acting on the free end of the tabs travels through the device to the inner shaft both in a serial direction along the length of the tabs via the curved connection, and in a parallel path through the VEM. A schematic of these load paths is shown in Figure 2.7.

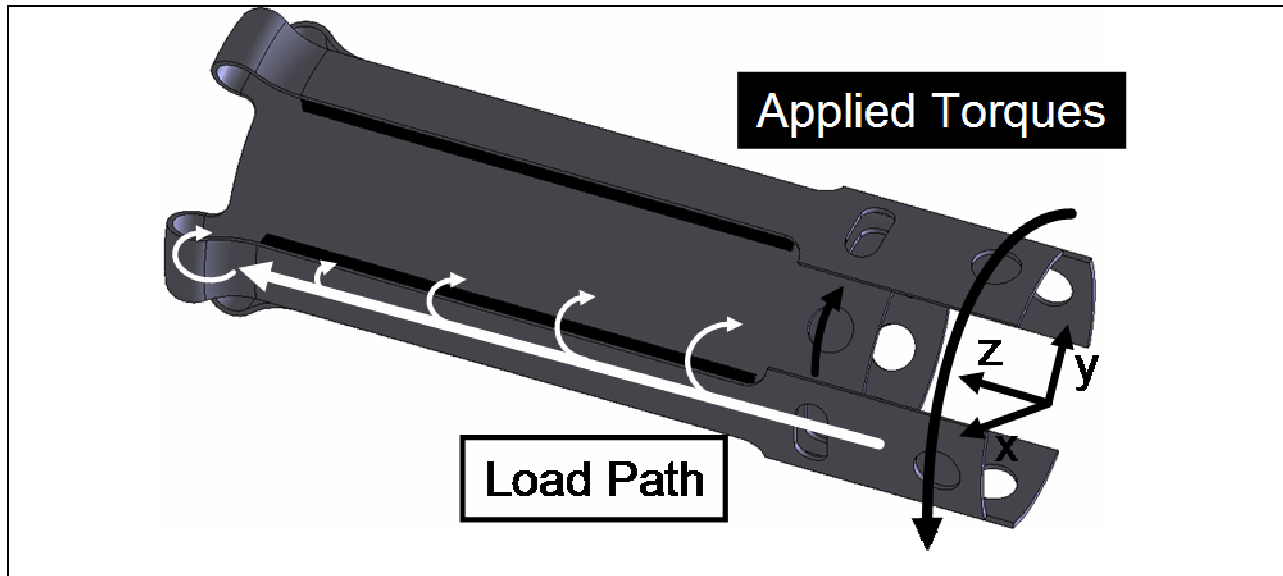


Figure 2.7 Torsional Load Paths of DVL

This is useful in a system situation where the applied control torque input is large where as the vibration torque input is low. Therefore, the load path of the two inputs could be separated, both protecting the VEM from failing and providing a more direct transfer of the desired torque inputs.

[Note the connection points to the upstream and downstream portions of a rotational system. The pair of circular holes in the inner shaft will be secured to the downstream portion of the system through use of a roll pin. The circular holes at the end of each tab will be connected to an adapter block, shown in Figure 2.9, which may be customized to join with the upstream portion of the system. Finally, the slots cut through each tab and the inner shaft will hold clevis pins and act as an emergency direct connection between the upstream and downstream portions in case the VEM or tabs fail.]

As the load is now shared amongst the elastic and viscoelastic materials, their properties and dimensions must be optimized to provide high levels of damping, and appropriate mechanical strength and stiffness for the system in which the device is to be implemented. Since the strain in the VEM is caused by relative displacement between the outer tabs and inner shaft, by making the tabs more compliant and the shaft more stiff the displacement between the two components may be increased. As alluded to in the last chapter, qualitatively, if the VEM stiffness is

comparable to that of the outer tabs, then it will absorb some of the load as strain energy and damp out vibrations. However, the VEM cannot be too stiff or there will not be enough strain and the damping of the device will decrease. According to Ungar, the loss factor of the total device is a ratio of strain energies developed in each of the materials weighted by their own respective loss factors [18]. This total loss factor may be calculated as:

$$\eta = \sum_i \frac{U_i}{U_{tot}} \eta_i \quad (2.5)$$

The other major design consideration is the amount of relative displacement of the tabs and inner shaft. Since this displacement varies along the length of the device, the VEM does not strain equally. Figure 2.8 shows how the VEM close to the free end of the tabs is strained the most while the VEM at the connection between the tabs and the inner shaft is not strained at all.

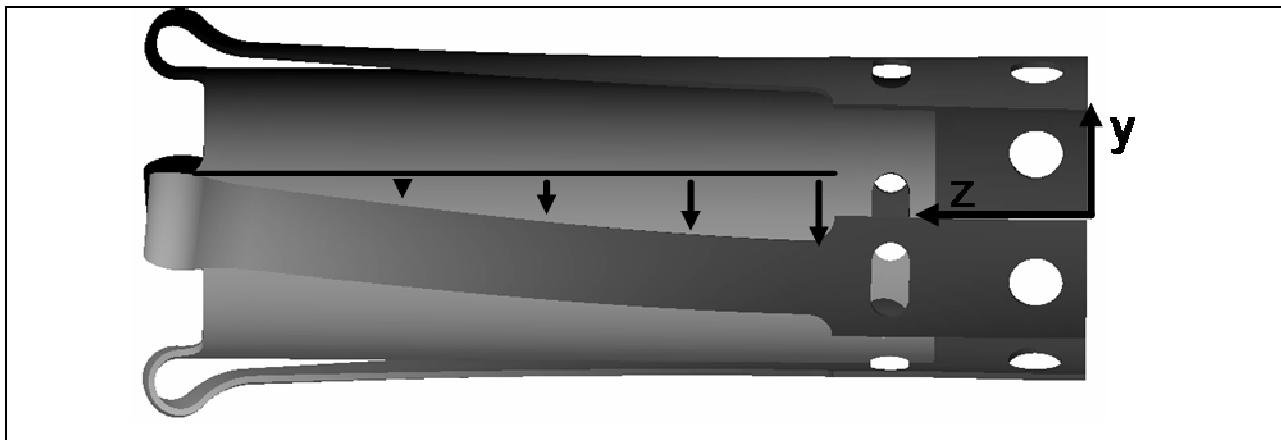


Figure 2.8 Plot of Relative Displacement of VEM vs Length

Therefore, the amount of the load absorbed by the VEM will vary with the length of the DVL, with the highest shear stresses at the edge of the shaft. In addition to the higher shear stresses, there will also be higher peeling stresses at the edges and possible delamination fatigue. This has been studied by Badre-Alam and may be avoided by locally increasing the VEM thickness along the edges of the tabs [19].

Several other practical design decisions were made in order to fabricate a prototype, shown in Figure 2.4. The most obvious change from Figure 2.6 is that the DVL cross-section is octagonal rather than circular. This change was made because of the difficulty in bending the tabs over the inner shaft and ensuring that the surfaces of the tabs and the shaft were concentric. Not only would this be difficult to accomplish, but the process would also cause a large amount of residual stress in the curved elements connecting the tabs to the inner shaft. By using an octagonal shape, reversing the concavity of the tabs after bending them over the inner shaft would not be necessary.

Outside of the design of the DVL itself, an adapter, shown in Figure 2.9, was designed and created to connect the device to a rotational system. The adapter supplied four thread locations to bolt down the ends of the tabs, and also provided an important protective feature. In the center of the extruded square, a circular recess was cut into the adapter, which would house a shaft from the downstream portion of the rotational system.

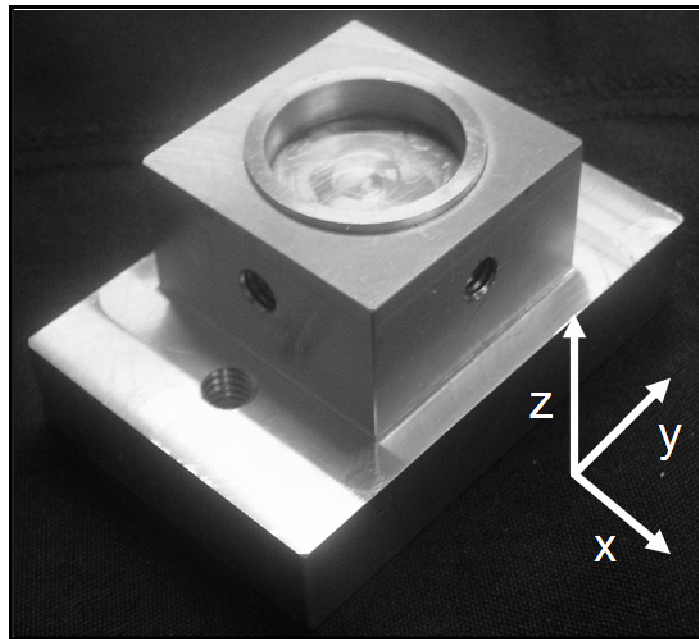


Figure 2.9 Adapter used to Mount DVL to Rotational System

This was important to include because the DVL is not intended to carry any bending moments that may result from installation into the rotational system. These bending moments could cause

the tabs to be pulled away from the inner shaft, in turn separating the VEM from the inner shaft. The recess also acts as an alignment feature for ensuring concentricity between the DVL and the downstream shaft of the rotational system. These considerations along with those involved in attaching the DVL to the downstream shaft of a rotational system will be discussed further in Chapter 4.

2.4 Summary

In this chapter, the designs for both devices have been presented. The important design parameters of the SAVI and DVL are:

SAVI

- Low-amplitude torsional stiffness
- Yield angle
- Stop engagement angle/gap spacing of engagement system

DVL

- Torsional stiffness
- Damping ratio

The major advantages that are to be exploited in the design of the SAVI are its ability to separate the loads of the rotational system, its simplicity and the potential for its components to serve multiple functions. The important issues for the design are the taper in the torsional spring created by the abrasive waterjet and the tight tolerances that are possible, depending on the device dimensions, for the engagement stop system. For the DVL, the most important consideration is the ratio of the stiffness of the VEM to the stiffness of the tabs. This determines the amount of load that is absorbed by the VEM, and hence, determines the damping and strength of the device. One major issue that may become a problem for future generation designs is the concavity of the tabs after bending. Also, the DVL must be protected from bending moments so that the VEM does not delaminate during installation into a rotational system.

CHAPTER

3 MODELING AND ANALYSIS

3.1 Purpose of Models

Now knowing what the major design considerations and parameters are, predictions must be made as to how the dimensions of each device affect their performance. This allows the designer at the very least to prioritize which elements of the design shall require the most work and also to potentially make changes to the design to improve the general performance or avoid certain potential pitfalls. More refined models may allow for optimization of these parameters to ensure the best performance possible. In addition to the predictions of the devices themselves, the rotational systems in which the devices will be used must be understood and the behavior of the total system after integration of either device must also be appropriately predicted. This way the proper device may be chosen early on and its parameters may be determined in light of the total system performance. The analytical models used for these purposes will now be presented. First, the models for determining the behaviors and choosing dimensions of the SAVI will be discussed, and the models for the rotational systems as a whole will follow. The necessary level of accuracy of all these theories will depend heavily on the requirements of the actual system being studied. However, for most moderately complex rotational systems the feedforward performance is important while a variable reduction of the upstream vibration is tolerable.

At the time of publication of this paper, a model for the DVL had not yet been completed. For now, the model of the SAVI was decided to be sufficient for the preliminary analysis of the performance of a CVA for the case study. Work is currently being conducted to generate a model for the DVL so that the damping and stiffness design parameters desired for a particular rotational system may be predicted. Nevertheless, a prototype of the DVL was still created and tested, as discussed in Chapters 4 and 5, to determine the practical design considerations concerning fabrication and the broad potential of the device.

3.2 Small Amplitude Vibration Isolator (SAVI)

The modeling of the SAVI was accomplished through finite-element simulations and a simple geometric relation for the size of the flange holes and pins in the interlocking stop engagement assembly. The torsional spring component was drafted in SolidWorks®, a CAD program, and then analyzed by CosmosWorks®, the accompanying FEA software, as shown in Figure 3.1.

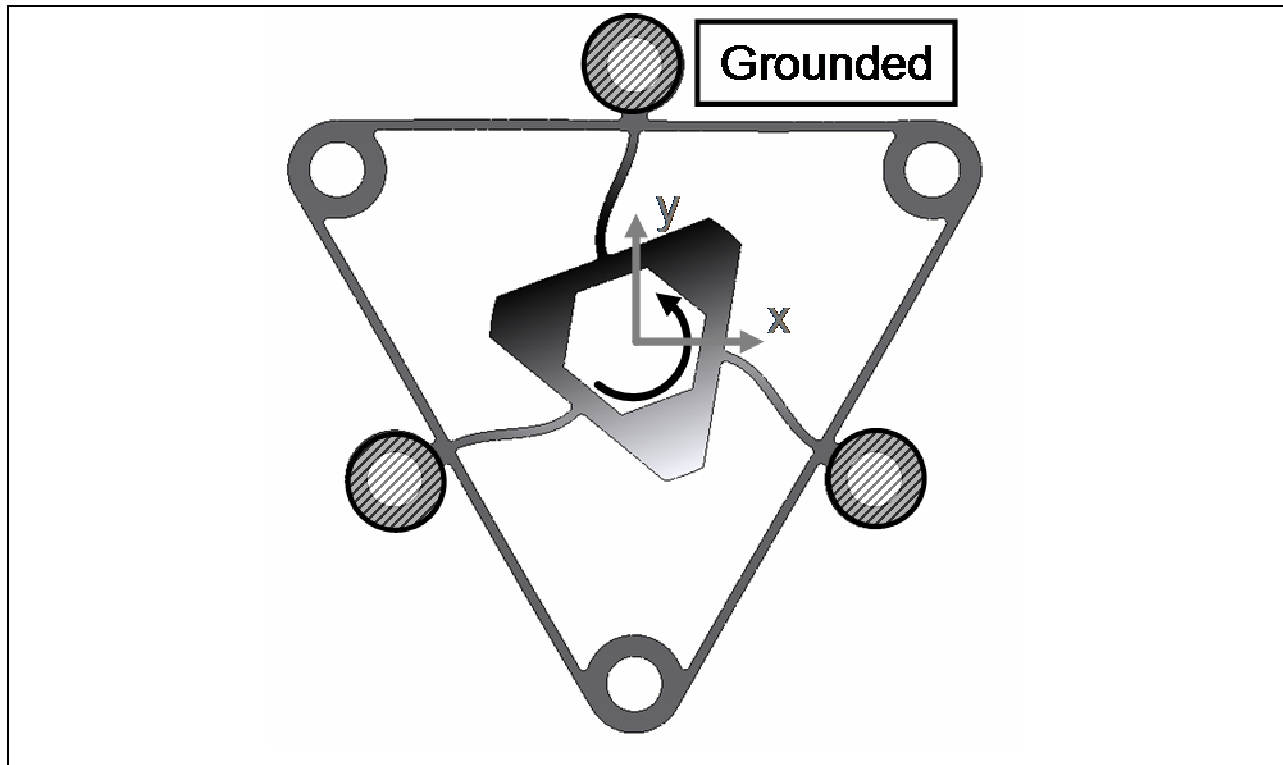


Figure 3.1 FEA Simulation

To calculate the stiffness of the device, a torque was applied to the inner surface of the component and the holes that would be connected to the upstream portion of the rotational system were grounded. By measuring the deflection of the torsional spring, the torsional stiffness of the component was calculated. Furthermore, any local stress concentrations were checked to determine the maximum deflection of the torsional spring that caused the first signs of yielding.

Looking at Figure 3.1, the elements of the torsional spring that are strained the most, given an applied torque, are the radial beams. Therefore, it seems likely that their bending stiffness dominates the torsional stiffness of the planar spring as a whole. The main parameters that affect the dimensions of the radial beams, and therefore their bending stiffness, are: (1) the width of the beams themselves, (2) the packaging diameter of the device, and (3) the thickness of the sheet of material from which the planar spring was cut. In order to understand the trends of how these dimensions affect the torsional stiffness of the SAVI, let's look at the formulae for the bending stiffness of the radial beams.

Figure 3.2 shows an enlarged view of the radial beams.

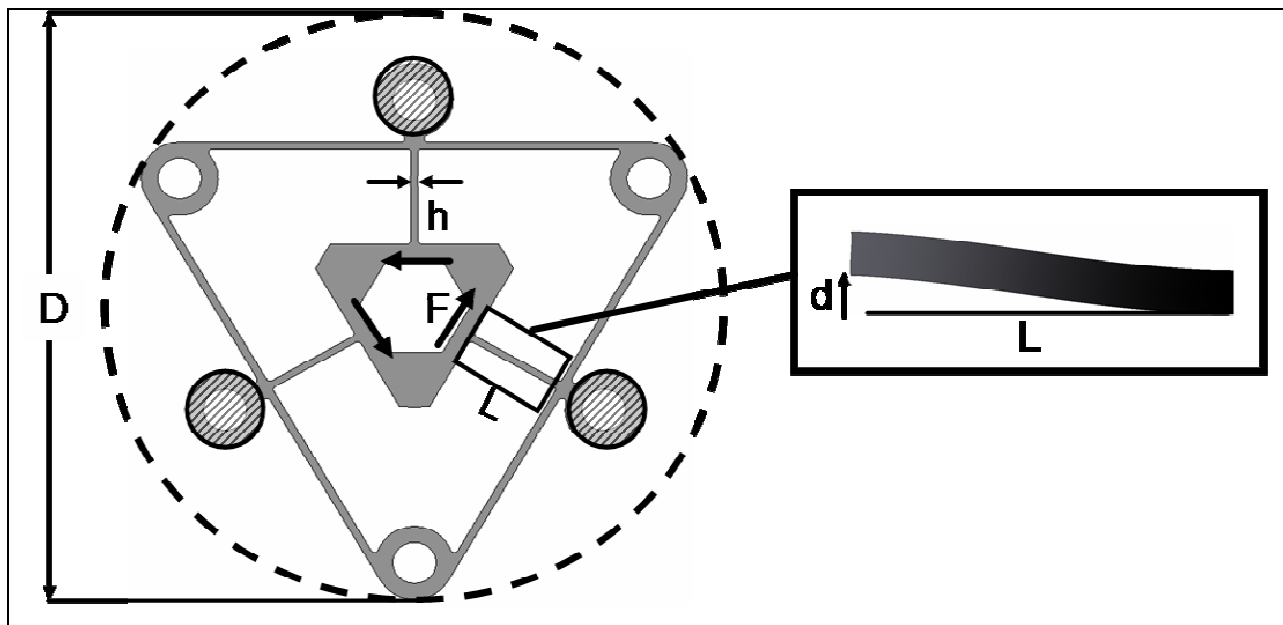


Figure 3.2 Enlarged View of Radial Beam

According to Bernoulli-Euler beam bending equations, for a horizontal force applied to the end of the radial beams at which there is a guided end condition, their linear deflection and stiffness are:

$$d = \frac{FL^3}{12EI} \quad (3.1)$$

$$K_L = \frac{E \cdot t \cdot h^3}{L^3} \quad (3.2)$$

Assuming that there is a proportional relationship between the overall diameter of the SAVI and the length, L , of the radial beams, the linear stiffness of the beams may be written as:

$$K_L = \frac{1}{C^3} \cdot \frac{E \cdot t \cdot h^3}{D^3} \propto t \cdot \left(\frac{h}{D}\right)^3 \quad (3.3)$$

where $L = C \cdot D$ and $C = f(D)$

According to Eq. 3.3, for a given part thickness, the linear stiffness of the radial beams is proportional to the cube of the nondimensionalized beam width $\frac{h}{D}$. Strictly, speaking C also may be a function of the diameter of the SAVI, which may violate this formula. Still, we would expect to see some direct relationship between the value $\frac{h}{D}$ and the torsional stiffness of the SAVI.

The other important design parameter is the maximum angular displacement that the torsional spring is capable of before first signs of yielding. Again, according to elementary beam theory, the maximum stress in the radial beams is:

$$|\sigma_{MAX}| = \frac{FL \cdot h}{2I} \quad (3.4)$$

Solving this equation for the force required to cause the maximum stress in the beam to equal the yield stress of the material, and then substituting this value into Eqn. 3.1, the linear deflection of the radial beams at yield is:

$$d_Y = \frac{C^2}{6} \cdot \frac{\sigma_Y D^2}{Eh} \propto \frac{\sigma_Y}{E} \cdot \frac{D^2}{h} \quad (3.5)$$

Although this value is not related to the nondimensional width of the beams, there are few important realizations to be made. First, the thickness of the part does not affect the maximum deflection of the radial beams, and therefore, of the torsional spring. This is advantageous because by varying this dimension, the stiffness of the SAVI may be adjusted without varying its maximum angular deflection. Second, the ratio $\frac{\sigma_y}{E}$ is an important measure of the maximum strain a material can undergo before it yields, and is often considered when designing a compliant mechanism, such as the torsional spring. By choosing a material that maximizes this ratio, the angular deflection until yielding of the SAVI can also be maximized. Third, as clearly seen from Eq. 3.5, the diameter of the SAVI has a much greater effect on its maximum angular displacement than the width of the radial beam. Therefore, in order to design a torsional spring with a low stiffness and large maximum displacement, it is important to make the diameter of the SAVI as large as possible given packaging constraints for the rotational system.

To verify these trends and provide a more accurate measure of the dependence of the two design parameters on the dimensions of the torsional spring, finite-element simulations were performed. Additionally, a 2.29 degree taper caused by an abrasive waterjet machine was measured for a 3.18 mm (0.125”) thick sheet of 7075-T651 aluminum, and added to the solid model of the torsional spring. This corresponds to a beam width variation of 0.254 mm (0.010”) across a 3.18 mm (0.125”) thick part. For this reason, there were practical limitations on the range of values for both the part thickness and the beam width. If the part thickness was large, then the beam width variation would also be large and possibly even be a significant fraction of the nominal thickness of the beams. Furthermore, if the beams were too small, then it is possible that the taper would cause the beam width to become zero on one face of the part, making the cross-section of the beams a triangle rather than rectangular or at the very least trapezoidal. Finally, since space is usually a premium in mechanical systems, the overall diameter of the SAVI would be restricted as well. Therefore, for the FEA study, a representative range of values, shown in Table 3.1, were chosen for the dimensions that would be reasonable for most applications.

Table 3.1 Dimension Ranges for FEA Simulation of Planar Torsional Spring

Dimension	Value Range	Step Size
Radial Beam Width (h)	0.762 – 1.52 mm (0.030 – 0.060")	0.254 mm (0.010")
Package Diameter of SAVI (D)	76 – 100 mm (3.0 – 4.0")	13 mm (0.5")
Part Thickness (t)	1.60 – 3.18 mm (0.063 – 0.125")	1.60 mm (0.063")

The results of the simulation are shown in Figure 3.3 – Figure 3.5.

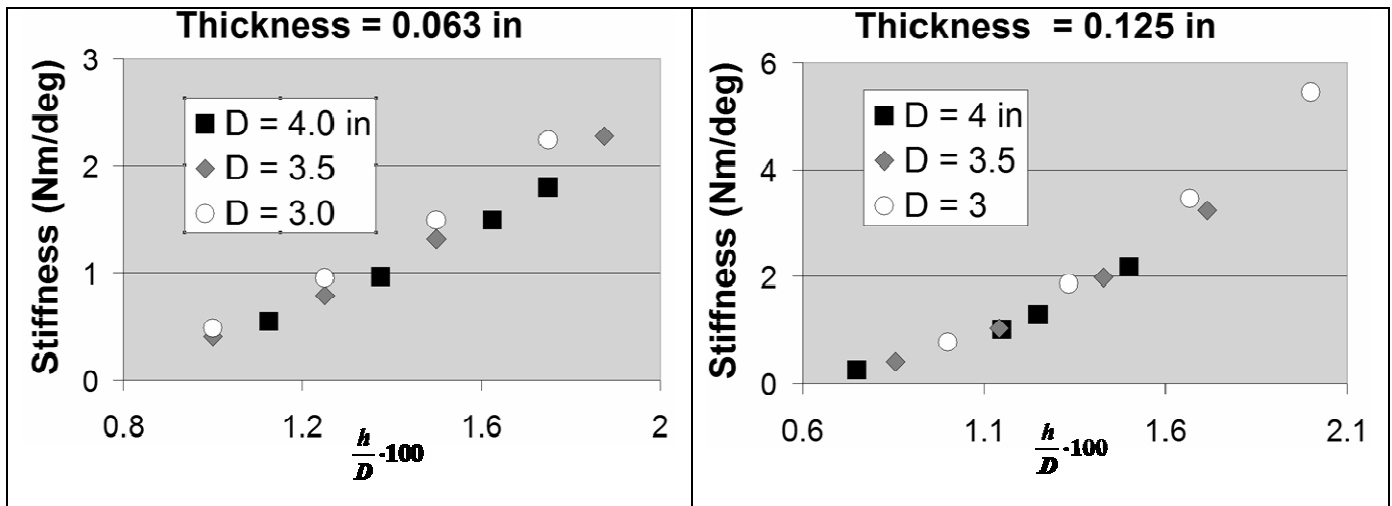


Figure 3.3 Two Plots of Stiffness vs Ratio

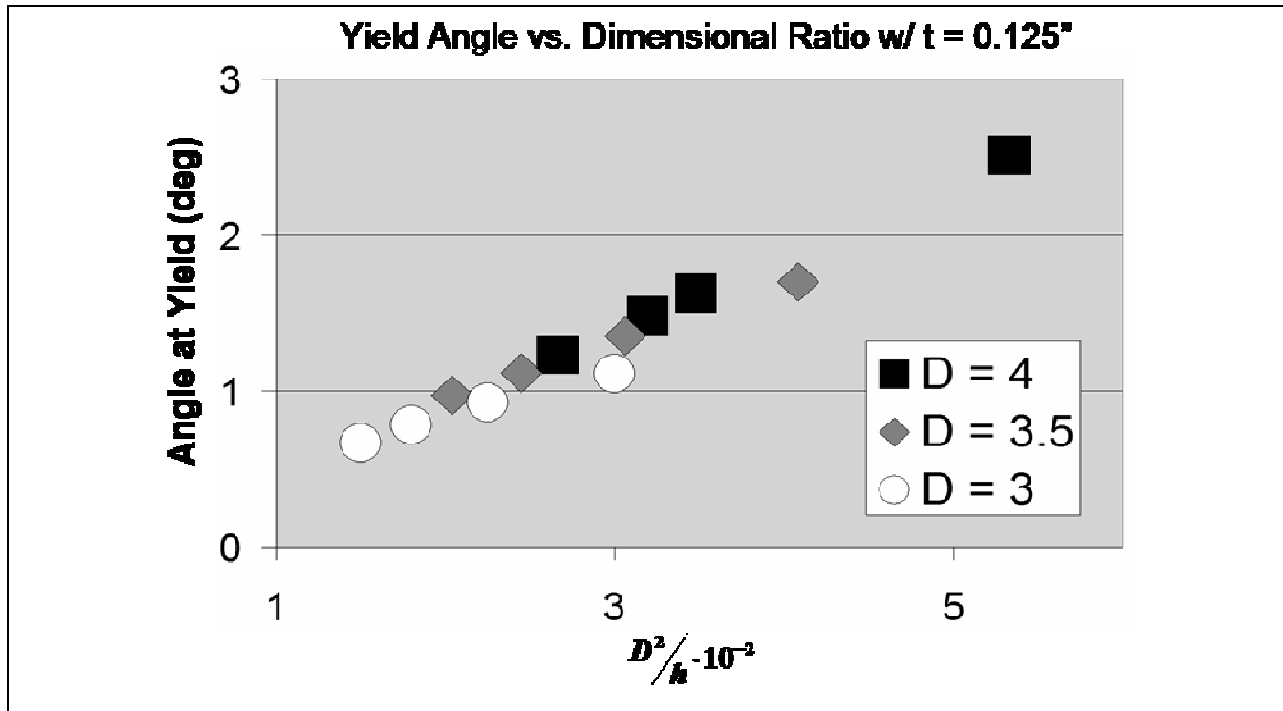


Figure 3.4 Plot of Yield Angle vs Ratio for $t = 0.125$ "

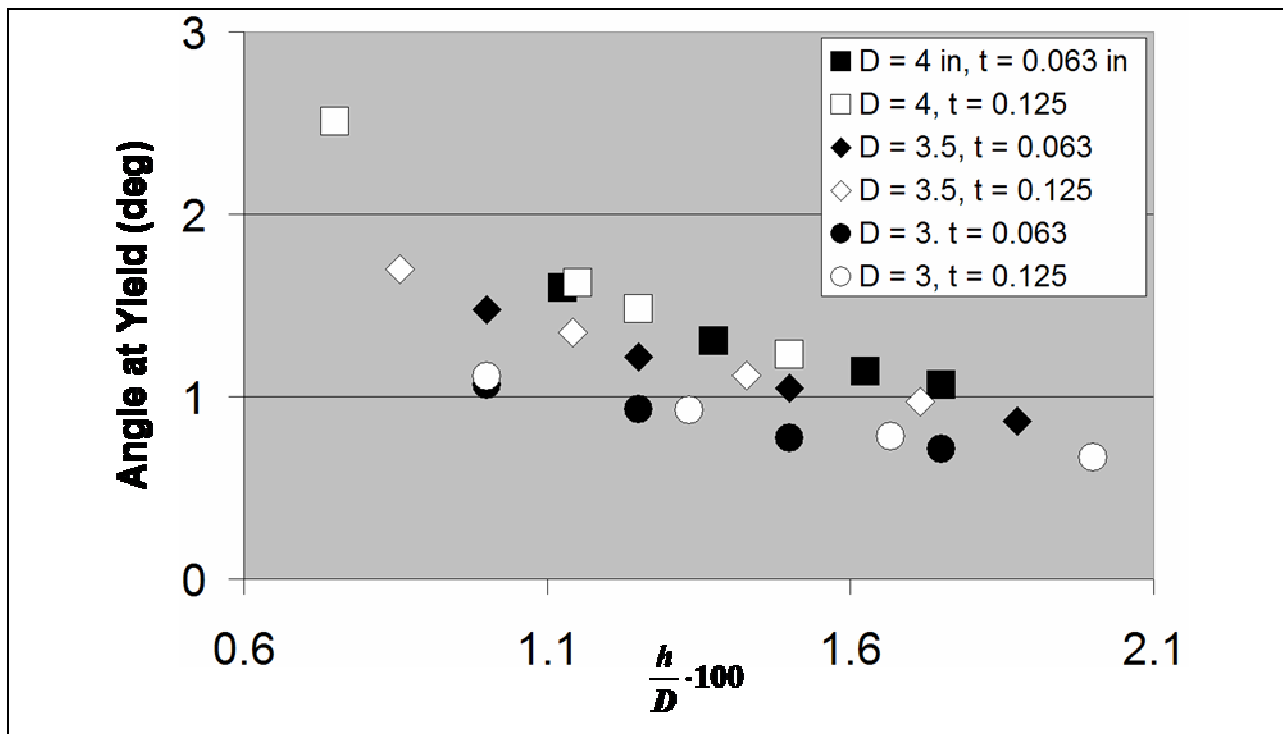


Figure 3.5 Plot of Yield Angle vs Ratio for both Part Thicknesses

In Figure 3.3 we see that the torsional stiffness of the planar spring does indeed follow a cubic trend with respect to the normalized beam with $\frac{h}{D}$. Furthermore, the part thickness changes the slope of this trend, as expected in Eq. 3.3. Interestingly, the stiffness curves for the different SAVI diameters do not line up, as they should if the torsional stiffness was simply proportional to $\frac{h}{D}$. Instead, as the diameter increases, the torsional stiffness tends to decrease, and this decrease is more pronounced for smaller part thicknesses. During the simulation, the value for C was calculated at each tested diameter. Table 3.2 lists the results.

Table 3.2 Calculated Values for C from Simulation

Diameter, D (mm, in)	Length of Radial Beams, L (mm, in)	Calculated Value for C
76 (3.0)	8.89 (0.350)	0.12
89 (3.5)	12.1 (0.475)	0.14
100 (4.0)	15.2 (0.600)	0.15

Clearly, C is a function the diameter of the SAVI, and monotonically increases as the diameter increases. According to Eq. 3.3, this means that the torsional stiffness should decrease for the same value of $\frac{h}{D}$ as the diameter increases, which is demonstrated in the simulation results.

Also, it is expected that as the thickness of the part increases, the effect of the variation of C on the torsional stiffness would decrease, which is also supported in Figure 3.3.

In Figure 3.4 we see that the angular displacement at which yielding first occurs varies linearly with respect to $\frac{D^2}{h}$ as expected. Again, there is some variation at different diameters, which is due to the changing value of C. Looking at Eq. 3.5, because of the variation of C, as the diameter increases the yield angle should increase as well. This trend is also seen in the FEA results.

Finally, Figure 3.5 depicts a plot of the yield angle with respect to $\frac{h}{D}$ for both values of the thickness, t , in order to demonstrate that this design parameter is independent of the part thickness. In the figure, however, the yield angle does seem to be slightly lower for smaller part thicknesses. This characteristic is due to the taper of the part caused by the abrasive waterjet. Due to the taper, as the part thickness increases, the variation between the beam widths on either face of the planar spring becomes greater. Since the beam width on one side is always equal to the nominal value, this means that the average beam thickness decreases as a function of the part thickness. Therefore, according to Eq. 3.5, the yield angle should decrease for increasing part thickness. Note that this effect of the taper will also cause the torsional stiffness of the planar spring to be slightly smaller than what may be expected from Eq. 3.3. In fact, if the taper was not included in the simulation, the resulting torsional stiffness values would be overestimated by more than 32 %.

Another effect of the taper caused by the waterjet that was alluded to earlier is a restriction on the part thickness of the torsional spring. For a large part thickness the taper in the part causes the beam width variation on either side of the spring to be large, the nominal value for this dimension may need to be increased to ensure that the radial beams do not have too narrow a cross-section. Although the average beam width can still be used to approximate the resulting stiffness, this causes a problem for the yield angle of the part. Now that the radial beams have a larger width on one face of the planar spring, for a given angular displacement the local stress at that face is very high, much higher than a thinner spring with the same taper and average beam thickness. Therefore, the yield angle will be significantly smaller, limiting the effectiveness of the SAVI. For this reason to increase the stiffness of the SAVI by using a larger part thickness, it is more appropriate to stack a few thin torsional springs than use one large one.

Using this information, the dimensions of the torsional spring may be chosen to provide the proper low-amplitude stiffness and angular deflection at yield to isolate a rotational system from a small amplitude upstream vibration.

The other design parameter, namely the angular position of the stop engagement, may be calculated directly from the geometry of the engagement assembly, seen in Figure 3.6.

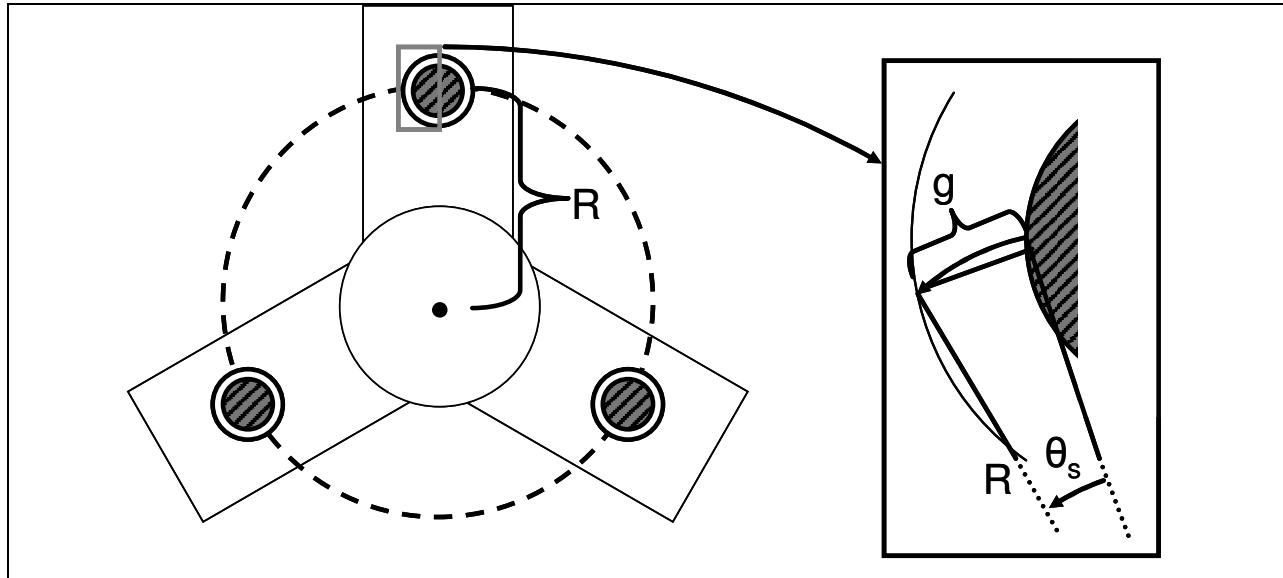


Figure 3.6 Geometry of Gap Spacing for Stop Assembly

For small stop engagement angles and large values of R compared to the radius of the pins, the gap spacing of the engagement assembly may be calculated as:

$$g = R \cdot \sin(\theta_s) \quad (3.6)$$

From this equation, we can see that manufacturing tolerances will become a limiting factor for small stop engagement angles. For example, the gap spacing required for a 2 degree stop angle given the other chosen dimensions for the fabricated prototype was on the order of 1.14 mm (0.045”), which is reasonably the tightest tolerance that a person may be expected to assemble the stop engagement system by hand. Future manufacturing processes may be able to achieve tighter tolerances, however, this is balanced by an increase in costs. Therefore, it is important to consider the design of the stop engagement system with a particular manufacturing process in mind.

3.3 Rotational Systems

In order to effectively predict the performance of either design in a given rotational system, it is first necessary to accurately model and understand the dynamics of the rotational system itself. This is required not only to choose the best concept early on in the design process but also is necessary for determining the performance of the total system once the device has been implemented. In this section, a simple and flexible lumped parameter model will be introduced that enables designers to rapidly determine the dynamic characteristics of a rotational system. Then methods will be presented for predicting the performance of both the DVL and SAVI.

3.3.1 Analysis of Rotational System Dynamics

As a design engineer interested in solving a vibration problem, the first important information one needs is the vibration regime of the system. This requires knowledge of the boundary conditions, the force inputs, the natural frequencies, the normal modes and the damping within the system. For many physical systems of moderate complexity, the simplest and fastest way to obtain an accurate estimate of these characteristics is through a lumped parameter model, like the one in Figure 3.7.

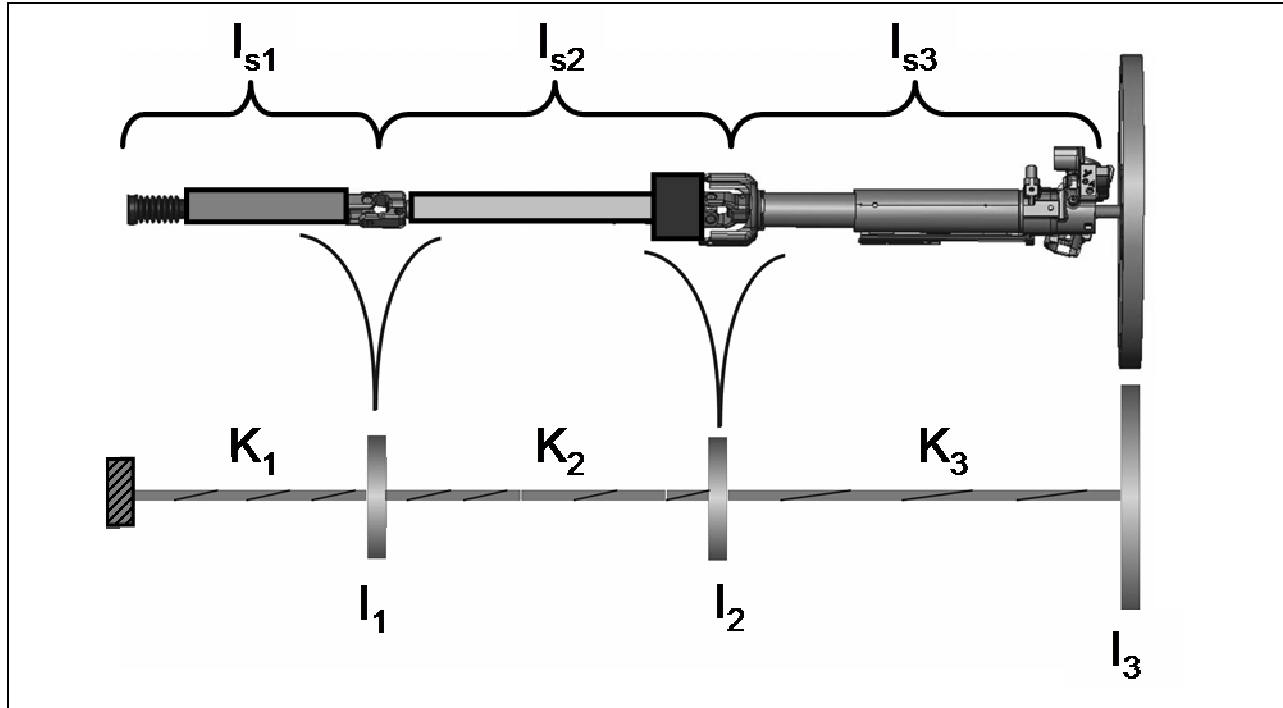


Figure 3.7 Lumped Parameter Model of Steering Column

The idea behind this form of modeling is to discretize a continuous system, in this case a steering column, into a series of springs and inertias. The level of accuracy of the results is dependent on the number of discrete inertias modeled, the appropriateness of the groupings of these inertias and the order of the frequency of the vibration under study. For example, the steering system shown in Figure 3.7 consists of three shafts and a steering wheel. This can be modeled as three inertias and three torsional springs. It was decided that it would be most appropriate to place the position of each discrete inertia at the connection between each element of the system. The magnitude of each discrete inertia component is the sum of half of the moment of inertia of each shaft at that connection, or:

$$I_i = \frac{1}{2}I_{s_i} + \frac{1}{2}I_{s_{(i+1)}} \quad \text{for } i < 3 \quad (3.7)$$

$$I_3 = \frac{1}{2}I_{s_3} + I_{sw} \quad (3.8)$$

The magnitude of each spring is the torsional stiffness of each shaft, which may be calculated directly or obtained from experimentation. This modeling method may be used for various rotational systems and extended to include any number of components.

However, this modeling approach is not appropriate for complicated systems. A main assumption of the model is that there is at most moderate damping in the existing system ($\zeta < 0.2$), so the natural frequencies and mode shapes may be calculated from an undamped model. In general, if this is not true of the physical system, then an exact analytical model of the rotational system is not possible, and numerical methods are required. Furthermore, if the groupings of the discrete inertias at the connection points of each element is inappropriate for the rotational system, or if one were interested in higher order frequencies, then the model would need to be discretized further. This means adding more inertia elements and torsional springs, whose magnitudes would be determined by some other method appropriate for that system.

Armed with a general model for an arbitrary rotational system, one may then calculate the natural frequencies and corresponding normal modes using classical multi-DOF analysis [20]. A Matlab® script was written which would read in experimentally determined inertia and stiffness values, calculate those that could not be found experimentally, and output the undamped natural frequencies and corresponding normal modes of the system. Additionally, if necessary, the script was capable of discretizing each component further using the same rules given above for the inertia elements, and approximating the added spring magnitudes from the rules governing springs in series.

For a specific desired level of accuracy, if the system could be simplified to a one-DOF model, then a useful estimate of the total effective damping in the system may be made as well. By using the mode shapes calculated from the multi-DOF model and applying a unit displacement at one discrete inertial element, the strain energy stored within each torsional spring may be calculated. If the damping ratio of each component can also be calculated from a hysteresis curve, like the one shown in Chapter 1, then the total effective damping in the system for each mode may be estimated using Eq. 2.5. This is useful if the rotational system may be represented by a one-DOF model and the proposed solution for reducing the upstream vibration is to add

damping in the system. With this information, a frequency response, similar to the one shown in Figure 3.8, of the original and modified system may be determined analytically.

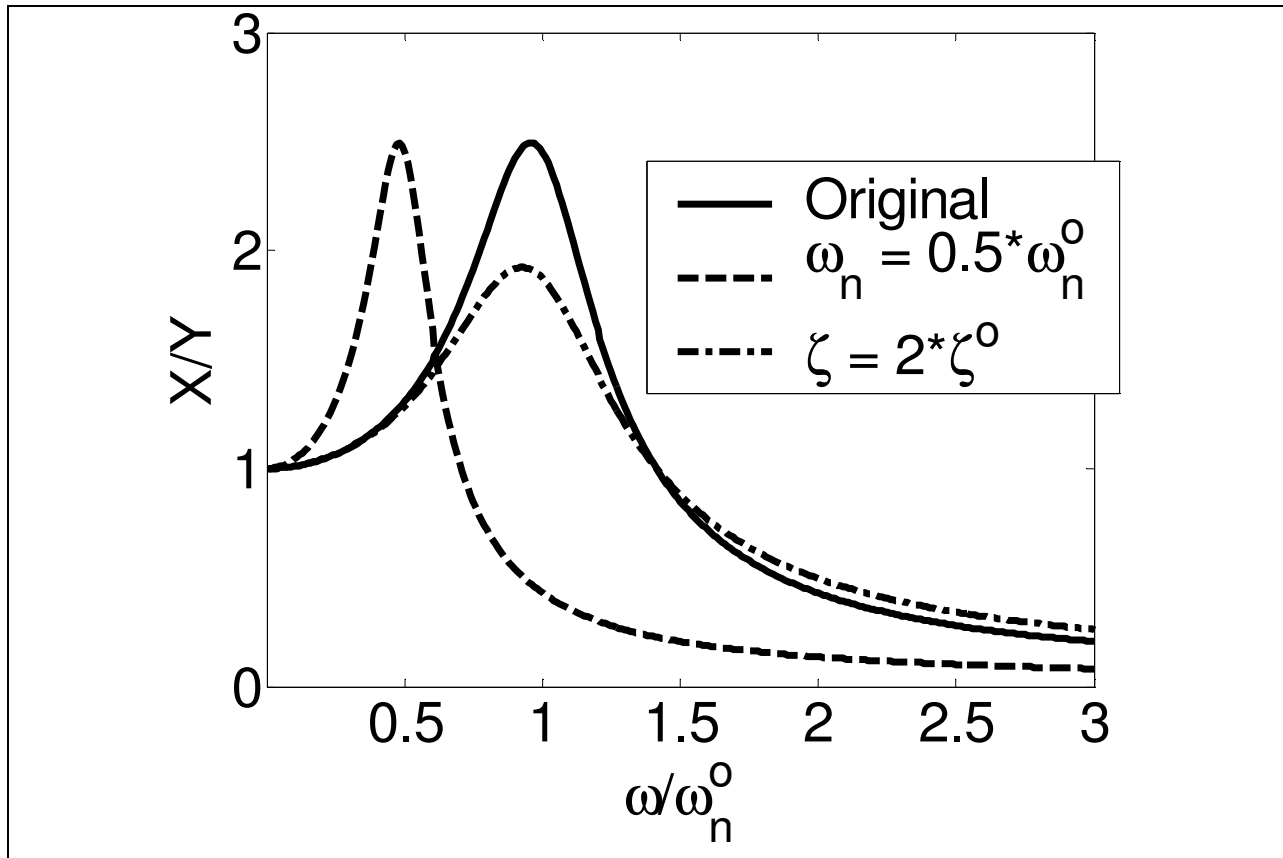


Figure 3.8 Frequency Response of Original System and Potential Responses of Modified Systems

From this figure, a designer can form a sense of the performance of the original system and what improvements are possible by adding more damping or changing the natural frequency of the system. Of course, this technique is not possible for more complicated systems or systems with large damping ($\zeta > 0.2$), in which case numerical methods are necessary.

Assuming that analytical methods are possible, once the natural frequencies, mode shapes and corresponding damping ratios of the system are calculated, the system response may be predicted for any combination of boundary conditions and force inputs. Therefore, preliminary design decisions may be made rapidly and more advanced analyses of the performance of a design may be predicted. The following sections outline how to decide which design is the most appropriate

solution for the vibration problem and how the performance predictions for both the DVL and the SAVI are made.

3.4.2 Determination of Effects of SAVI

The benefits to using the SAVI are: (1) performance improvements are possible for both resonating and non-resonating systems, and (2) the potential improvement provided by changing the natural frequency of the system, seen in Figure 3.8, is far greater than that from added damping. Of course, the SAVI modifies the low-amplitude stiffness of the system, so it is not the appropriate solution for a system whose stiffness properties must not change or where the amplitude of the upstream vibration is on the same order as that of the feedforward input.

To determine the performance of the SAVI, the lumped parameter model cannot be used alone because of the limitation to linear stiffness elements. The lumped parameter model can still be used to rapidly characterize the original rotational system, but a more advanced dynamic analysis CAE tool, like ADAMS®, will need to be used to evaluate the performance of the modified system. The procedure for this evaluation is as follows:

1. Model the system described by the lumped parameter model in a non-linear dynamic analysis CAE tool.
2. Input the SAVI as a non-linear spring element into the CAE model.
3. Determine the relationship between the performance metrics, i.e. percent reduction and delay, and the SAVI parameters, which are the low-amplitude stiffness and the stiffness transition point.
4. Select parameters that provide the best performance for the modified system.

An example of this procedure will be shown in the case study of automotive nibble described in Chapter 5.

3.3.3 Determination of Effects of DVL

As stated earlier, the DVL is useful when the vibration problem is due to a resonance in the system and the stiffness or inertial characteristics of the system cannot be altered. As seen in Figure 3.8, the upstream vibration may be successfully reduced without changing the natural frequency of the system, meaning that the performance of the system in other areas is unaffected.

The following procedure may be used to determine the effectiveness of the DVL and for what stiffness characteristics should the DVL be designed:

1. Insert the DVL as a stiffness element into the lumped parameter model described above.
2. Recalculate the undamped natural frequencies and mode shapes.
3. Determine the total effective damping for the mode shape of interest.
4. If the total damping is moderate and the system can still be reduced to one-DOF, then generate the frequency response of the modified system.
5. Calculate the percent reduction of the vibration at the excitation frequency, and any change in the natural frequency of the system.
6. Evaluate the performance benefits and trade-offs to using the DVL to select appropriate design parameters.

Through this procedure, the effectiveness of the DVL may be determined for many applications.

3.4 Summary of Modeling

In this chapter:

1. FEA simulations were performed to predict the performance characteristics for the SAVI based on its dimensions.
2. An understanding was gained from these simulations for what parameters are most critical to the performance of the device.
3. An analytical model was produced that can:
 - a. Rapidly and simply evaluate the vibration characteristics of a rotational system and predict the performance of the system modified by either device.

- b. Aid in selecting which device to use for a given vibration problem.
4. Design guidelines were laid out that:
- a. Describe under what conditions either the DVL or SAVI should be chosen as the design solution.
 - b. Determine an accurate prediction of the performance and trade-offs for either device in any application.
 - c. Allow for the selection of the performance characteristics of either device that result in the optimized performance of the modified system.

Important things learned from the model for the SAVI is that the taper caused by the abrasive waterjet can significantly affect the performance of the SAVI in almost every area. Also, the critical dimensions were determined to be the width of the radial beams, the overall diameter of the device, and the part thickness of the torsional spring. The major performance parameters of the SAVI listed in Chapter 2 were related to ratios of these dimensions to verify general performance trends and aid in dimension selection. Finally, the engagement stop angle is limited by the tolerances associated with the chosen manufacturing process. This is important not only for the placement of the stiffness transition point for the SAVI but also for the yield angle of the torsion spring, since the engagement stops must protect it from yielding. In the next chapter, the process of fabricating each device will be discussed.

CHAPTER

4 FABRICATION

4.1 Goals

The purpose of this chapter is to illustrate the many issues dealing with the fabrication of the devices that were directly considered in their design, and to explain the major challenges and goals for building the initial prototypes. Recall in Chapter 1, two metrics used to assess the designs were (1) simplicity and (2) robustness. Here, simplicity referred to the manufacturability, implementation, maintenance and cost of the devices, and robustness referred to the performance sensitivity in part due to manufacturing variations. The term manufacturability is intended to cover all of the vagaries involved in large and small-scale production of the devices, including geometry feasibility and process capabilities, like tolerances, cutting forces, etc. Nevertheless, at this point only a handful of prototypes were actually produced, and large-scale manufacturing techniques are left for future work. The main goals of these initial prototypes are to prove that each of the concepts is physically realizable and works as intended. In Chapter 5, a discussion will be given of how the prototypes of both the SAVI and DVL were tested, and the results will be compared with those predicted by the analytical models described earlier.

4.2 Small Amplitude Vibration Isolator (SAVI)

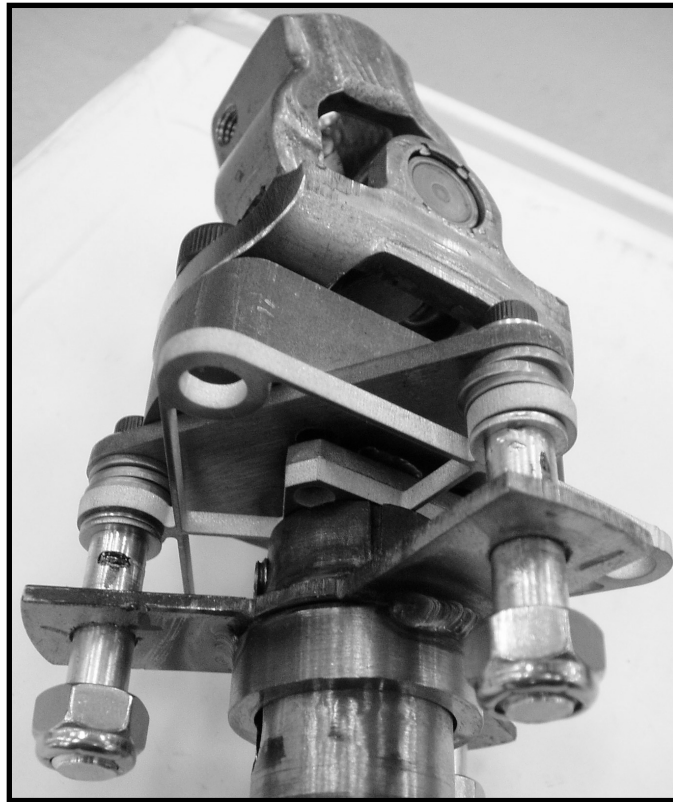


Figure 4.1 SAVI Final Prototype

When the SAVI was originally designed, it was intended to be directly installed into a component of the steering column of a light-duty pickup truck, shown in Figure 4.2. Therefore, the fabrication process is composed of several operations specifically designed to aid in retrofitting the device to the existing system. Although this greatly simplified the installation of the SAVI into the vehicle steering system, the fabrication process described herein is not generally applicable to rotational systems. Consequently, future designs and manufacturing procedures may benefit from redesign. Nevertheless, the procedure described here lays out the fundamental steps required to build a SAVI prototype and presents some of the main concerns involved.

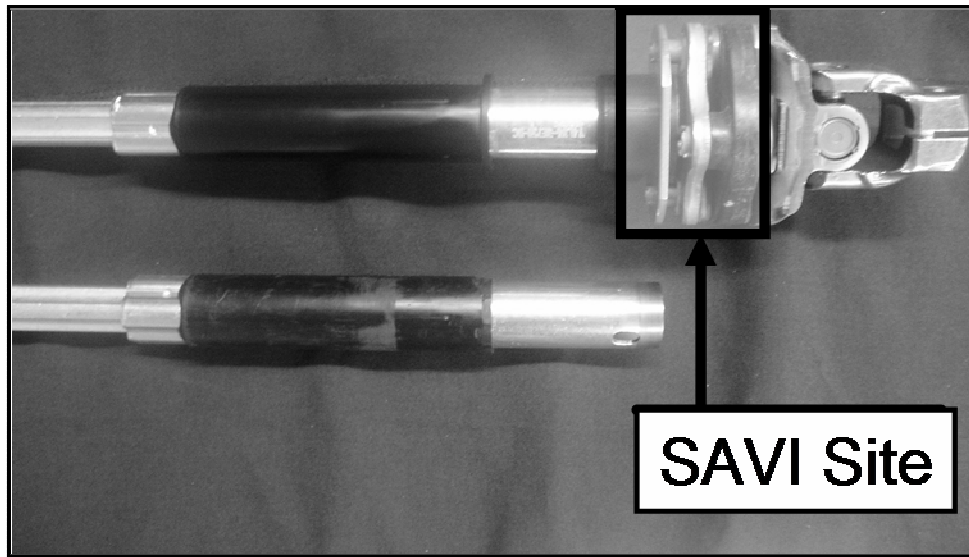


Figure 4.2 Steering Component to be Retrofitted with SAVI

A major advantage to the SAVI is that most of its parts may be built separately and in parallel to each other. Once all the components have been made, they can then be rapidly assembled or unassembled if necessary. As will be shown, this is not true for the DVL, which is fabricated through a serial process and has long cycle times. On the other hand, because most of the components of the SAVI were made separately, there were some issues aligning them during assembly. This was particularly true in the assembly of the stop engagement system, which required very tight tolerances.

The major components required in the fabrication and assembly of the SAVI are:

1. The planar torsional spring
2. The stop engagement system, which consisted of:
 - a. Engagement pins
 - b. Flange
3. Adapters used to connect to the upstream and downstream portion of the system to the SAVI

Due to the concurrent nature of the fabrication process, the production of each component will be described first. The procedure for assembling all of the components together will then follow. In cases when the fabrication and assembly are interrelated, the best attempt will be made to explain both and the reasons behind any design decisions.

4.2.1 Fabrication of Individual Components

The planar torsional spring was cut from a sheet of 7075-T651 aluminum by an abrasive waterjet machine, as stated earlier. This material was chosen for the device because of its high yield strength to elastic modulus ratio and low cost compared to titanium. Since the prototype was intended to be a proof-of-concept only and not an actual production version, fatigue issues associated with aluminum were not considered as the final usable prototypes would be made from spring steel or perhaps a polymer. Fatigue calculations would be carried out during the engineering analysis for the final prototype.

The engagement pins, shown in Figure 4.3, were cut from round aluminum bar stock. They were internally and externally threaded to connect with the bolts used to secure the torsional spring to the upstream adapter, and to have a lock nut threaded on each of their ends. The lock nut was used to prevent the entire assembly from sliding apart axially in case the torsional spring failed. As may be seen in Figure 4.1, the nuts would interfere with the holes drilled into the flange if this were to happen. Although the handling performance would become very poor, the driver could safely stop the vehicle with losing directional control.

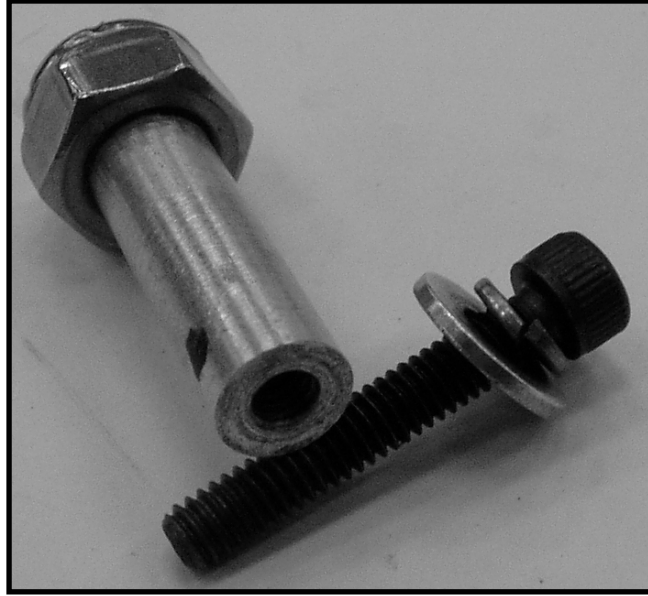


Figure 4.3 Engagement Pin with Connection Bolt and Lock Nut

The flange used to engage with the pins, shown in Figure 4.4, was cut from two pieces of steel and welded together. In order to properly position the hole locations, the flange was placed over the modified component of the steering column shown in Figure 4.2. Once all the other components had been fabricated and assembled on the same shaft, the positions of the engagement pins were marked on the flange. These points were subsequently drilled out to the appropriate size and the flange was replaced onto the shaft and permanently welded to it. This procedure will be explained further during the description of the assembly process.

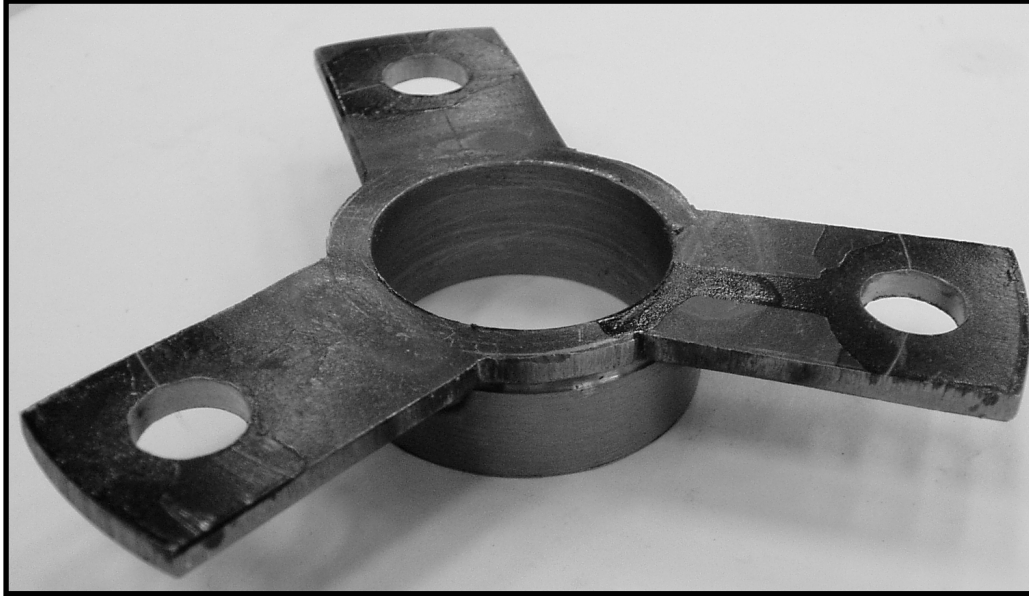


Figure 4.4 Flange Sub-Assembly

An exploded view and the fully assembled prototype are shown in Figure 4.5 and Figure 4.6 to demonstrate how both the upstream and downstream adapters were designed and assembled with the rest of the device. The upstream adapter consists of a triangular plate, hexagonal bar and a mounting block, which is attached to the yoke from the existing steering column component. The hexagonal bar was pressed into the mounting block and into the central hole of the triangular plate. Each component was then welded together to form a permanent sub-assembly, which collectively is called the upstream adapter. This adapter was then raised off the torsional spring by a set of washers and secured through three of the spring's holes with bolts. These same bolts are threaded into the engagement pins, as shown in Figure 4.6.

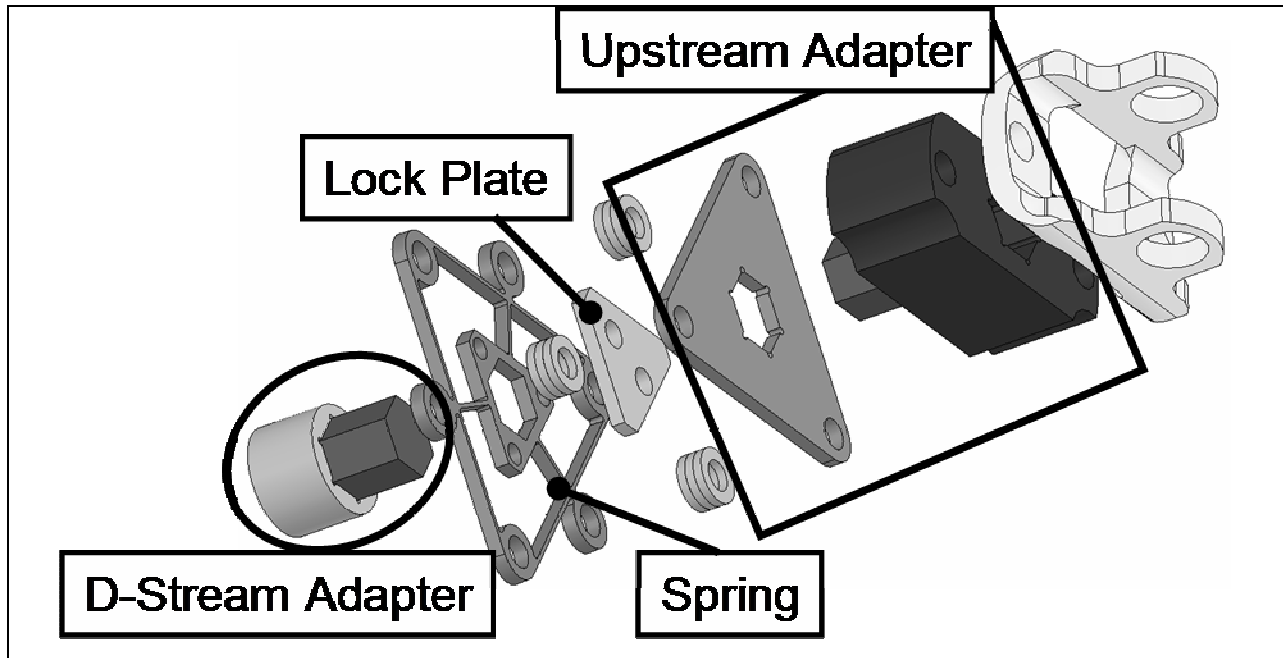


Figure 4.5 Exploded View of SAVI Assembly

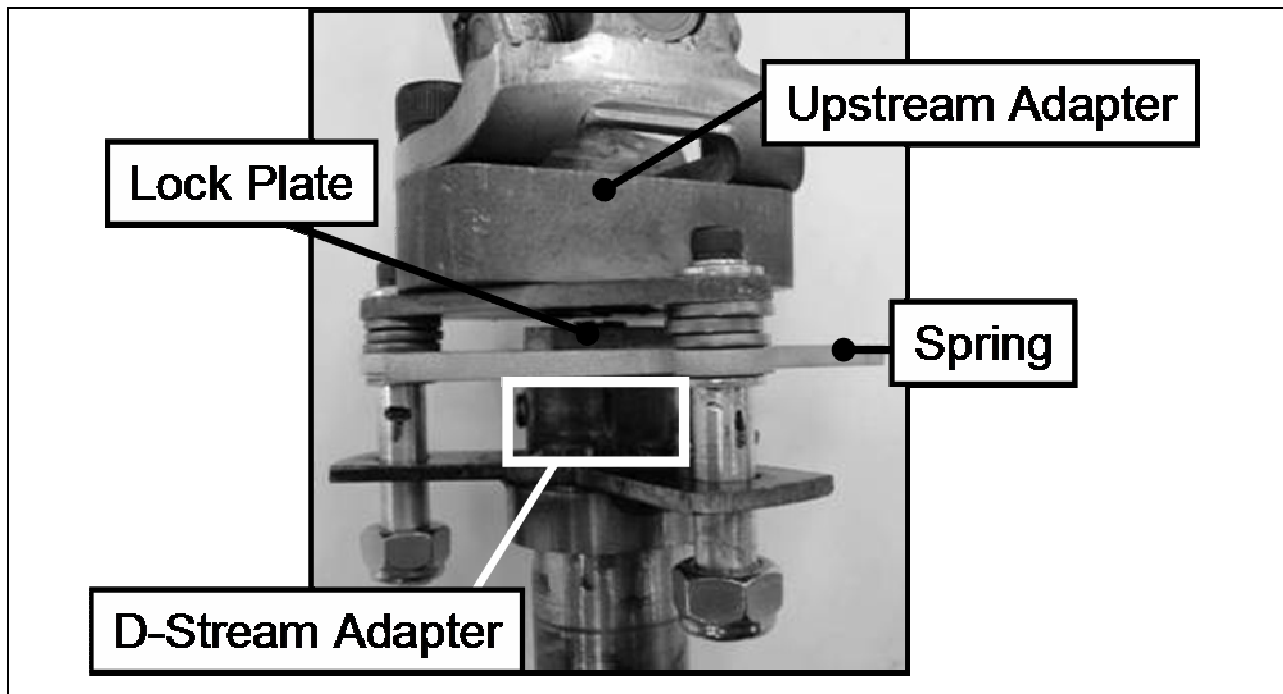


Figure 4.6 Side-View of Fully Assembled SAVI Prototype

The downstream adapter is composed of a round shaft with a hexagonal hole cut in it and an accompanying hexagonal bar. The two were initially press fit together and then the round shaft

was welded to the end of the steering column component. However, the residual stresses created during the welding process loosened the press fit between the round shaft and the hexagonal bar. Therefore, a set screw was used to secure the hexagonal bar in the rounded shaft, as seen in Figure 4.6. This adjustment was beneficial because now the amount of the hexagonal bar that was exposed could be varied, which meant that a variably thick torsional spring could be pressed onto the exposed hexagonal bar. However, this also prevented the torsional spring from lying flush with the round shaft when the SAVI was fully assembled. Nevertheless, the amount of angular misalignment was slight and not an important issue.

The last component in the assembly was the lock plate, shown in Figure 4.5. This part was used simply to prevent the torsional spring from detaching from the hexagonal bar in the downstream adapter, during either installation of the device into the steering column or operation of the vehicle. It was secured to the hexagonal bar in the downstream adapter by two countersunk screws.

A major design goal in fabricating the SAVI was to keep the device as simple as possible, which allowed for rapid turnarounds on future generation prototypes and convenient experimentation. Every single component of the SAVI assembly shown in Figure 4.5, with the exception of the two hexagonal bars, the washers and the torsional spring, were cut from steel using the abrasive waterjet. This was because of the machine's ability to cut complicated shapes, like the hexagonal cut-outs, simply and relatively rapidly. Hexagonal bars were used to connect several different components because the shape could transmit a torque more effectively than a rectangle. Press fits were used in all possible situations to reduce the part count and allow for rapid and easy assembly. Finally, any component that would not need to be disassembled was welded to again reduce the total number of individual parts and simplify assembly.

4.2.2 Assembly Procedure

With each of the components comprising the SAVI device built, the final device, shown in Figure 4.1, could be assembled. In order to fully convey the major assembly steps and challenges, we shall start from the determination of the hole positions in the flange.

The full assembly process required to mate all the components of the SAVI and form a final device are:

1. Slide flange onto steering shaft
2. Assemble SAVI mechanism
 - a. Expose proper amount of hexagonal bar in downstream adapter and lock bar into place with set screw
 - b. Press fit planar torsional spring on downstream adapter
 - c. Attach lock plate to top surface of torsional spring
 - d. Affix upstream adapter to torsional spring using bolts and engagement pins
3. Mark hole locations on flange
4. Disassemble SAVI mechanism
5. Remove flange from steering shaft and drill out hole locations
6. Place flange back on steering shaft
7. Reassemble SAVI mechanism
8. Slide flange into proper position so engagement pins fit in holes
9. Attach lock nuts to engagement pins to hold flange in place
10. Weld flange to steering shaft
11. Disassemble SAVI mechanism
12. File holes to greater diameter if necessary to account for any misalignment
 - a. Ensure clearance for upstream vibration
 - b. Ensure stops engage before torsional spring yields
13. Reassemble SAVI mechanism for last time

Clearly there are many steps involved in taking the individual components and assembling them into the final device. Since many of these steps are self-explanatory, we will focus only on those that are important to the assembly process and present certain problems.

The press fit of the torsional spring, shown in Figure 4.7, was an example of an advantageous use of a normally negative side-effect to a fabrication process. As stated in Chapter 3, the taper

caused by the abrasive waterjet creates certain performance problems and dimension limitations for the torsional spring. However, by choosing the proper dimension for the central hexagonal hole in the spring, the taper may be used to form a very secure yet removable interference fit on the hexagonal bar. This makes disassembly, which is required more than once in the above procedure, and changing the torsional springs for different testing, very convenient.

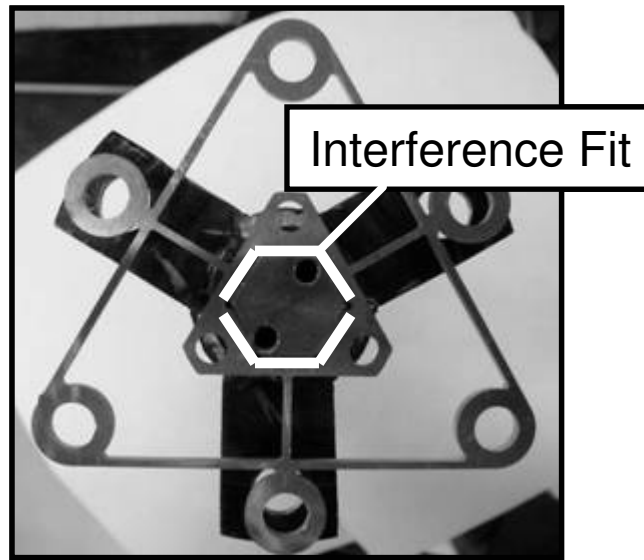


Figure 4.7 Interference Fit of Torsional Spring onto Downstream Adapter

An enlargement of the SAVI assembly is shown in Figure 4.8 to demonstrate the full functionality of the stop engagement system. Of course the primary functions of this assembly are to (1) create the non-linear stiffness profile for the SAVI to work properly, (2) prevent the torsional spring from yielding, and (3) provide both an angular and axial connection between the upstream and downstream portions of the steering column in case the torsional spring fails. However, the engagement system also provides three other important side functions:

1. Absorb any moments applied to the mechanism and prevent them from damaging the torsional spring.
2. Protect the bolts connecting the entire assembly to the upstream adapter from experiencing any bending moment or shear loads created by the stop engagement.
3. Allow for rapid assembly and disassembly.

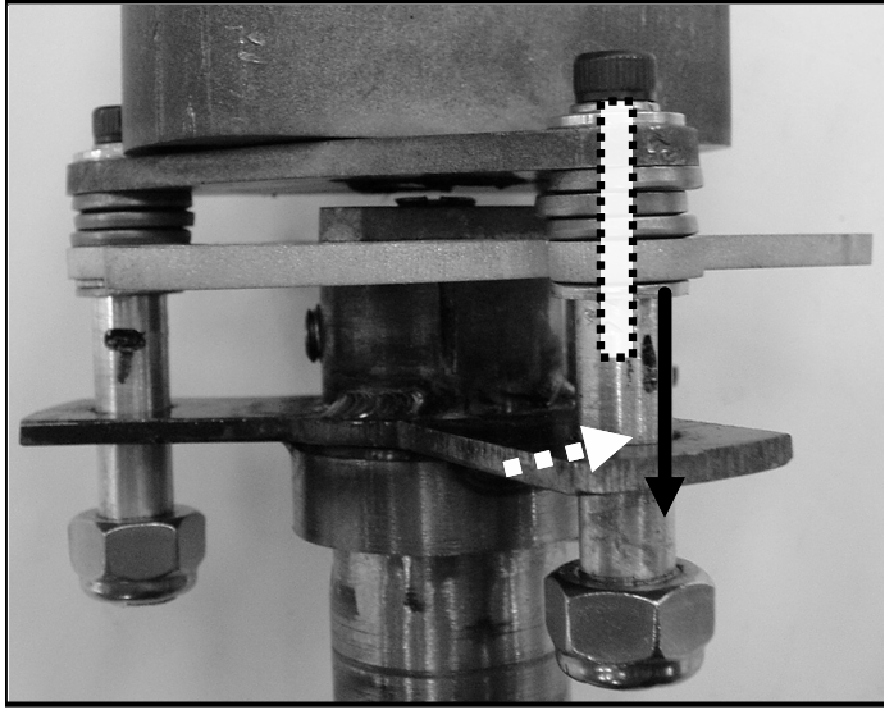


Figure 4.8 Enlargement of Stop Engagement Sub-Assembly

Because the gap between the pins and the flange is very small, any moment applied to the shaft as the part is installed into a vehicle is resisted by the engagement system. This prevents the weak torsional spring from yielding during installation. This was found to be a necessary function of the device, since many torsional springs were broken during testing as a result of torquing the steering column bolts to their intended values. Furthermore, bolts are weak in shear because of the sharp cuts needed to form their threads. By tightening the ends of the engagement pins against washers positioned beneath the triangular adapter plate, the friction in this interface took up the shear load, shown by a dashed arrow, applied to the solid portion of the pins. Additionally, the width of the pins provided a lever arm for a resistance force, shown in solid black, to counterbalance the bending moment created by the shear force on the pin. Finally, because the bolts threaded directly into the pins, they also provided the clamping force necessary to hold the entire assembly together. This eliminated the need for extra parts, further simplifying the assembly process. There is no doubt that the engagement assembly was the most versatile component of the SAVI.

The most problematic part of the assembly process was properly aligning and sizing the holes in the flange. First, it was difficult to properly mark the center of the hole locations by judging off the position of the engagement pins once the SAVI mechanism had been assembled. However, since each of the components had been fabricated separately, without common referencing, this seemed like the most accurate and expedient method. Once the holes were drilled and the device reassembled, none of the pins had clearance in the holes. This was a problem because without any gap between the pins and the flange, the upstream vibration would be transmitted through the steering column. Therefore, the holes had to be filed on their appropriate sides to allow for this gap. Still, this was not an easy process because one had to be careful not to oversize the holes or the torsional spring would not be protected from yielding. Iteratively, the pins were inserted, the holes checked for clearance, the pins were removed, the holes filed, and the pins reinserted, until there was the appropriate amount of clearance.

In general, the fabrication of the SAVI was straight-forward with the exception of the sizing of the flange holes. However, once the SAVI sub-assemblies were welded together and appropriately placed, the SAVI mechanism could be assembled and reassembled in a few minutes. This was crucial for rapid testing of prototypes and generation of redesigns. In contrast, the DVL took hours to assemble to a rotational system and, once in place, it could not be easily removed. Note the other differences between it and the SAVI, as the fabrication of the DVL is discussed in the following section.

4.3 Damping Vibration Link (DVL)

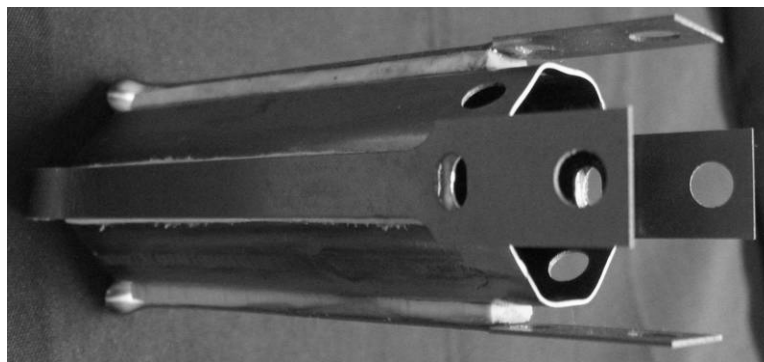


Figure 4.9 DVL Final Prototype

4.3.1 Summary of Failed Attempts

There had been a few earlier incarnations of the DVL before the one shown in Figure 4.9 was finally made. Although these previous attempts were discarded, it is again noted that they were discarded only for reasons of inefficiency in building an early prototype. In fact, the following “failed” attempts at fabricating a prototype may very well be more efficient and cost-effective methods for large-scale production manufacturing.

The initial idea for producing the inner shaft and outer tabs was to start with a pre-cut sheet and performing a deep drawing process, shown schematically in Figure 4.10.

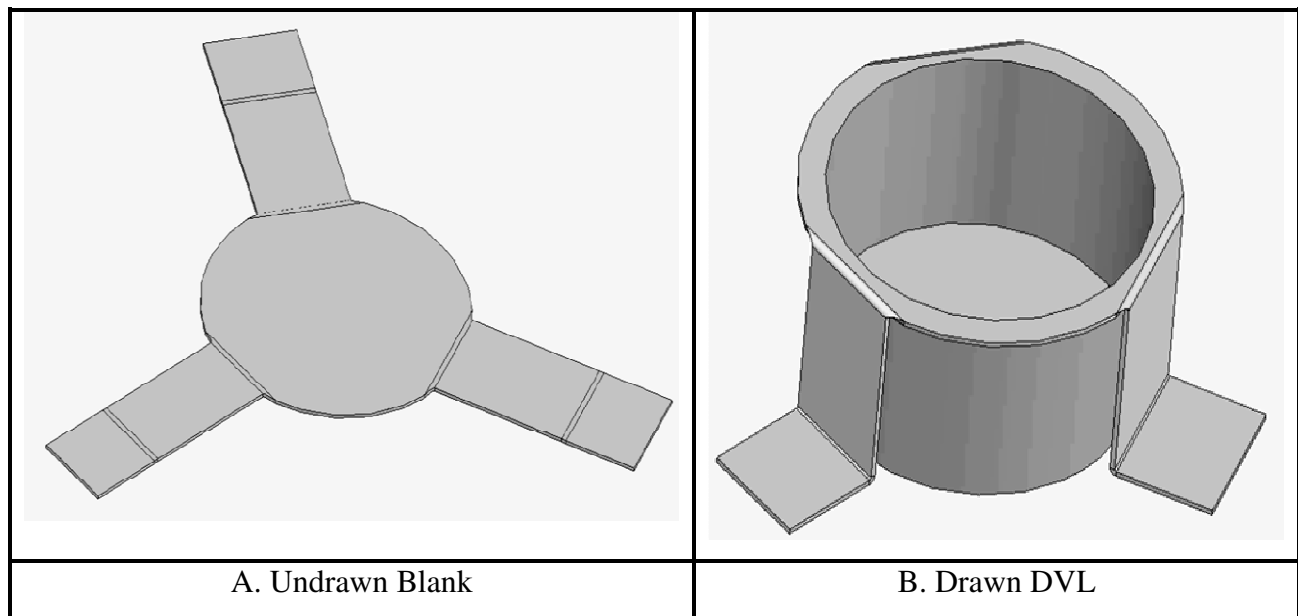


Figure 4.10 Deep Draw of DVL

There were several problems encountered with this process. First, the drawing itself imposed certain geometric constraints on the size and depth of the device, and was also difficult to perform properly. Since drawing in many ways is as much of an art as a science, die sets needed to be iteratively fabricated through trial and error until the final drawn shape was made properly without failure. Second, it was difficult to apply the proper amount of force on the blankholder to keep the undrawn material from wrinkling under the compressive hoop stress created by

forcing larger diameter material into a smaller diameter hole. Third, given the desired dimensions of the device and its overall geometry, it would have been impossible to bend the tabs over after drawing the inner shaft using a press brake. Fourth, the tabs, which were to form the other constraining layer for the VEM, needed to be bent to form concentric arches about the inner shaft. While not impossible, looking at Figure 4.10, this would have been a difficult task given that there was not any available equipment for this step.

Another idea, shown in Figure 4.11, was to start with a round tube, laser-cut the tabs and then bend them back over the tube. This process has a problem similar to the latter one mentioned for the deep draw.

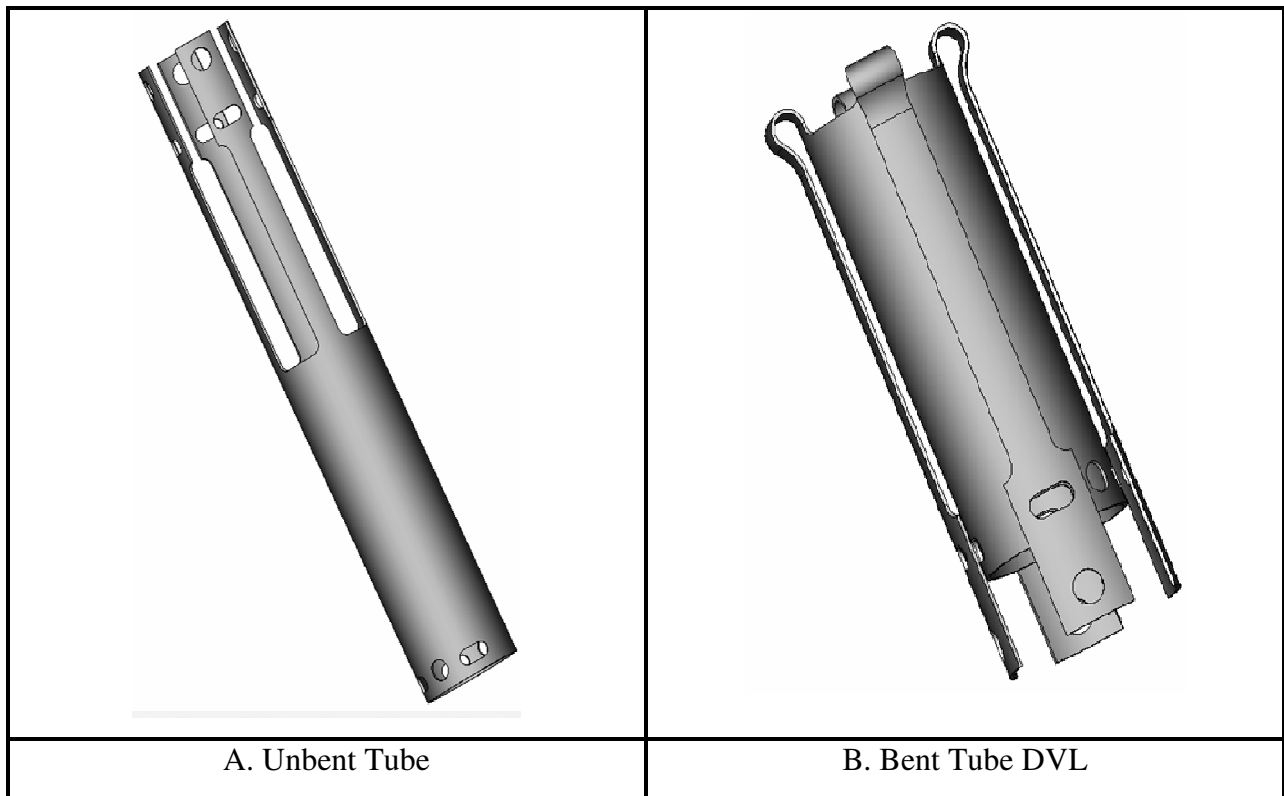


Figure 4.11 Bending of Round, Pre-Cut Tube

Clearly, in Figure 4.11A, the curvature of the tabs is the same as that of the inner shaft. However, after bending the tabs down over the shaft, the curvature of the two constraining layers of the VEM would be in opposite directions. For the curvature of the tabs to be concentric with the inner shaft, they would have to be bent along their length. Besides being difficult, this step

would create a large amount of residual stress in the arched connections between the shaft and the tabs, which could shorten the fatigue life of the device.

To avoid this last bending operation, an octagonal shaft was chosen over a round one. This way, once the tabs had been bent down, they would already be parallel to the inner shaft and the formation of the metal portion of the DVL would be complete. Of course the shaft did not need to be octagonal for this to work, but eight sides was the best choice for performance, strength and installation. The only remaining problem with this process was acquiring the octagonal shaft itself. Since manufacturers would not produce a shaft to our desired specifications for a small volume order, we had to create one ourselves.

4.3.2 Fabrication Procedure

The overall procedure for creating the DVL prototype shown in Figure 4.9 is broken into three general steps: (1) forming the pre-cut octagonal inner shaft, (2) bending the outer tabs into the proper position, and (3) bonding the VEM to the metal constraining layers. As previously mentioned, it was not possible to purchase an octagonal shaft with the correct dimensions. It was also troublesome to machine a stock shaft to the proper size and to cut in the features of the device. The cutting forces produced by conventional milling machines damaged the thin part and residual stresses present in the original shaft warped the part after material was removed. Consequently, the features were first cut into a flat sheet of low-carbon 1006 steel using an abrasive waterjet. Low-carbon steel was chosen for its good formability, which will be important in creating the inner shaft and bending the tabs. Each resulting part, shown in Figure 4.12, was then folded four times using a finger brake at 45° bends to form one half of the octagonal shaft, as seen in Figure 4.13. Two halves were then butt-welded together, finishing the shaft.

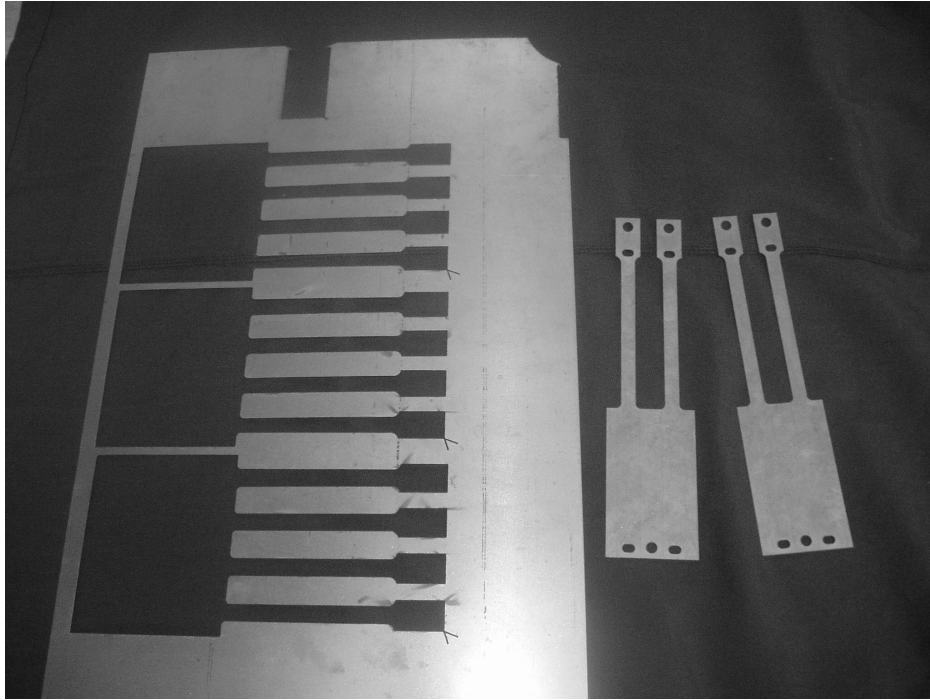


Figure 4.12 Feature Cutout from Flat Sheet

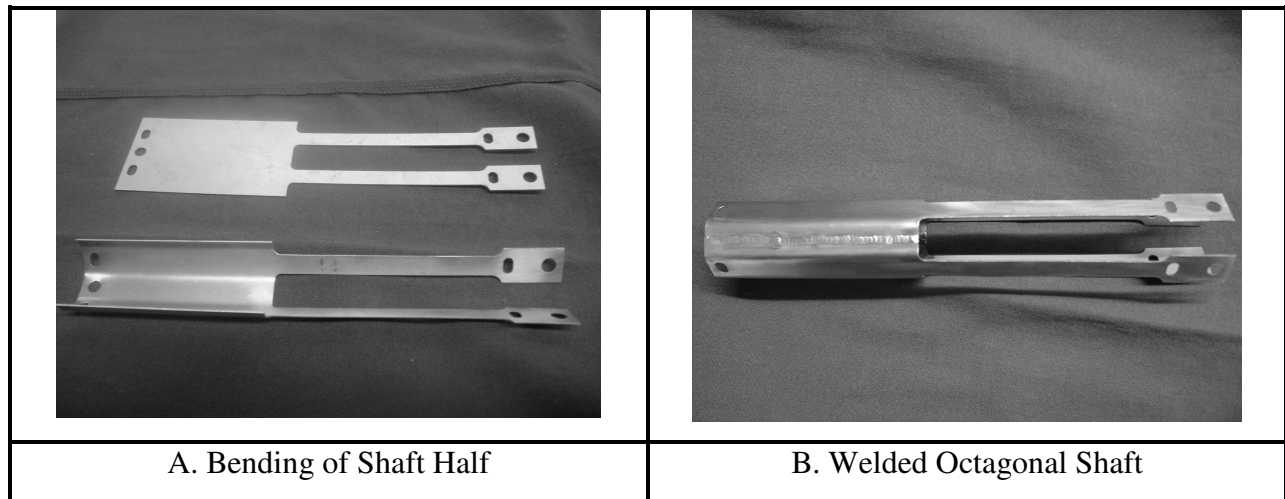


Figure 4.13 Bending and Welding to Form Octagonal Shaft

Since all of the faces of the metal skeleton to which the VEM is to be bonded is now conveniently exposed, the surfaces of these faces were prepared to provide the best bonding site for the adhesive according to the manufacturer's specifications. Now that the shaft is completed, the next step is to bend the tabs.

This step required two bends – one to fold the tabs over the shaft, the other to ensure the two surfaces were parallel. Some fine tuning was also necessary to remove any springback and provide preload against the VEM. The first bend was initiated by hand with a dowel pin placed at the connection between the tabs and the shaft. The part was then placed in a vice with two dowel pins for each tab placed at the proper bending locations, and a dowel pin inserted in the corresponding slots of the shaft and tabs to aid alignment. This is shown in Figure 4.14. The vice was then closed until the bends formed the proper shape. This was repeated for each of the four tabs.



Figure 4.14 Formation of Primary Bends in Tabs

For this step, the bend radii were not critical, but the alignment of the safety slots and the minimum unbent length of each tab were. These parameters were ensured to be met through the use of the dowel pins. In the following step, the other important parameters of gap distance between the tabs and the shaft, and the preload of the tabs were achieved. By placing a plastic spacer with a thickness about 0.127 mm (0.005”) larger than the desired gap distance under the bend in the tab, we visibly see the springback of the bend (Figure 4.15). By pressing the tab against the surface of the shaft with the plastic spacer at different locations, the springback was not only removed but actually reversed, as seen in Figure 4.16. This creates a preload against the VEM, which again is slightly thinner than the plastic spacer, once it is inserted between the tabs and shaft, and ensures a strong bond between the two materials. The spacer was made to be

larger than the VEM because the larger the gap distance was at the connection points, the larger springback was in the tab. Although this meant that the gap distance would be slightly oversized at the connection points, using a larger spacer ensured that there would be no springback present when the VEM was inserted.

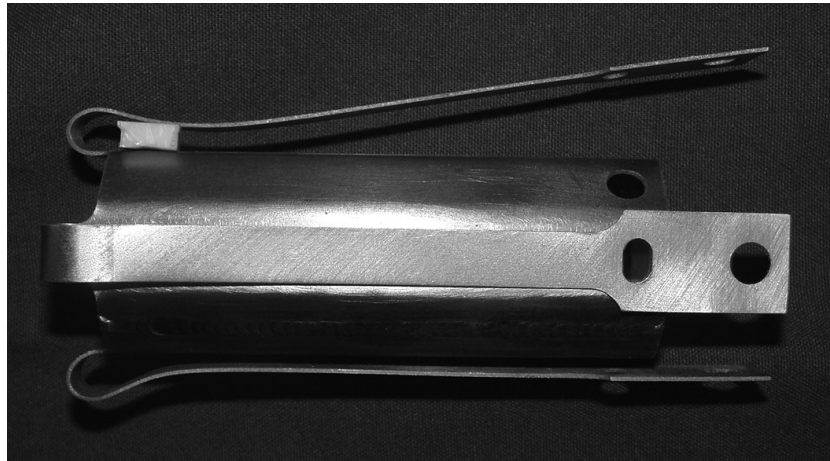


Figure 4.15 Pronounced Springback after Bending Process



Figure 4.16 Reversal of Springback into Preload

Now that the metal portion of the DVL has been formed and bent into its proper shape, the final step is to insert and bond the VEM. EAR C-1100 [21] was chosen as the VEM because of its maximum loss factor of 1.04 and its large range of operating temperatures. After cutting the VEM and preparing its surface, 3M Scotch-Weld DP810 [22] acrylic adhesive was generously applied to both sides of the VEM and then slid into place under each tab. The excess adhesive was wiped off and rubber bands were wrapped around the DVL to apply pressure. The entire

assembly was then left overnight to cure. Once the rubber bands were removed, the fabrication was complete resulting in the prototype originally shown in Figure 4.9.

4.3.3 Assembly with Rotational System

Now that the actual device had been built, the next step was to assemble it to a rotational system. Although the DVL was not used in a real-life situation, this assembly was necessary for experimentation and is not a trivial problem. Therefore, it was important that any difficulties in the assembly process be discovered so that possible design changes or identification of critical issues could be made. There are two steps required to assemble the DVL with an actual system: (1) connecting the downstream portion to the inner shaft, and (2) connecting the upstream portion to the tabs through the adapter. The steps must be performed in this order for reasons that will be explained later.

The assembly of the DVL with the downstream portion of a rotational system consists of the following steps:

1. Preparation of downstream shaft and adapter for assembly.
2. Connection of inner shaft and downstream portion of system through a roll pin.
3. Alignment of downstream shaft with adapter recess.

4.3.3.1 Preparation

In order to illustrate the assembly process, a demonstration of the assembly of the DVL to the vehicle steering shaft shown in Figure 4.17 will be given. Here, the DVL will replace another sub-assembly in the shaft. As seen in the figure, slots must be cut in into the shaft which will hold the roll pin connecting the shaft to the DVL. Slots are milled instead of holes so that the alignment of the shaft and the DVL may be adjusted and to not over-constrain the alignment of the shaft and the adapter, which is shown in Figure 4.18.

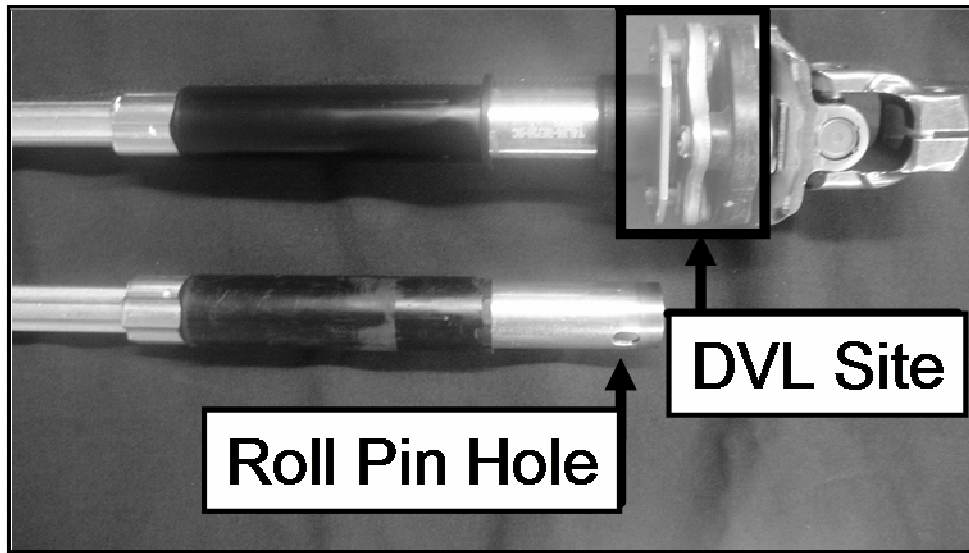


Figure 4.17 Downstream Shaft of System to be Connected to DVL

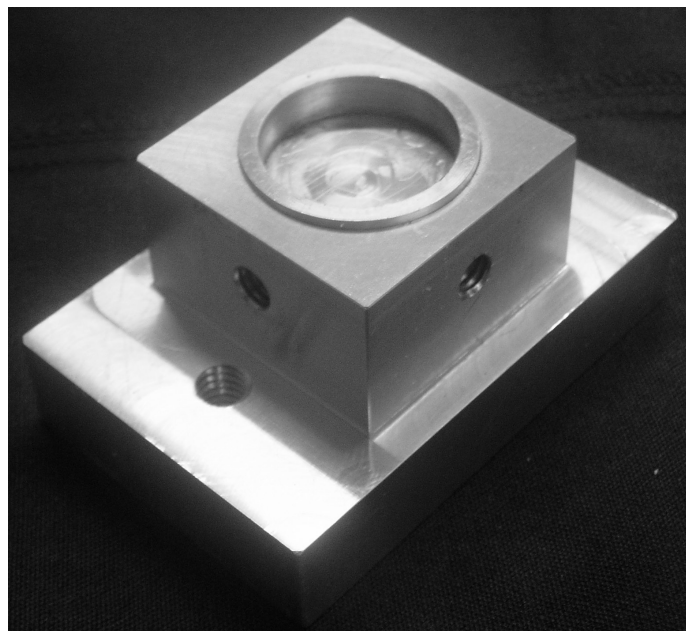


Figure 4.18 Adapter Used to Connect Reverse Section of Shaft to DVL

The adapter has been pre-machined to be assembled with the yoke at the upstream end of the shaft, and the recess has been appropriately dimensioned to properly hold the shaft for alignment. Next the steering shaft must be connected to the inner shaft of the DVL.

4.3.3.2 Connection of DVL to System Shaft

The method for connecting the inner shaft of the DVL to the steering shaft is to hammer a roll pin through the holes in the inner shaft of the DVL and the slots cut into the steering shaft. As this is a rather violent process, precautions must be taken to not damage the tabs or separate the VEM from either constraining layer. To this end, the DVL was supported in a vice, as shown in Figure 4.19, so that any loads placed on the DVL during the hammering would not be transmitted to the tabs.

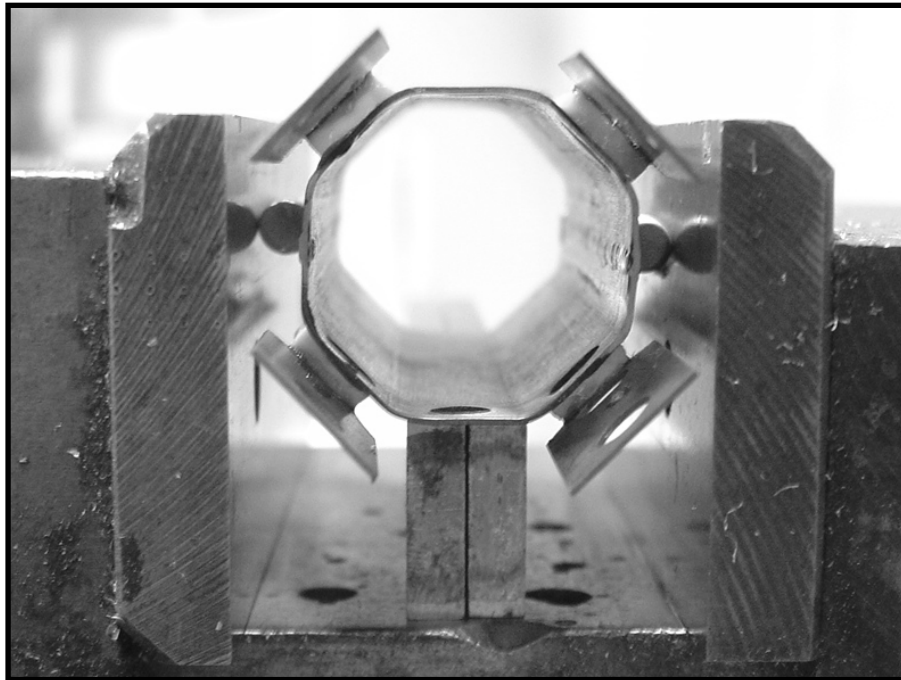


Figure 4.19 Support Configuration of DVL for Insertion of Roll Pin

The steering shaft was then supported and aligned inside the inner shaft of the DVL so that the slots were at the same axial location as the holes in the DVL, as shown in Figure 4.20.* A plastic spacer and dowel pins were used to raise the shaft off the surface of the DVL so that the steering shaft could be concentrically aligned with the DVL inner shaft and the adapter.

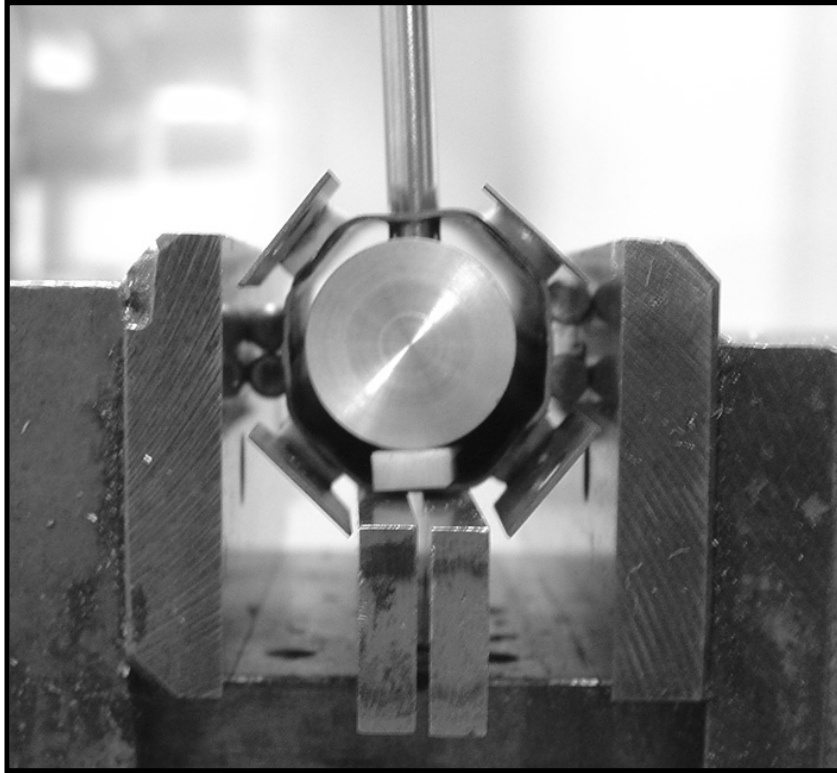


Figure 4.20 Alignment of System Shaft for Roll Pin Insertion*

The roll pin was then hammered through the hole locations in the DVL and shaft until the pin was about equally exposed on either side of the DVL. At this point it is not necessary to make the steering shaft perfectly concentric with the inner shaft of the DVL. This will be done as the adapter is connected to the tabs of the DVL.

* Picture is of solid aluminum shaft, not steering system shaft. However, the method is the same.

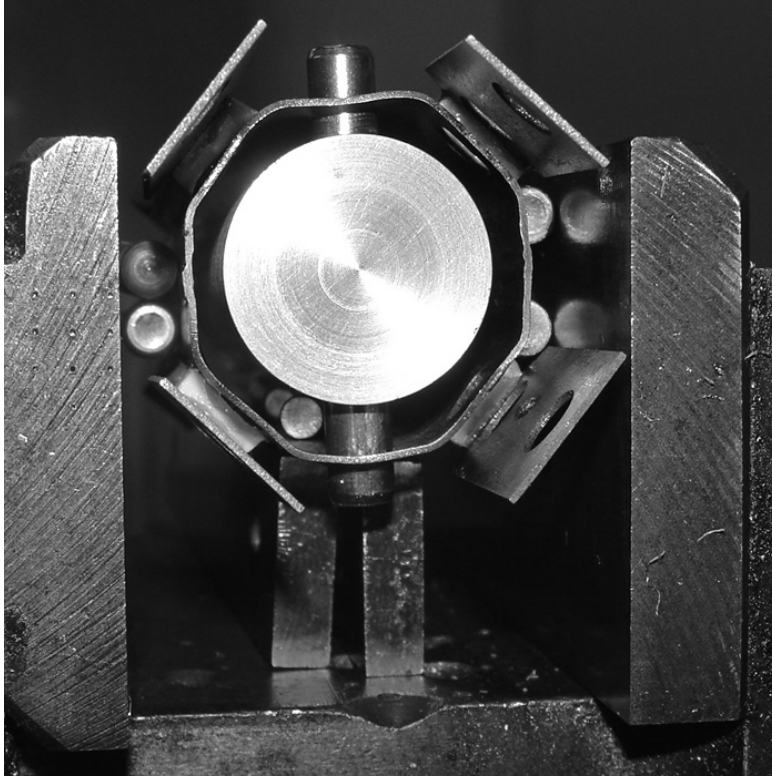


Figure 4.21 Final Position of Roll Pin*

4.3.3.3 Alignment of System Shaft with Adapter Recess

The assembly of the DVL and the steering shaft was then fitted with the adapter. Any misalignment between the end of the steering shaft and the recess of the adapter could be managed by lightly hammering the roll pin in either direction until the adapter fit properly between the tabs of the DVL. Finally, bolts were used to clamp the tabs down to the square extrusion of the adapter. The very last step was to bolt down the yoke to the opposite end of the adapter, connecting the upstream portion of the system to the DVL.

The fully assembled system is shown in Figure 4.22 and Figure 4.23.

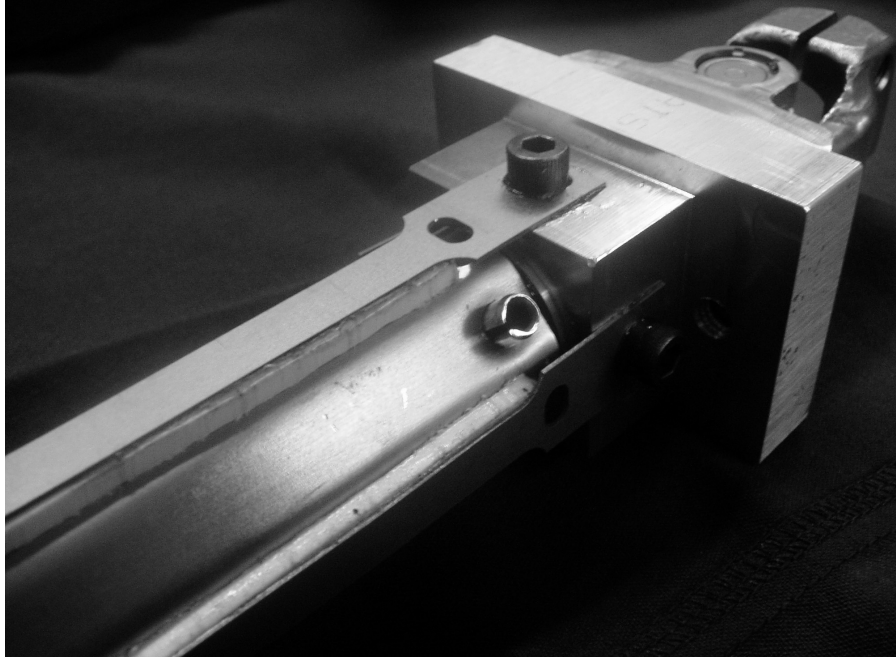


Figure 4.22 Alignment of Shaft and DVL with Adapter

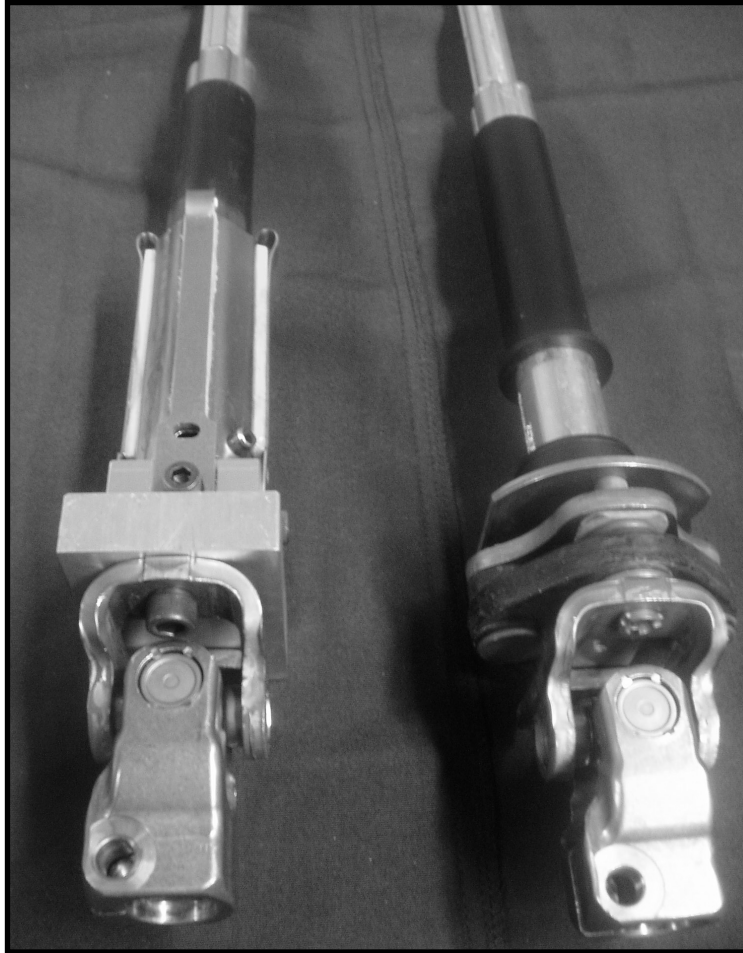


Figure 4.23 Comparison of Final Assembly of Shaft and DVL with Original Shaft

4.3.4 Important Fabrication Issues

Overall, the fabrication procedure was successful and repeatable. Yet, there were several important steps in the process that required extra care and posed a few problems. First, the formation of the inner shaft of the DVL suffered from human error and tolerance stack-up. Bending the sheet metal halves four times by 45° and ensuring that the bend lines were parallel was difficult to do by hand with a finger brake. Typically, the errors in each bend stacked-up causing the edges of each shaft half to be skewed and off-parallel by a couple degrees (see Figure 4.24). Therefore, a pair of halves did not mate perfectly to form an octagon. Still, the misalignment could be compensated by hand and through the welding process.

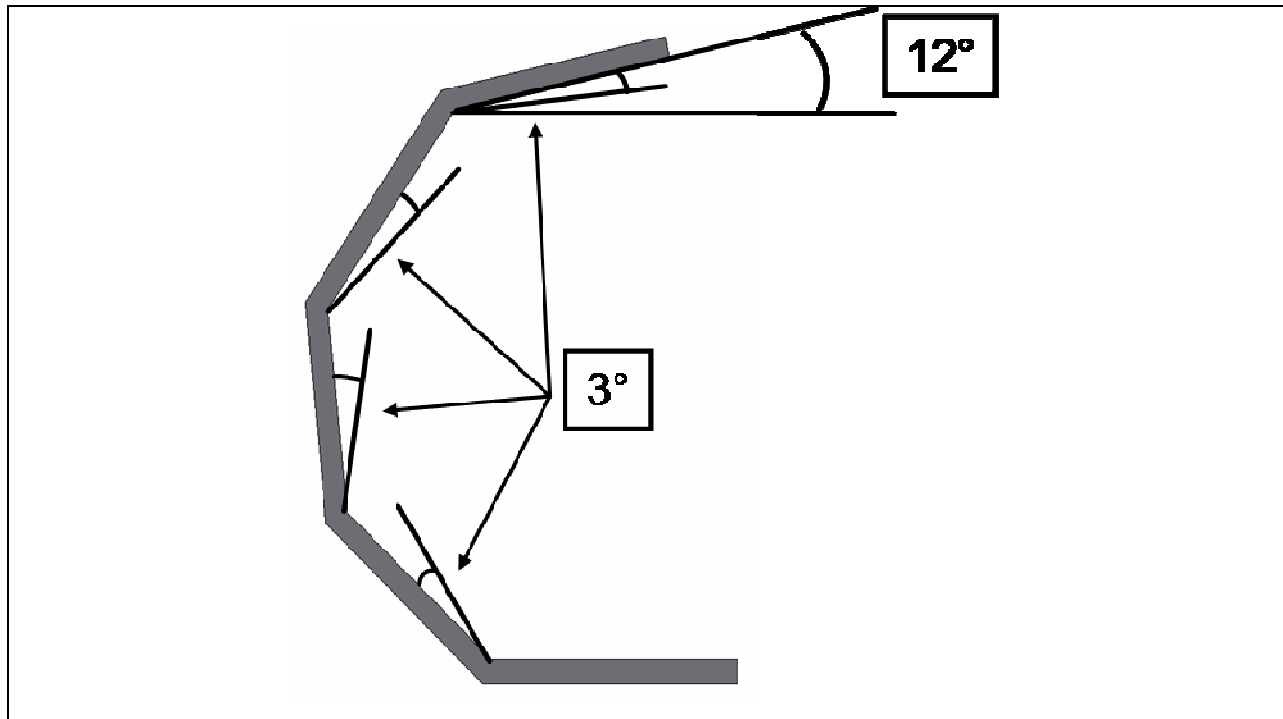


Figure 4.24 Stack-up of Errors in Bending Angles for Inner Shaft

Second, forming the bends in the outer tabs was not done by a machine at all and required some skill. The dowel pins at the connection points provided the proper radii to the bends, and the pins that fit through the safety holes ensured that the tab ends were at the proper distance from the edge of the inner shaft. However, neither the position of the bends lines nor the gap separation between the tabs and the shaft were deterministically controlled. Moreover, the second pair of bends was made more difficult due to the fact that the one of the previously bent tabs, rather than the flat inner shaft, was now in contact with the lower surface of the vice. Therefore, the device could not rest flat as the second pair of tabs was bent.

Third, bonding the VEM to the metal substructure was very messy and the adhesive could not be evenly distributed across the bonding surfaces. Adhesive was applied generously to both sides of the VEM purposely to account for some of it being removed as the VEM was slid into place. This caused excess adhesive to collect near the free ends of the tabs and on the inner shaft. This excess adhesive needed to be carefully removed so that it did not form a direct bond between the inner shaft and the tabs. Furthermore, the VEM did not lie perfectly flush against the total area of the bonding surfaces because of some structural irregularities, like divots and bends, in the

metal tabs and shaft. However, this nonconformity was localized and compensated by the potting nature of the adhesive.

Fourth, the assembly of the DVL with the downstream shaft is a very violent and cumbersome process. The holes in the DVL through which the roll pin lies are purposely undersized to ensure a tight fit, there is a significant amount of resistance provided by the inner shaft of the DVL to the hammering process. This resistance and the violent nature of the hammering causes damage to the walls of the inner shaft, shown in Figure 4.25.

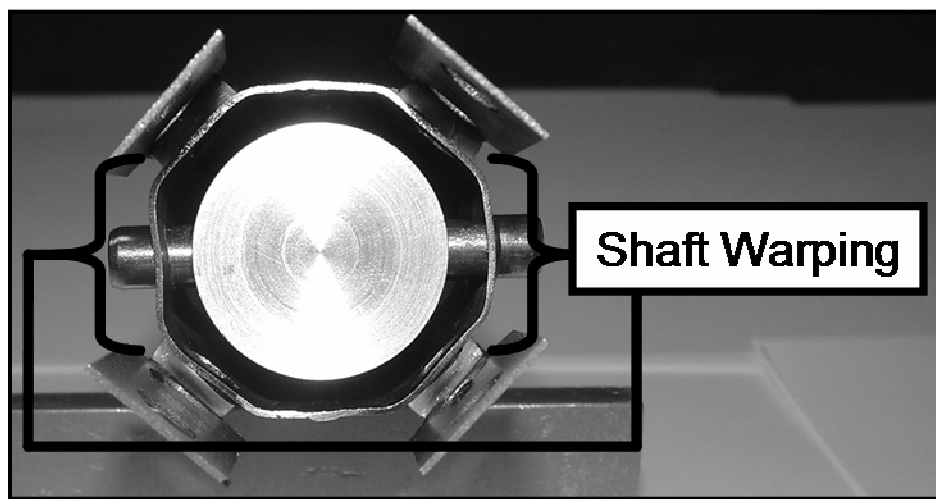


Figure 4.25 Warping Damage to Inner Shaft from Hammering

Furthermore, the precautions and preparations that needed to be taken because the hammering was so violent made the entire assembly process cumbersome and lengthy. As seen in Figure 4.20, the multitude of dowel pins, parallel plates and plastic spacers required to support the inner shaft and ensure that the tabs were unloaded was difficult to set up and made the work area very cramped. In addition, the shaft must be concentrically aligned with the DVL and adapter after the roll pin is inserted. It would be preferable to align and support the shaft first by connecting the DVL tabs to the adapter and inserting the shaft in the adapter recess. This would reduce complexity, cycle time and make sure that the shaft does not have to be adjusted after it is secured to the DVL.

Although this solution was convenient for an initial prototype, using a roll pin to connect the DVL to the downstream shaft was not the best choice and should be reevaluated. As a roll pin is tapered, the fit on either side of the assembly is not symmetric, leaving the possibility for backlash. Moreover, given the distance between the four crimping points on the roll pin, the assembly is over-constrained. If any of the holes is slightly oversize, either as a result of the fabrication or hammering process, the roll pin will not conform to the diameter of that hole and may not provide a secure connection. The very fact that it takes several paragraphs to explain the connection of the DVL to the downstream portion of the system and one sentence to explain the connection with the upstream portion indicates that another solution is desirable. Possible future alternatives are shrink-fitting or welding the inner shaft directly to the downstream shaft. Although these more permanent methods are not desirable for a proof-of-concept prototype, they would be much more economical and effective for large-scale manufacturing.

Two final notes about the connection of the adapter to the DVL that are important to consider are the use of grease to lubricate the adapter recess and the sizing of the square extrusion. The grease is necessary to prevent the downstream shaft from binding with the recess of the adapter, therefore, bypassing the DVL altogether. The lengths of the sides of the square extrusion on the adapter were also adjusted for the DVL prototype. During the preparation step, before assembling the prototype with the downstream shaft, the length of each side of the extrusion was purposely made between 0.254 – 0.127 mm (0.005 – 0.010”) shorter than the distance between the pair of opposing tabs. This ensured that when the tabs were bolted to the adapter there was a slight preload pushing the tabs against the VEM and not pulling them away from it, preventing any inadvertent delamination.

In all, the entire process of fabrication the DVL prototype and assembling it to the rotational system took about ten hours per device. Of course, this procedure would not be used for large-volume manufacturing. Some of the other methods that were initially investigated but not pursued, such as sheet metal forming and laser cutting, could potentially be used for production manufacturing. If the substructure could be made of a plastic rather than a metal, injection molding or even vacuum forming could be effective manufacturing methods. A detailed fatigue study of the DVL was not conducted for this thesis. However, delamination problems could be

circumvented by increasing the thickness of the VEM at the edges of the tabs, or by anchoring the VEM to the substructure by molding it through a weave or feature matrix in the material.

4.4 Summary

There were many important practical design considerations learned from the fabrication of each prototype. For the SAVI, a major convenience is the parallel fabrication of many of its components and the simplicity of the device. The part count was reduced as much as possible by permanently bonding many of the sub-assemblies together, and by having several components serve multiple design purposes. This allowed for rapid assemblies, testing and design changes for later generation prototypes. However, this also caused difficulties in aligning each of the individual components together. For this reason, future designs should use a master reference so that each sub-assembly is ensured to fit properly with their respective mates.

The DVL fabrication process leaves much to be desired. Part of the problem is the nature of the design. Due to the coupling between the VEM and the elastic constraining layers, the fabrication was performed in a serial procedure; the different components could not be built independently like in the SAVI. Also, the assembly of the DVL with a rotational system is difficult. In order to avoid permanent methods for the initial prototypes, complicated and lengthy nonpermanent methods were employed. Furthermore, more automated methods for bending the inner shaft and tabs are necessary in the future. One advantageous design change that was a result of the fabrication effort was using an octagonal cross-section rather than a circular one. This removed the necessity to reverse the concavity of the tabs after they were bent over the shaft.

CHAPTER

5 EXPERIMENTAL VERIFICATION

The purpose of this chapter is to experimentally verify the models developed in Chapter 3 and the broad capabilities of the DVL. First, the SAVI will be tested for its low-amplitude stiffness and its yield angle. Large amplitude (10's Nm) torque testing was performed to find the gross characteristics of the SAVI, and small amplitude (100's mNm) torque testing was conducted to determine its performance on the scale of possible upstream vibration. Then the lumped parameter model will be verified by testing a portion of a steering column to determine its natural frequency and mode shape. Finally, the DVL prototype will be testing to get a general idea of the potential effectiveness of this device compared to conventional damping treatments.

5.1 Testing of SAVI

It is necessary to verify the accuracy of the FEA simulation presented in Chapter 3, which is used to determine the proper dimensions of the torsional spring of the SAVI given certain desired design parameters. Based on the requirements for the steering system described in the case study of automotive nibble, a SAVI was designed with the design parameters shown in Table 5.1. From the models presented in Chapter 3, the following dimensions of a torsional spring, cut from 7075-T651 aluminum, and the stop engagement system were chosen. Looking at the table, there seems to be a problem with the chosen dimensions for the SAVI. Although the stiffness prediction from the model is 1 % off from the desired value, the yield angle is nearly 50 % less than what is desired. Notwithstanding this error, the dimensions were chosen for the following reasons:

1. The maximum acceptable diameter for the SAVI based on the constraints of the system was 89 mm (3.5”).
2. Because of thickness limitations created by the taper in the torsional spring, the part thickness could either be chosen as 1.60 mm (0.063”) or 3.18 mm (0.125”). Based on the

models, a torsional spring with a thickness of 1.60 mm (0.063”) and a stiffness around 2 Nm/deg would have a yield angle of less than 1 degree. Therefore, a part thickness of .18 mm (0.125”) was the better choice.

3. As explained in Chapter 3, the yield angle estimates determined from the models are for the first signs of yield in the part. This is important for high-cycle fatigue failure, but since the SAVI prototype fabricated needed only to prove the capability of the concept, such a lifetime was not necessary. As will be seen, even with these dimensions, the part does not exhibit gross yielding until after 2 degrees, which is greater than the stop engagement angle provided by the gap dimension in Table 5.1.

Table 5.1 Selected Values for Design Parameters and Dimensions of SAVI

Design Parameter	Desired Value	Predicted Value from Chosen Dimensions
Low-Amplitude Stiffness	2 Nm/deg	1.98 Nm/deg
Yield Angle	>2 degrees	1.11 deg
Stop Engagement Angle	2 degrees	2 degrees

Dimensions	Selected Value
SAVI Package Diameter	89 mm (3.5”)
Radial Beam Thickness	1.27 mm (0.050”)
Torsional Spring Part Thickness	3.18 mm (0.125”)
Stop Gap Clearance	1.14 mm (0.045”)

The large gross characteristics of the torsional spring were tested using an MTS torque instrument, which measured the stiffness of the SAVI as well as its yield angle. As the upstream vibration may occur at very small amplitudes, like in the case study of the steering system discussed in Chapter 6, low-amplitude testing was also required to verify that the stiffness of the torsional spring did not vary with amplitude. This was conducted on a AR2000 Rheometer capable of torques in the range of mNm. Based on these experiments, the models were shown to

predict the low-amplitude stiffness of the torsional spring to within 1 % error. The complete non-linear stiffness profile and the angular displacement at stop engagement of the SAVI were not tested. However, based on results from the case study presented in the next chapter, and the characteristics of the torsional spring used in that situation, it was determined that the angular displacement at stop engagement could be fabricated at about 2 degrees.

5.1.1 MTS Testing of SAVI

In order to test the gross stiffness and the yield angle, a SAVI mechanism, fully assembled except for the stop engagement system, was tested in an MTS torque instrument as shown in Figure 5.1. A low frequency sinusoidal torque with a maximum amplitude of 2 Nm was applied to the SAVI assembly in order to generate a fully reversed loading plot of its stiffness. Then a torque ramp was applied to determine the yield point of the device. The results of these experiments are shown in Figure 5.2 and Figure 5.3, respectively.



Figure 5.1 Testing Setup for MTS Experiments

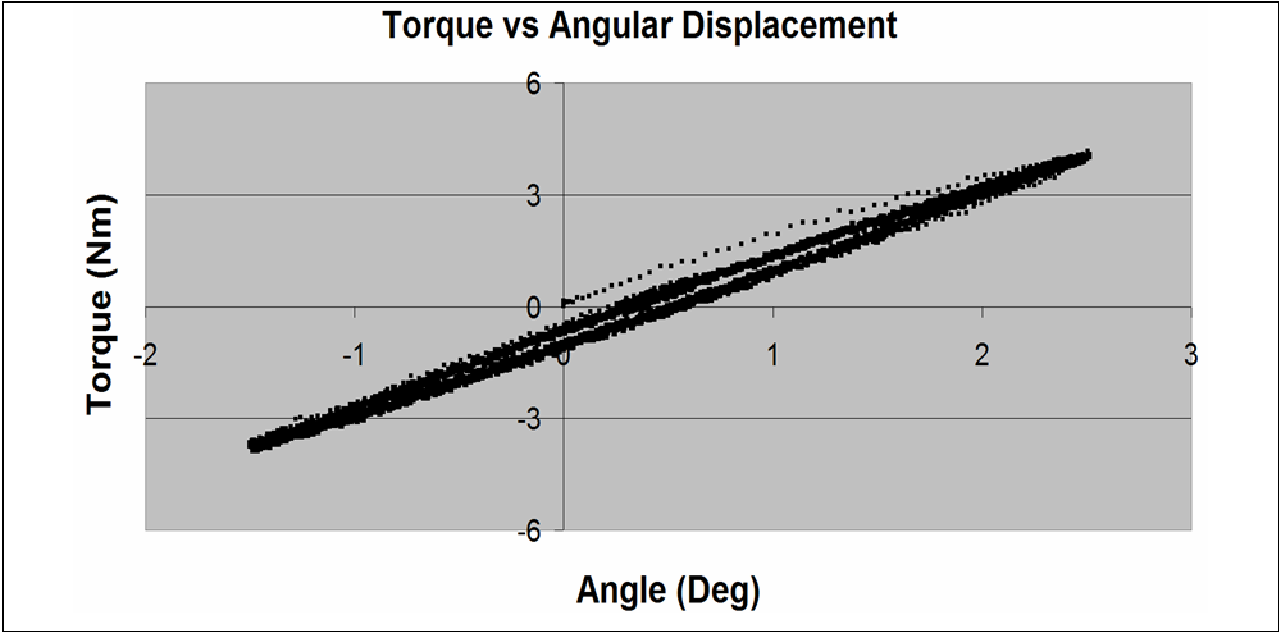


Figure 5.2 Plot of Reversed Loading Curve for SAVI

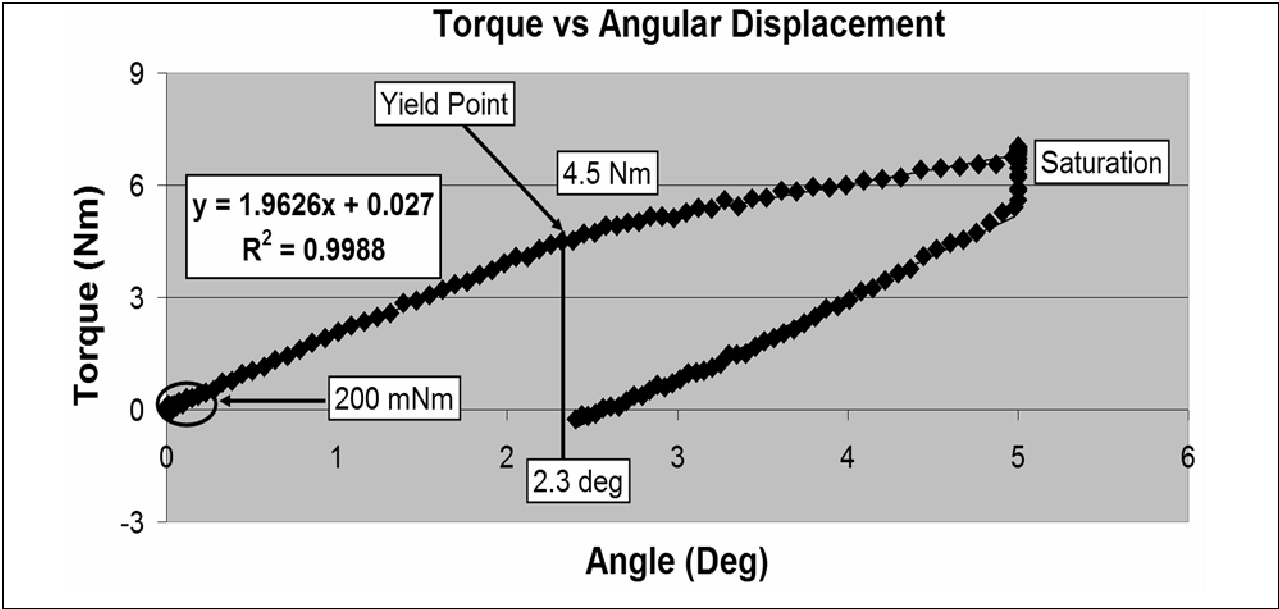


Figure 5.3 Plot of Torque Ramp

According to both tests, the stiffness of the SAVI was calculated as 1.96 Nm/deg, and from Figure 5.3, it was estimated that the yield angle for the device was 2.3 degrees. The torsional stiffness value agrees with the FEA simulations to within a 1 % error. Although the simulations

indicate that the SAVI will not survive repeated loaded beyond a couple hundred cycles, this limitation does not apply to our needs for the prototype. What is important is that the gross yielding of the SAVI occurs beyond 2 degrees, which is the angular displacement at which the stops engage and absorb the torque load in the device.

As a final note, notwithstanding the fact that the SAVI was coupled in series with the steering shaft, the above results are considered an accurate measurement of the torsional spring itself. This is because the torsional stiffness of the shaft is in the range of 20 Nm/deg, which is an order of magnitude greater than the measured stiffness of the SAVI. Furthermore, as will be seen, the low-amplitude stiffness of the torsional spring alone matches the large amplitude data shown above.

5.1.2 Low-Amplitude Testing of SAVI

Now that the overall characteristics of the SAVI have been determined, the low-amplitude torsional stiffness of the mechanism must be found to ensure proper isolation of the upstream vibrations present in the vehicle. These vibrations were found to deflect the SAVI at an amplitude of about 0.25 deg, far less than the stop engagement angle. Given the large amplitude stiffness of the SAVI, this would require a measuring instrument capable of torques on the scale of 100's mNm and high measurement resolutions. An AR2000 Rheometer, which is typically used to test the viscosity of fluids, is capable of these requirements, and hence, was chosen to determine the stiffness of the SAVI at these small amplitudes. The testing setup for this experiment is shown in Figure 5.4.



Figure 5.4 Test Setup for Rheometer Testing

The torsional spring was raised off the support surface by washers, which were affixed to both the through holes of the planar spring and the support by superglue. Discrete torque levels, ranging from 0 – 200 mNm and separated by 20 mNm increments, were applied to the torsional spring via the hexagonal adapter. With the application of each torque level, the angular displacement of the spring was measured and recorded. Three loading cycles of this nature were applied and the results are plotted in Figure 5.5.

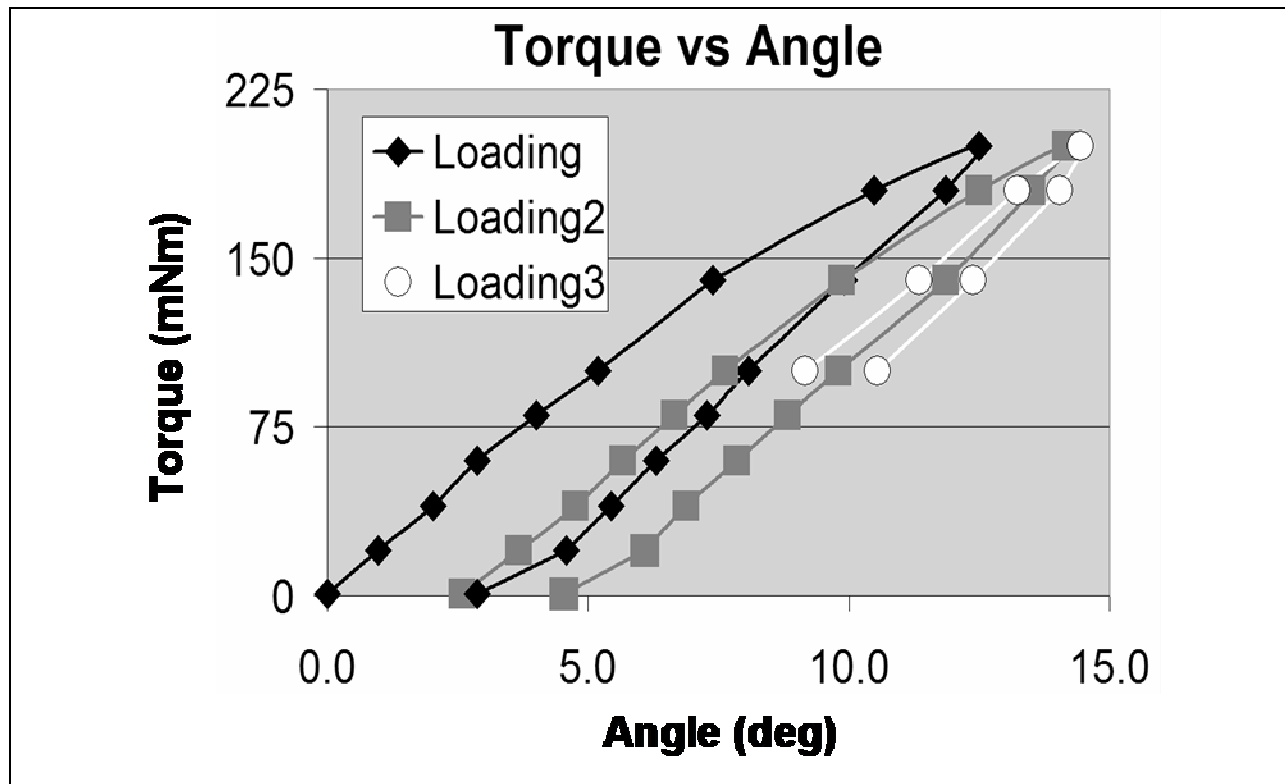


Figure 5.5 Results from Rheometer Testing

Although there is significant hysteresis in the measurements, the average of the linear sections of all three loading and unloading curves is 2.06 Nm/deg. This average measurement was considered to be a sufficient validation of the low amplitude stiffness testing of the SAVI. One possible reason for the hysteresis in the plots and the variation in the measured stiffness values between the individual loading curves is that the rheometer is not designed to apply such large torques at a constant displacement. Although 200 mNm is not a relatively large torque value, that this the maximum output of this specific rheometer. Plus, typical experiments conducted with this equipment do not stall the motor but run it at a constant velocity. Despite the fact that the AR2000 is capable of running the torque testing described above without damaging the motor, the performance of the instrument may be hindered by excessive heat generation. Nevertheless, the results demonstrate that the low-amplitude torsional stiffness of the SAVI matches the measurements calculated from the MTS machine.

5.2 Verification of Lumped Parameter Model

The accuracy of the lumped parameter model, described in Chapter 3, which is used to rapidly and conveniently characterize the dynamic properties of a rotational system, needed to be verified. For this purpose, an experiment was conducted on part of the steering column of a light-duty pickup truck, shown in Figure 5.6.

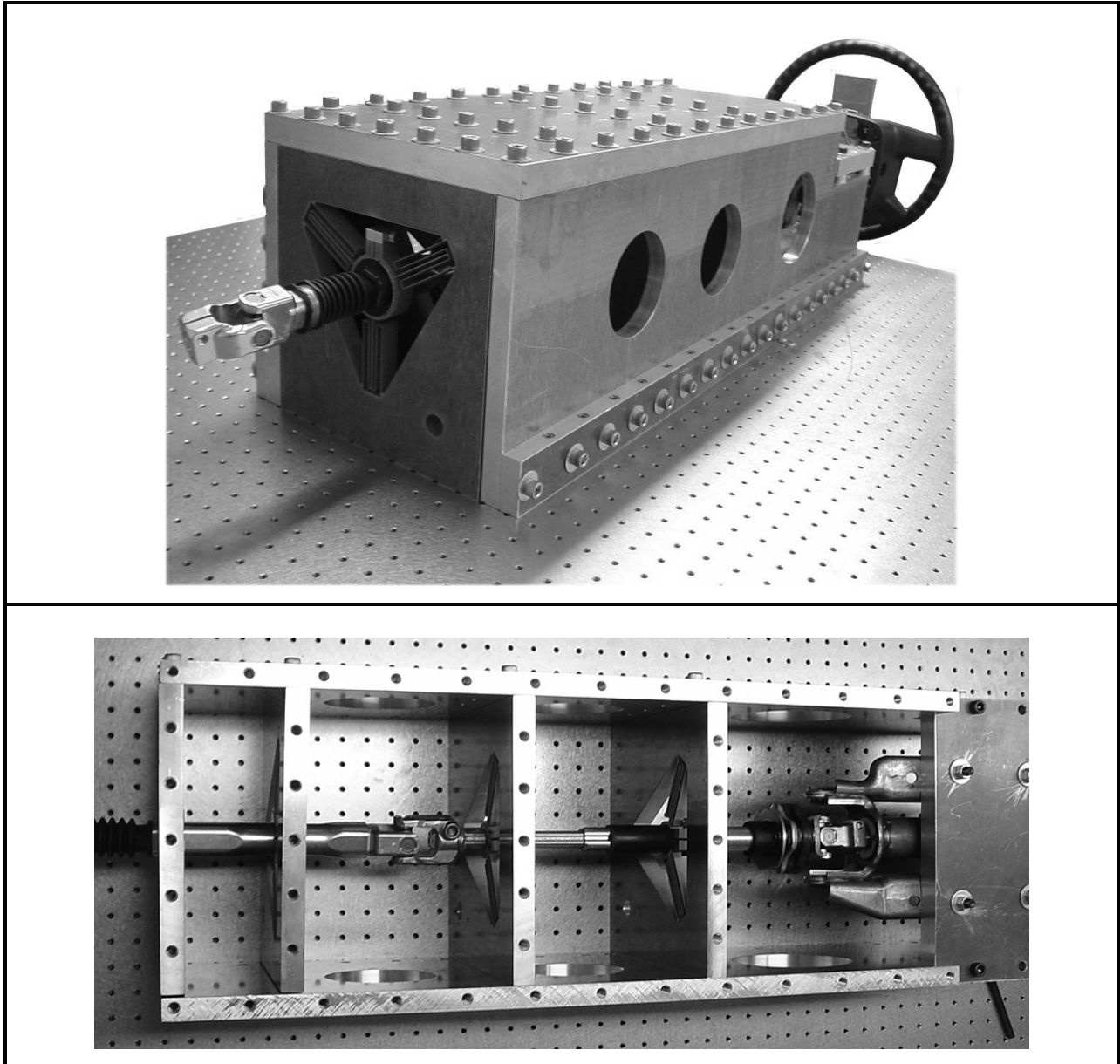


Figure 5.6 Experimental Fixture for Characterization of Steering Column

In the figure, one can see an aluminum block attached to the center of the steering wheel. This block serves the dual purposes of (1) emulating the moment of inertia of the airbag (not installed for safety reasons) and (2) providing a structure which would excite the column via a mechanical impulse.

The steering column was supported by a novel revolutes flexure, designed by the author and Professor Martin Culpepper, which allowed for rotations about the steering column's main axis, but restricted motions in all other directions [23]. Each flexure was bolted on the fixture's side and top by $\frac{3}{8}$ inch bolts. The fixture assembly was bolted through the mounting rails to an optical table. Each steering column component was then assembled within the test fixture. Tri-axial accelerometers (PCB 356B08) were placed at nine points along the steering column, with one above and the other below the axis of rotation. An impact hammer (PCB 086B03) was used to excite the system. A dynamic analyzer (SigLab 20-42) calculated the transfer functions, coherence plots and time responses of each accelerometer. Data was sampled at 512 Hz with a frequency resolution of 0.13 Hz. The results of the experiment are shown in Figure 5.7 and Figure 5.8.

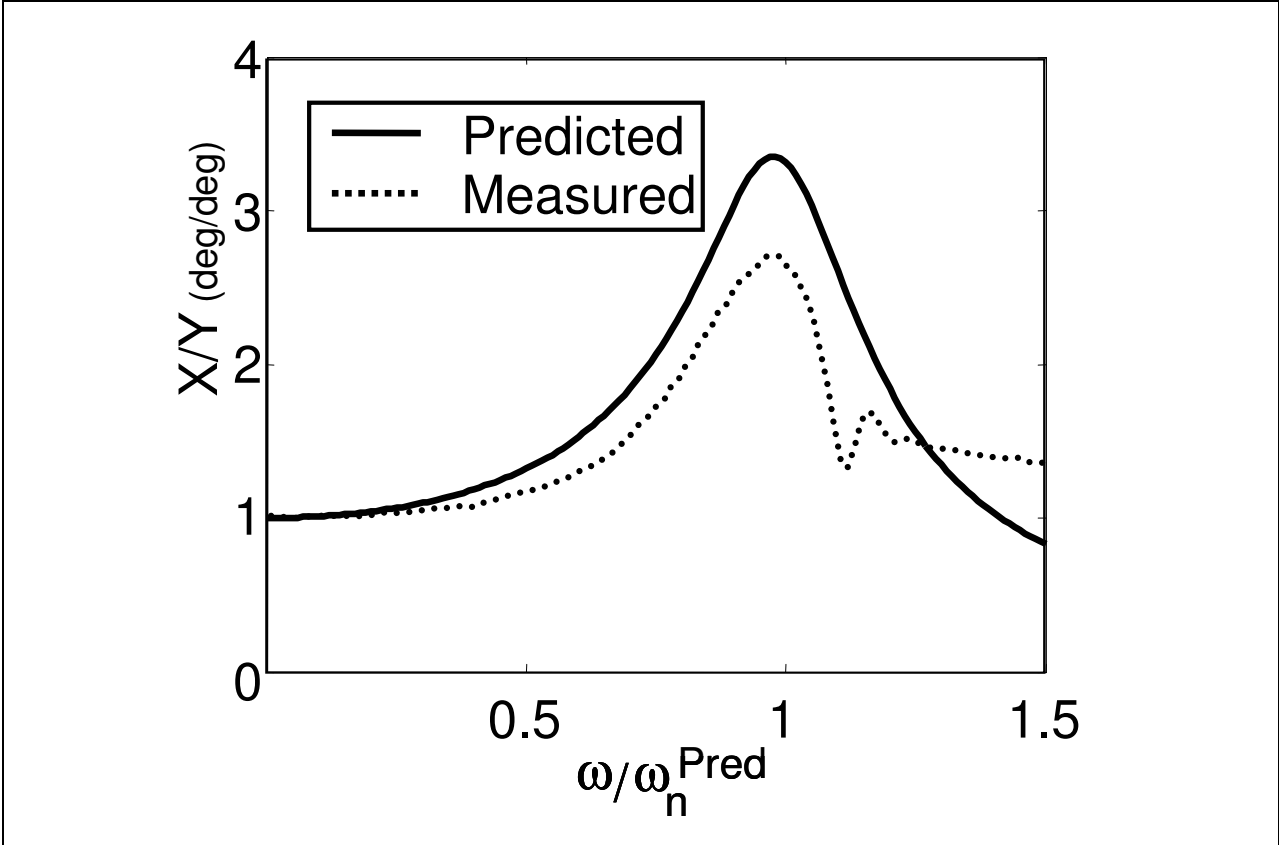


Figure 5.7 Measured Transfer Function of Steering Column

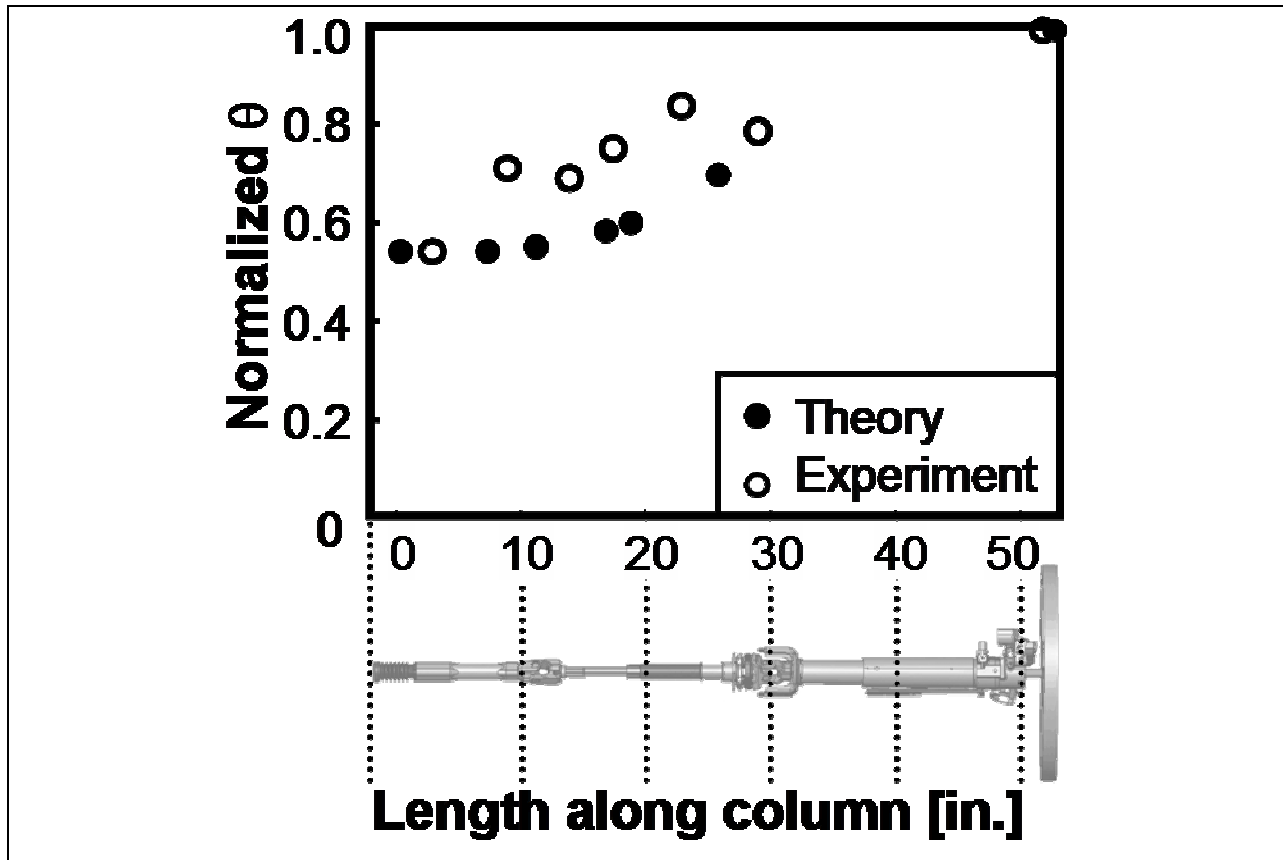


Figure 5.8 Measured and Predicted Mode Shape of Column

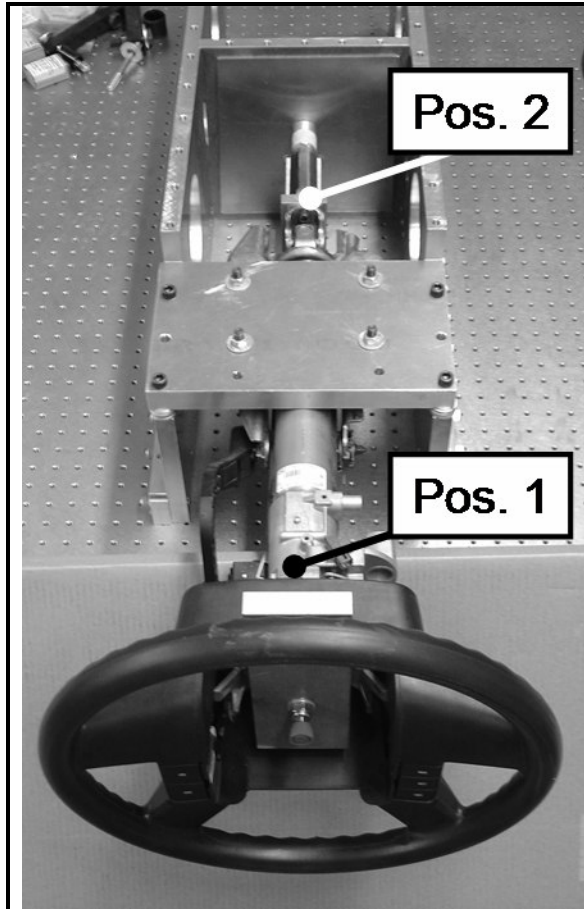
The steering column natural frequency and damping ratio were measured as 11.7 Hz and 0.083, respectively, whereas the predictions from the lumped parameter model of the steering column suggested a natural frequency of 11.5 Hz (-1.7% error) and a damping ratio of 0.05 (-40% error). The comparison between the measured and expected transfer functions for the steering column is shown in Figure 5.7. The large amount of error in the damping calculation may be explained by the errors in calculating the fundamental mode shape of the column, discussed below, and the uncertainty of the inherent damping present in the bearings of the upper steering shaft. The discrepancy between the trailing ends of the two curves shown in Figure 5.7 can also be explained by the fact that the theoretical curve is a plot of a single-DOF system. The actual system, which is represented by the measured curve, has many DOF, each of which has its own mode and is coupled to the other modes in the system.

As the mode shape is useful for determining the damping of a system, we now turn our attention to the rotation amplitude of various components within the steering column. Figure 5.8 presents data which describes the rotation at discrete locations along the steering column. The data is normalized with respect to the rotation amplitude of the steering wheel at resonance. Although the data matches well at the endpoints of the analysis, errors of 20% to 30% are observed at various points in between. It is interesting to note that the points which exhibit the large error are either located on components that have a finite clearance between them and the adjacent component in the steering column, or are constructed of differing materials, i.e. u-joints, safety crush/sliding joints, etc.. These components cause the dynamics to be, to some degree, non-linear. Therefore, it would be expected that the linear lumped parameter model does not completely agree with the measured data.

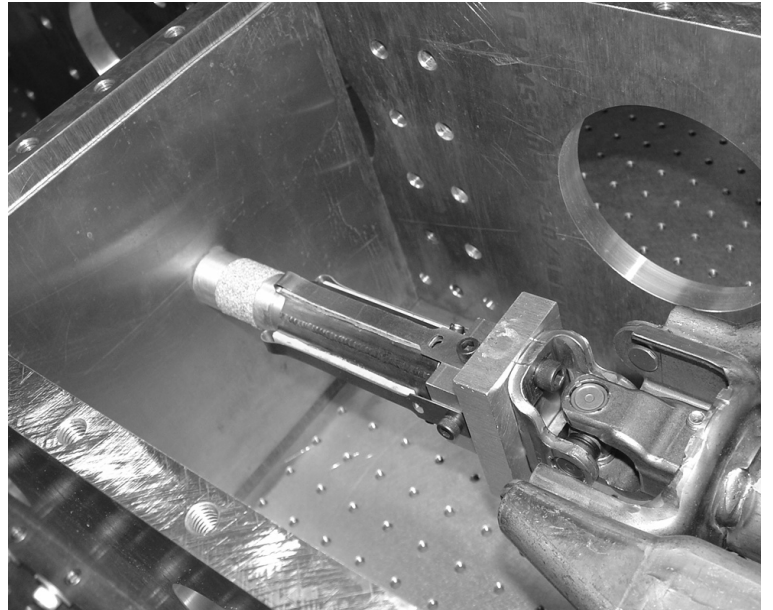
The hypothesis that the non-linear components in the steering column are the sources of error in the above experiment is supported by the experiment conducted on the DVL, which uses a similar test setup. Although the parts of the model that remain to be validated, namely the prediction of the mode shape, are used to determine the properties of the DVL, certain methods are employed to confirm the model's accuracy. Still, the above experiment demonstrates both the capabilities and limitations of the linear lumped parameter model.

5.3 Dynamic Testing of the DVL

The general capabilities of the DVL were tested in the fixture shown in Figure 5.9. Here the DVL was connected directly to the steering shaft of the steering column via the adapter. The other end of the DVL was fixtured to an aluminum shaft, which is in turn bonded to a metal plate via superglue. Similar to the test conducted on the entire column, the system was excited by hitting the inertia block connected to the steering wheel with an impact hammer. Using the same equipment as before, ten averages were taken of the resulting transfer function of accelerometers placed at two different positions along the system length: (1) just behind the steering wheel, and (2) on the adapter block. The first natural frequency of the response, corresponding to the fundamental mode of the system, is plotted in Figure 5.10.



A. Accelerometer Positions



B. DVL Installation

Figure 5.9 Experimental Setup for Testing of DVL

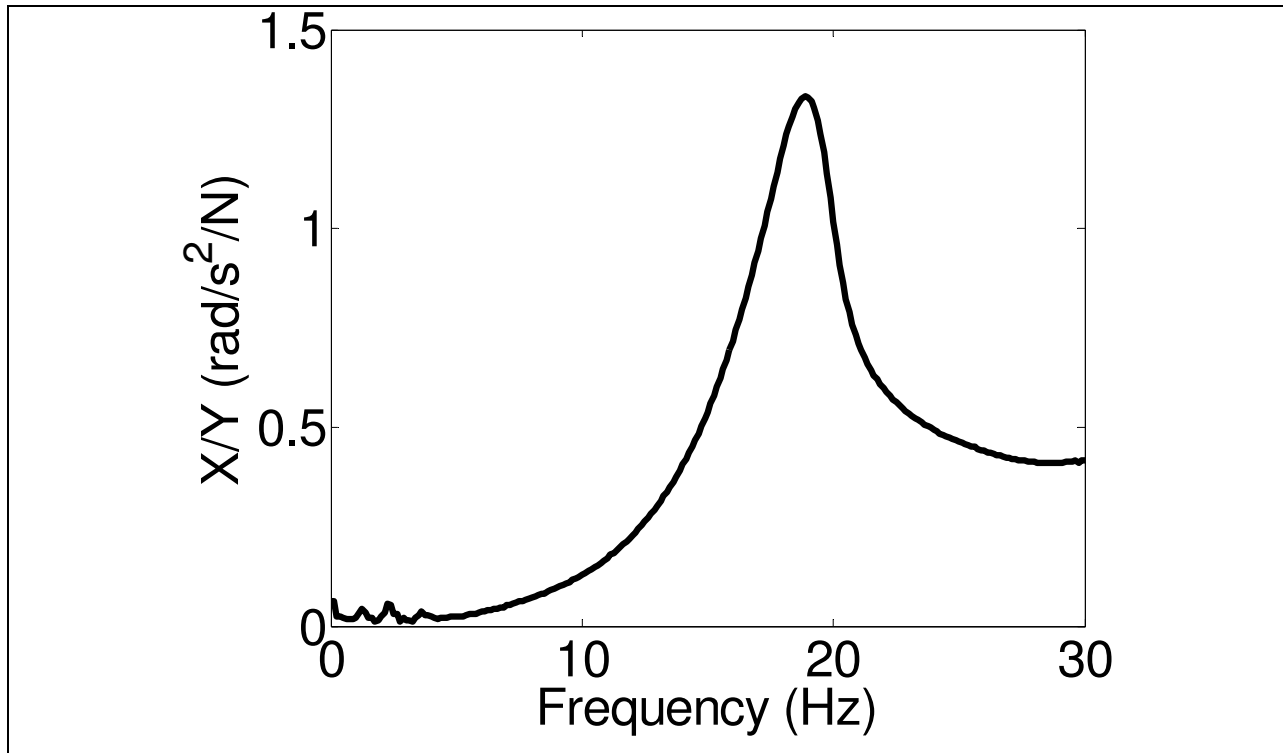


Figure 5.10 Measured Transfer Function of Accelerometer Response

From the transfer functions measured at the two indicated positions along the system length, the natural frequency, total damping ratio and mode shape of the system were calculated as shown in Table 5.2. From the measured natural frequency, the stiffness of the DVL was calculated as 17.9 Nm/deg. Using this data and approximating the effective rotational inertia of the DVL, the lumped parameter model was used to predict the natural frequency and the mode shape of the system to both check the experimental data and the accuracy of the model. The results are also shown below.

Table 5.2 Measured and Predicted Results of DVL Experiment

Dynamic Characteristic	Measured Value	Predicted Value	Percent Error (%)
Natural Frequency	18.9 Hz	19.6 Hz	3.7
Mode Shape	$\begin{Bmatrix} \theta_1 \\ \theta_2 \end{Bmatrix} = \begin{Bmatrix} 1 \\ 0.526 \end{Bmatrix}$	$\begin{Bmatrix} \theta_1 \\ \theta_2 \end{Bmatrix} = \begin{Bmatrix} 1 \\ 0.570 \end{Bmatrix}$	8.4
Total Damping Ratio	0.082	---	

With knowledge of the stiffness of all of the components in the system and the overall mode shape, an estimate of the damping ratio of the DVL was calculated, using Eq. 2.5, as 0.084. It should be noted that this is an overestimated value, which was calculated using the assumption that the steering shaft does not have any damping. Since there are roller bearings in the steering shaft assembly, this is not generally true. Furthermore, the calculated stiffness of the DVL is not without some error. As stated in Chapter 4, the overconstraint of the roll pin caused there to be a small amount of play between one of the holes in the inner shaft of the DVL. Therefore, the torsional stiffness calculated above is lower than the actual value for the DVL. Nevertheless, both values for the damping and stiffness of the DVL are good approximations of the device's potential performance.

5.4 Summary

From both large and small amplitude torque testing of the SAVI, the actual torsional stiffness value of the device was found to be within 2 % of the predicted values from FEA simulations. The predictions for the yield angle made by the simulations were also found not to apply to gross yielding of the torsional spring but rather as a design consideration for high-cycle fatigue failure. Although the stop engagement angle was not tested, the case study presented in the following chapter suggests that the engagement angle was properly fabricated by hand to less than 2 degrees.

The lumped parameter model was shown to make accurate predictions of the natural frequency (within 4 % error), and can make approximations of the mode shape of simple linear systems to within 10 % error. For more complicated, non-linear systems, the natural frequency predictions are also accurate, however, the mode shape and damping calculations can vary significantly from experimentation. For such systems, it is recommended to check the information obtained from the lumped parameter model with more sophisticated software.

By testing a prototype of the DVL, the potential performance for damping in a CVA was shown to be moderately high. Although this initial prototype was not optimized, damping ratios on the

order of 0.08 have been achieved. If an analytical model is developed for the DVL and the dimensions optimized, it is possible that the damping ratios may be increased further. Additionally, the stiffness of the DVL may be designed to be similar to that of the other components in the system. For the prototype described in the thesis, a torsional stiffness of at least 17.9 Nm/deg was achieved. Therefore, the DVL should be able to transmit any desired torque input through the rotational system just as well as any other component in that system, allowing for high attenuation of resonant vibrations with minimal effect on the primary performance of the system. Table 5.3 compares the performance of the DVL with the optimum values for other torsional dampers of similar dimensions. As a first attempt, placing viscoelastic material directly in the load path of the rotational system, rather than indirectly coupling it through an external treatment, makes for difficult analysis but provides a very competitive performance with existing damping technology.

Table 5.3 Potential Damping Ratios for DVL and Conventional Damping Methods

DVL	Concentric Tubes [9]	External Treatment [8]
0.08	0.05	0.06

CHAPTER

6 CASE STUDY: AUTOMOTIVE NIBBLE

This chapter discusses the application of both the Damping Vibration Link and Small Amplitude Vibration Isolator towards the problem of automotive nibble in light-duty pickup trucks. First, a general description of the problem will be given, followed by a detailed analysis of the steering sub-system. The suitability and performance of each device will then be discussed. The SAVI was chosen as the most appropriate solution, which provided a 60 % reduction in vibration amplitudes.

6.1 Background

Automotive nibble is the rotational vibration of the steering wheel in a vehicle. Generally, it is a low-amplitude, low-frequency upstream vibration transmitted from the wheel assembly to the steering wheel through the suspension system and steering linkages. While the phenomenon does not affect driving performance or safety, it has been a major perceived quality issue in the automotive industry, particularly in the light truck market. This is directly demonstrated in the warranty numbers and reports of customer satisfaction. Although warranty costs associated with repairs for nibble are less than a few million dollars per year, for roughly every 100 trucks sold there are 3.9 customer complaints about nibble. In a 2004 Initial Quality Study, J. D. Power Associates found consumers rated nibble as the number one problem in the “Ride, Handling, and Brake” category [24]. In order to improve customer satisfaction, companies throughout the automotive industry have attempted to reduce or eliminate nibble for over a decade.

As a result, there is a large volume of literature on this topic. Previous studies have investigated the causes of nibble, how it affects various vehicle sub-systems, its transmission between these systems, and what may be done to solve the problem [25 – 32]. Unfortunately, nibble is a system level issue and its removal requires modifications throughout the vehicle. Competing performance requirements on each of the involved sub-systems restrict the extent of these modifications and have made finding a solution to nibble extremely difficult.

Therefore, this is an ideal application for a CVA, such as the DVL or SAVI. First, the upstream vibration frequency is typically around 13 – 14 Hz, which is significantly greater than the frequency of the turning inputs provided by the driver. Second, because nibble is a consumer satisfaction concern and does not cause any vehicle performance issues, eliminating the source of the problem is not necessary. This is particularly beneficial because the sources of vibration are still not completely understood in industry. Furthermore, the other components involved in propagating the vibration up to the steering wheel, i.e. the suspension, steering gear, etc., are pre-designed to meet other performance requirements and cannot be modified significantly to accommodate nibble. Instead, the effects of nibble on the various individual sub-systems can remain unchanged as long as the driver is simply isolated from these effects. Hence, as discussed in Chapter 1, a CVA acting as a mechanical low-pass filter would effectively eliminate the higher frequency vibrations of nibble while properly transmitting the handling commands from the driver. In the next section, the fundamental issues behind nibble will be explained in more detail.

6.2 Problem Definition

6.2.1 Kinematics

A basic graphical representation of nibble in a vehicle with independent front suspension and McPherson struts is shown in Figure 6.1. A harmonic force is applied to the tire and generates a turning motion on the wheel. The resulting motion is then transmitted to the steering system via the tie-rods attached to the wheel spindle and then up to the steering wheel.

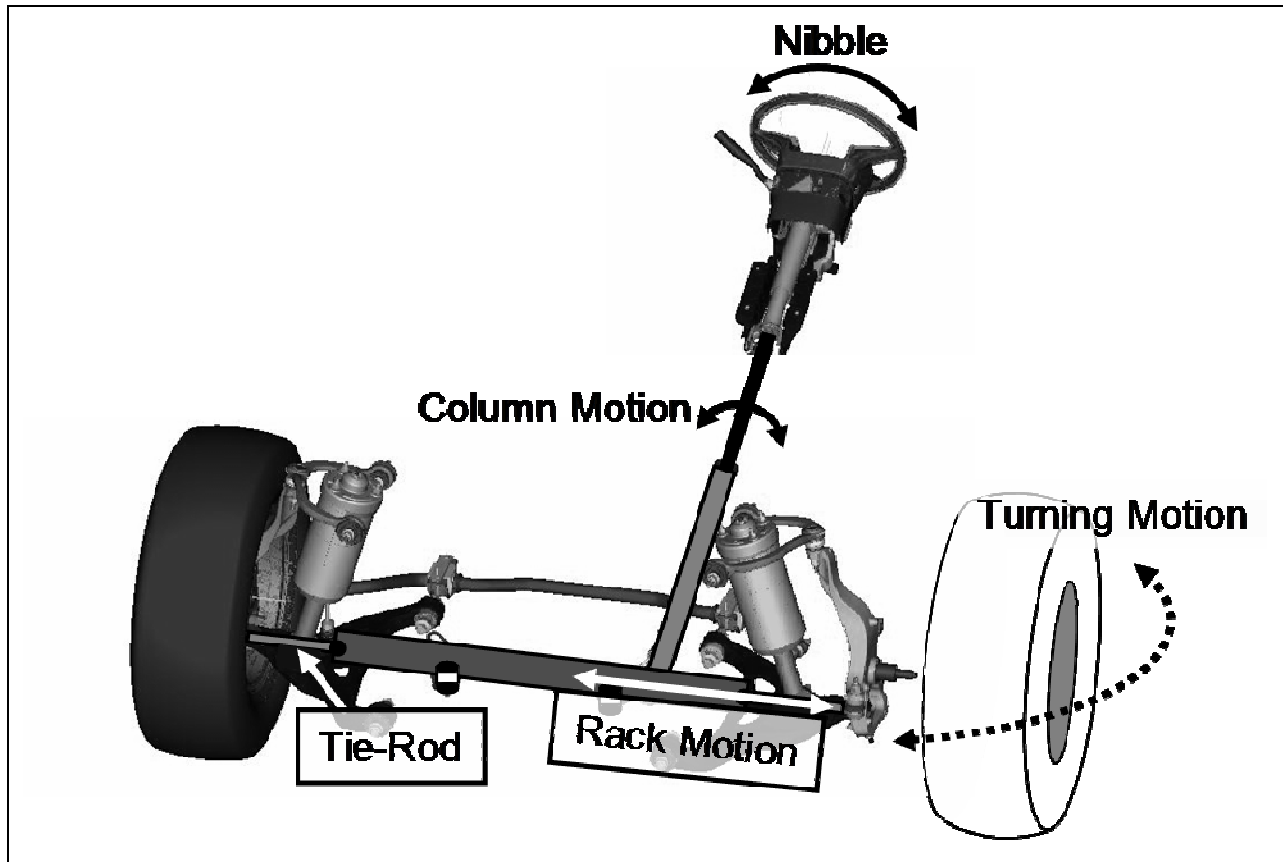


Figure 6.1 Transmission of Nibble

The turning motion causing nibble arises for two main reasons: direct rotation about the wheel spindle, and longitudinal translation of the suspension system. Of course, if the force input on the tire is a moment about the wheel spindle, then the wheel will turn. However, it is not intuitively obvious how longitudinal, or fore-aft, translation of the wheel-strut assembly can cause a similar turning input. The kinematics of this transformation is shown in Figure 6.2. As the wheel moves forward, the control arms force the system to pivot about the bushings located on the frame. Although the wheel never actually rotates about its spindle, a turning motion is sent through the tie-rods due to the steering angle, α , created by the pivoting action about the bushings. For a similar reason, vertical motions of the wheel may also cause a displacement input on the tie-rod and simulate turning. However, through simulations and a kinematic analysis, longitudinal translation was found to be the major cause of turning inputs [25-26].

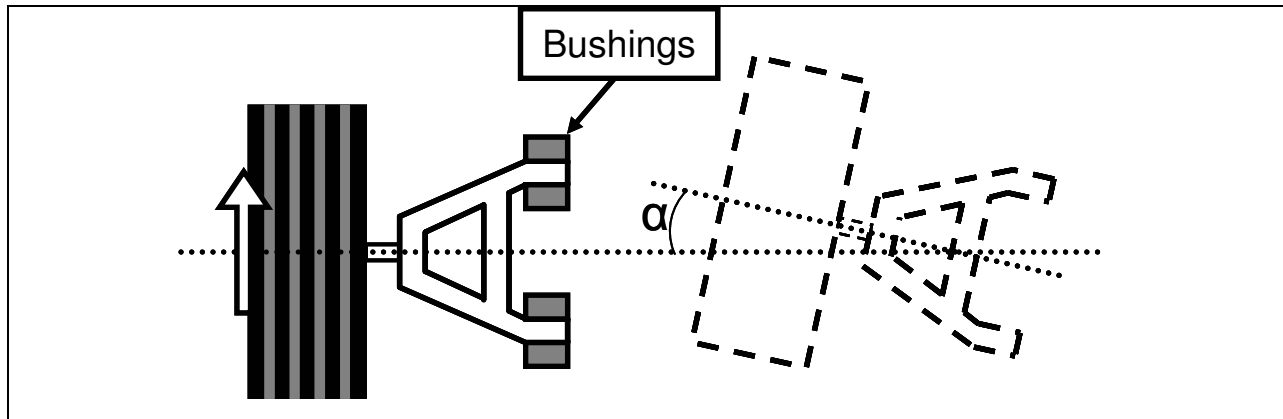


Figure 6.2 Kinematics of Turning Motion Caused by Longitudinal Translation

6.2.2 Sources

The possible sources of the input force at the tire are:

1. Static and dynamic wheel imbalance
2. Tire geometric and material irregularities
3. Brake torque variations (BTV)
4. Self-excited wheel shimmy
5. Road Irregularities

Here, only the more significant factors will be discussed, but substantial information is available for each source [25 - 29]. An obvious force source for nibble and one that is easily reproduced for testing is wheel imbalance. Wheel imbalance is a mass defect of the wheel assembly. Instead of the wheel mass being uniformly distributed, there are areas of mass concentrations about the circumference of the wheel. As the wheel spins, the centripetal forces resulting from this imbalance can either cause longitudinal translation of the suspension (static imbalance), or direct rotation about the wheel spindle (dynamic imbalance). In practice wheel imbalance is not usually a major cause of nibble. In order to generate a moderate amount of nibble vibration, test engineers typically apply an imbalance mass of 30 g to the outer rim of the front tires [25]. However, the industry standard for the minimum accuracy of wheel balancing equipment is 7 g [33], with some manufacturers achieving accuracies of 1 g [34]. Hence, wheel imbalance is not

considered as significant a force source for nibble as tire irregularities or BTV. Nevertheless, because these other sources are more difficult to model and reproduce, wheel imbalance is typically employed to generate nibble under testing conditions.

Tire irregularities are prominent causes of nibble primarily through longitudinal translation of the suspension. Due to non-uniformities in ply wrappings and shape, tires typically apply tangential and radial force variations (TFV and RFV, respectively) to the road as the vehicle is moving. These force variations in turn affect the position of the wheel with respect to the vehicle body. Tangential force variations are generally of more concern than RFV because these forces are applied parallel rather than perpendicular to the road surface. This consequently creates longitudinal motion in the suspension and steering wheel nibble. Like BTV, the forces generated due to TFV may be much higher than those caused by typical wheel imbalances, and therefore is a more significant cause of nibble.

Brake torque variations also cause longitudinal motion of the suspension by inducing a relative displacement between the wheel and the vehicle body. The underlying cause of BTV is variations in the thickness of brake rotors along their circumference. Thermal growth and local spots of high friction due to temperature exacerbate the problem [27]. Essentially, because the material thickness varies along the circumference of the rotor, the brake pressure, and consequently the brake torque, applied by the calipers varies as a function of the wheel rotation. This fluctuation in brake torque causes the longitudinal position of the wheel to oscillate, exciting the longitudinal mode in the suspension and causing nibble. Like TFV, brake torque variation is a complicated issue and cannot be as easily controlled as wheel imbalance. Therefore, although these two phenomena are more important sources of nibble, they are not commonly used to generate nibble under controlled experiments. Additionally, because the primary causes of nibble are not fully understood, previous attempts at reducing nibble have focused on other factors related to its intensity.

6.2.3 Factors Affecting Nibble Severity

In order to reduce the effects of these force sources on the steering system, considerable research has been conducted on the various components that determine the amount of nibble that is transmitted up to the steering wheel [25, 30 – 32]. A list of these factors for a vehicle with McPherson strut suspension and rack-and-pinion steering (Table 6.1) is shown below.

Table 6.1 Factors Affecting Nibble Severity in System Shown in Figure 5.3

#	Factor
1	Effective Wheel-Strut Assembly Mass
2	Caster Offset of Wheel-Strut Assembly CoG
3	Kingpin Offset of Wheel-Strut Assembly CoG
4	Fore/Aft Stiffness of Front and Rear Bushings on Lower Control Arm
5	Fore/Aft Stiffness of Front and Rear Bushings on Upper Control Arm
6	Position of Front and Rear Control Arm Bushings
7	Position of Outer Tie-Rod Ball Joints
8	Position of Inner Tie-Rod Ball Joints
9	Position of Rack Mounts
10	Stiffness of Rack Mounts
11	Friction/Damping in Rack
12	Torsion Bar Stiffness
13	Steering Wheel Moment of Inertia
14	Steering Wheel Radius
15	Transmission Ratio between Rack and Pinion
16	Hydraulic Power Assist Boost Curve Characteristics
17	Hydraulic Damping

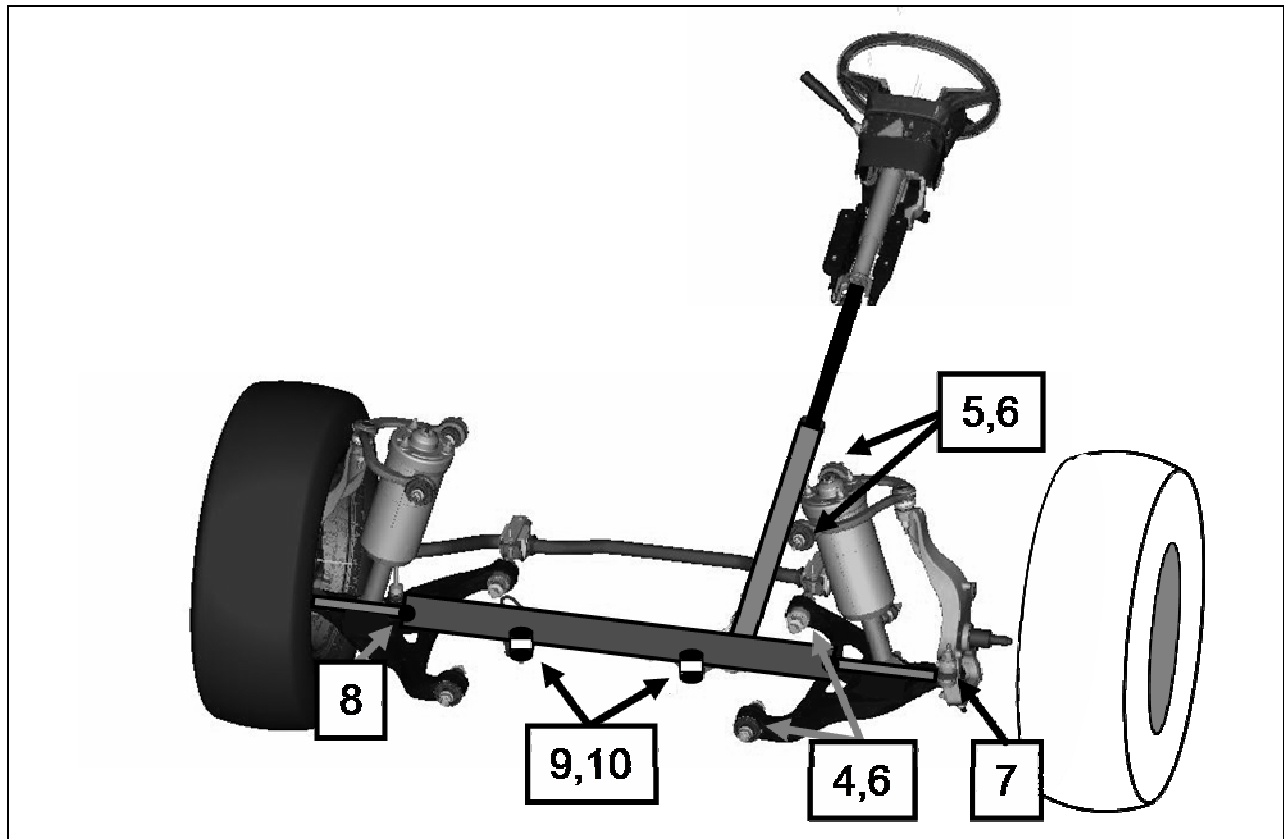


Figure 6.3 Schematic of McPherson Strut Suspension with Rack-and-Pinion Steering

Looking at Table 6.1, it becomes clear why nibble is such a problem in the light truck market. These vehicles usually have large tires and a strong frame to support the loads expected of a truck, meaning the effective mass of the wheel-strut assembly is large. However, the front suspension is kept relatively soft to provide a comfortable ride. This creates a suspension system that is particularly susceptible to resonance vibration in a longitudinal direction. Furthermore, trucks with a rack-and-pinion steering system for improved handling also have lower gear friction than those with a recirculating worm gear, reducing the damping losses in the system. Finally, trucks typically have larger steering wheels than passenger cars, further amplifying the amount of nibble felt by the driver.

Sensitivity analyses have been conducted to identify the most significant of these factors [25, 30, 32], and vehicle manufacturers have adjusted their parameters to achieve the lowest possible nibble amplitudes. However, because each of these adjustments seriously affects the performance of other areas, i.e. handling, ride comfort, safety, packaging, etc., they have been

restricted along with their effect on nibble. For this reason, other solutions are required. Considering the steering system, including the rack-and-pinion, steering column and steering wheel, as a rotational system, it was determined that either the DVL or SAVI could be used to reduce the nibble upstream vibrations without significantly affecting the other aspects of vehicle performance.

6.3 Functional Requirements

The functional requirements of the design were to:

1. **Reduce Steering Wheel Vibration** – The single reason for even considering an alteration to the steering system is to reduce the amplitude of the nibble vibration. There is no hard requirement that needs to be met since the problem is of a subjective nature. However, since vehicle manufacturers will reasonably add an additional element to the steering column only if there a significant benefit for doing so, the author chose to set a 30 % reduction of the nibble amplitude as a requirement.
2. **Transmit Turning Input from Driver** – No matter how much the nibble vibration is attenuated, if the driver does not have control over the vehicle then the device will not be useful. Therefore, a second requirement is that the torque/displacement input from the driver must get transmitted to the rack-and-pinion. This is a binary requirement, without consideration of degree of effectiveness. The degree is covered in the third functional requirement.
3. **Minimize Unsatisfactory Delay or Reduction of Road Feel** – The final requirement is that the device does not cause customer dissatisfaction by negatively affecting the handling performance of the vehicle. This includes introducing an unacceptable time or angular delay between the response of the vehicle and the driver input, as well as an over-isolation of the driver from tangible upstream from the road. In other words, there needs to be some degree of upstream from the tires although the upstream vibration is to be

reduced. Again, this requirement is purely subjective and a quantitative measure could be determined only after designing an initial prototype.

6.4 Constraints

Being a retrofit application, there were several constraints imposed upon the design:

1. **Cost** – The cost per device must be on the order of one dollar.
2. **Manufacturing** – The new technology had to be implemented with a minimal change in the transfer line's core machinery. New processes could be employed, but they must utilize existing equipment within the company so that any change would require minimal capital investment.
3. **Space** – Depending on the chosen location in the steering system for the position of the device, there is a size restriction on the design. The device can not directly interfere with the operation of any other component in the vehicle, and also needs to ensure a certain distance from nearby objects so that the steering column can rotate unimpeded given any assembly errors or part failure.
4. **Environment** – If the device is to be installed in the engine cabin, then the design must also be able to withstand and function under various extremes of environmental conditions. This includes temperature, humidity, salt, dirt, ice, etc.
5. **Stiffness** – There are some hard constraints on the minimum allowable stiffness of the entire column and its components. The device must meet these constraints for both overall stiffness and on-center stiffness, which is the stiffness of the column in the angular range before activation of the hydraulic power assist.

6.5 Design Selection and Optimization

The procedure for determining which design concept to use, the DVL or the SAVI, and what parameters either one should be designed to have so that all functional requirements may be met is as follows:

1. Identify the area or sub-system within the total steering system in which the device will be implemented.
2. Characterize the sub-system dynamics using the rotational system model developed in Chapter 3, and determine the response from external forces or displacements.
3. Choose the appropriate solution method and design strategy based on the functional requirements and constraints.
4. Calculate the required design parameters to achieve the best performance by the procedure described in Chapter 3.
5. Generate the design topology using the modeling techniques for the specific device, described in Chapter 3, to satisfy the design parameters.

6.5.1 Subsystem Identification

Since the only rotational element of the steering system is the steering column itself, the steering column was chosen as the focus of the design area. The steering column is composed of three separate units: the lower shaft, the intermediate shaft and the steering shaft. The steering shaft connects the steering wheel itself and is fully enclosed within an exterior jacket (see Figure 6.4). Therefore, the possible position of the device was focused further to the lower and intermediate shaft, shown in Figure 6.4.

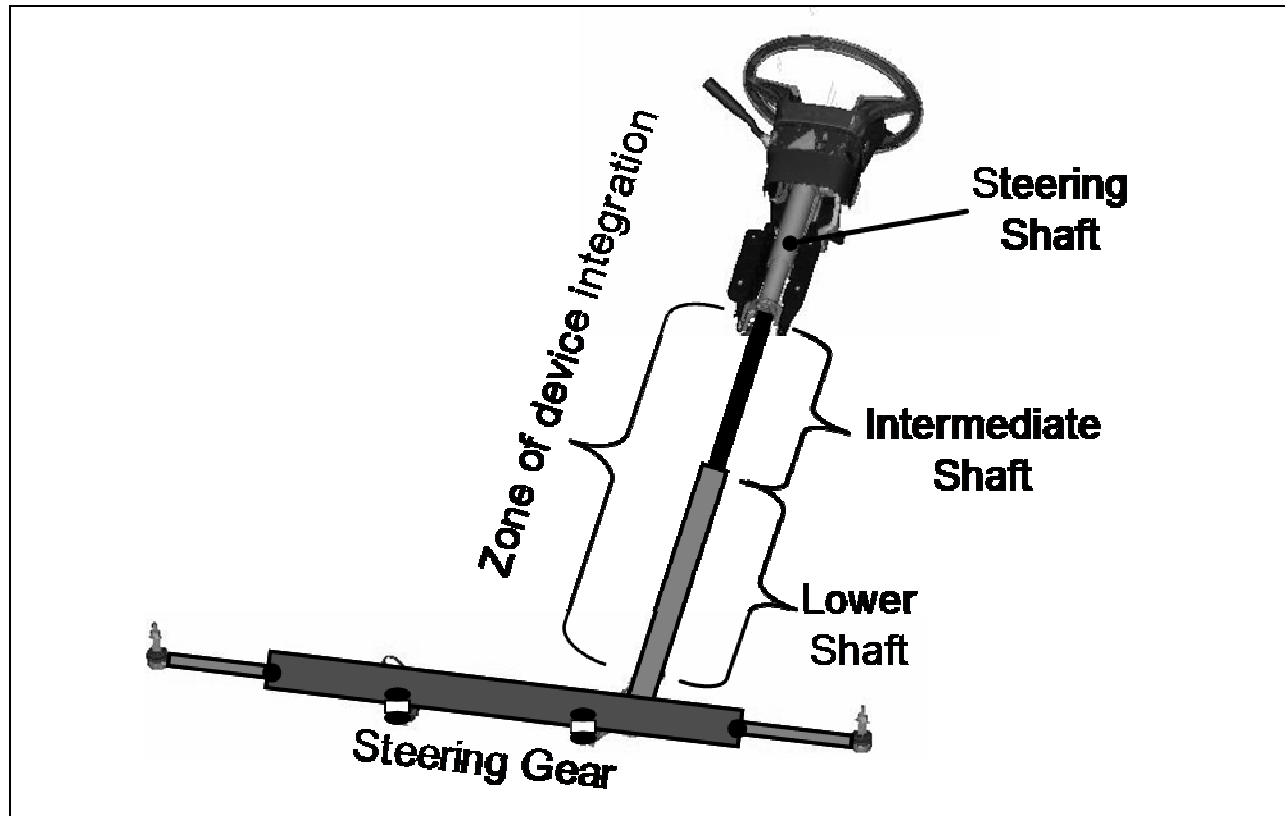


Figure 6.4 Potential Working Space for Design

6.5.2 Characterization of Sub-System Dynamics

Before developing a model of the steering system, certain assumptions about each component needed to be made. Inside the steering gear assembly, between the lower shaft and the pinion, is an element called a torsion bar, which is essentially a compliant torsional spring that activates the valves for the hydraulic power assist. As the stiffness of the torsion bar (T-bar) is in series with the column and is an order of magnitude less than any other column component, the T-bar must be included in the dynamic model. Although the hydraulics system, including the fluid volume, the piston and the pump, was expected to add some stiffness and damping to the system, it was not modeled initially for purposes of simplicity. The influence of the hydraulics on the system would be determined later through experimentation and then used to refine the model. Therefore, the major components that required modeling were the torsion bar, each element of the steering column and the steering wheel. The high rigidity of the rack and its coupling to the

large mass of the suspension elements leads to the assumption that the rack-and-pinion assembly is a rigid support for the torsion bar and the rest of the steering column.

With these assumptions, the steering system may be analyzed. The stiffness of each component of the steering column and the moments of inertia of the lower shaft, intermediate shaft and steering wheel were experimentally measured. This information along with the nominal value of the T-bar stiffness and a calculated moment of inertia for the steering shaft was input into the Matlab® script mentioned in Chapter 3. The corresponding lumped parameter model and the calculated values of the first two natural frequencies and their mode shapes are shown in Figure 6.5 and Table 6.2, respectively.

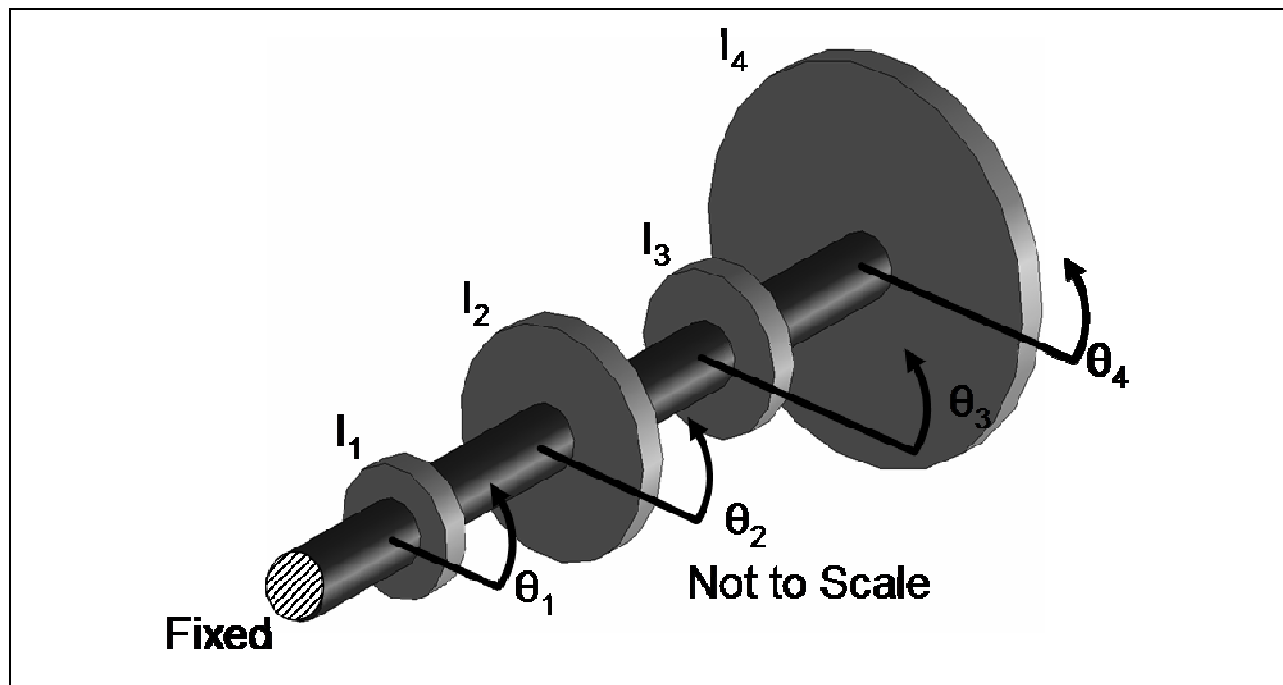


Figure 6.5 Lumped Parameter Model of Steering System

Table 6.2 Calculated Natural Frequencies and Normal Modes

Frequency Order	Natural Frequency (Hz)	Normal Mode Shape
1	5.7	$\begin{Bmatrix} \theta_1 \\ \theta_2 \\ \theta_3 \\ \theta_4 \end{Bmatrix} = \begin{Bmatrix} 0.81 \\ 0.87 \\ 0.96 \\ 1.0 \end{Bmatrix}$
2	160	$\begin{Bmatrix} 99 \\ 92 \\ 32 \\ -1.0 \end{Bmatrix}$

Looking at the results, it is clear that only the first natural frequency is important to consider for determining the response of the system to an input force with a frequency of 13 Hz. Also, since the magnitudes of I_1 through I_3 are two orders less than that of I_4 , this system can effectively be reduced to a one-DOF translational model under support motion, shown in Figure 6.6. Here, the pinion, whose displacement is assumed to be known, was considered to be the support for the rest of the system.

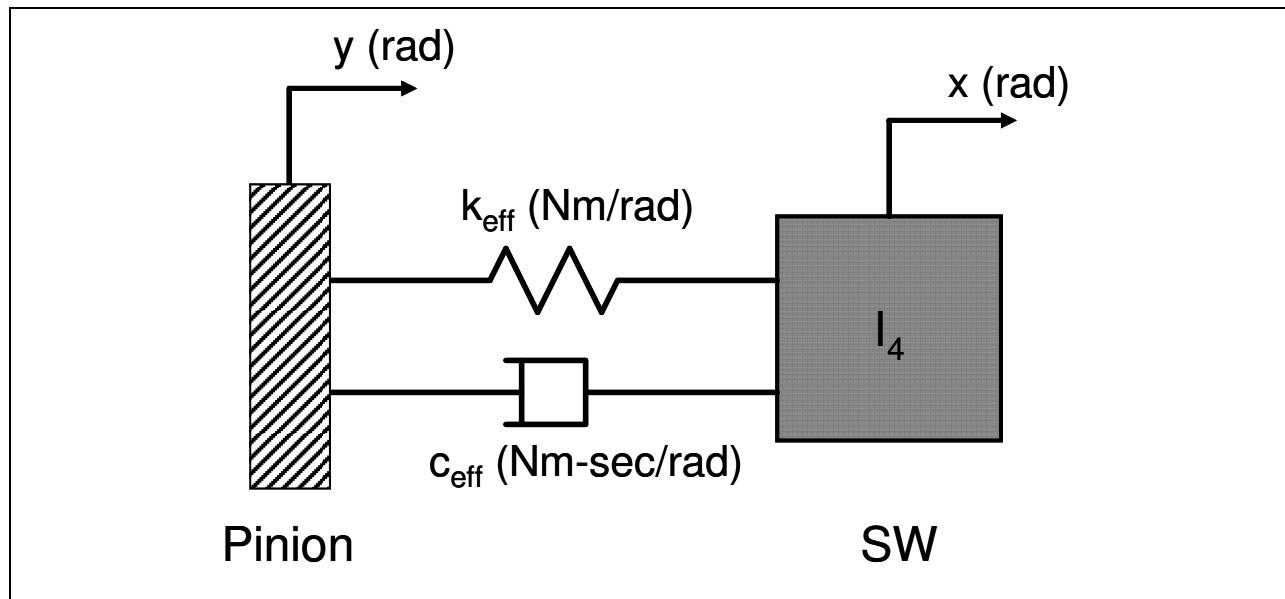


Figure 6.6 One DOF Translational Model of Steering System

The value of k_{eff} is the effective spring constant of the series of springs representing the stiffness of the torsion bar and each shaft component. After calculating the damping ratio of each element in the model from their respective hysteresis curves, the total damping ratio in the system for the first normal mode was estimated as 0.01 from Eq. 2.5. As a first estimate, the frequency response due to support motion of the model shown in Figure 6.6, neglecting the effects of the hydraulics, was calculated and plotted in Figure 6.7.

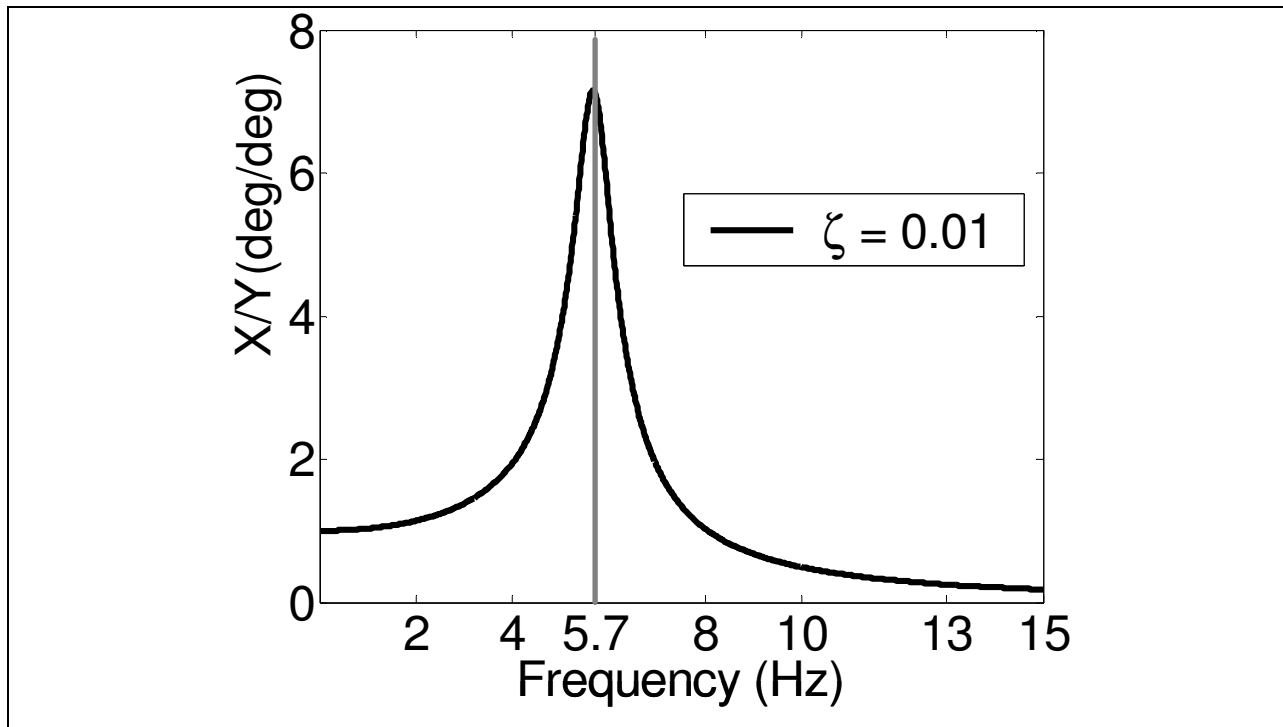


Figure 6.7 Frequency Response of One DOF Model of Steering Column

6.5.3 Choice of Design Strategy

As may be seen from the figure, at an input frequency of 13 Hz, the system is already in vibration isolation. Therefore, adding damping will have a negative effect on the system, and the only two possible methods for reducing the nibble response is to increase the inertia of the steering wheel or decrease the stiffness of the column. This means that the DVL is not a useful design for this application. The SAVI may be used effectively by lowering the natural frequency of the system and pushing the 13 Hz response further into vibration isolation. However, because there is a constraint on the stiffness of the column and a functional requirement to minimize

delay, the exact non-linear stiffness characteristics of the SAVI must be precisely designed. First, a more accurate model of the steering system must be developed, including the effects of the hydraulics. This was done through experimentation.

6.5.4 Design Optimization

Validation of Theoretical Analysis

The two main purposes for performing experimentation are to validate and refine the analysis of the steering system, and to test future prototypes to gauge their performance once they are finally installed in an actual vehicle. To this end, the full front-end of the subframe of a light-duty pickup truck, including all the components of the steering system, was assembled and fixtured to a bedplate, as shown in Figure 6.8.

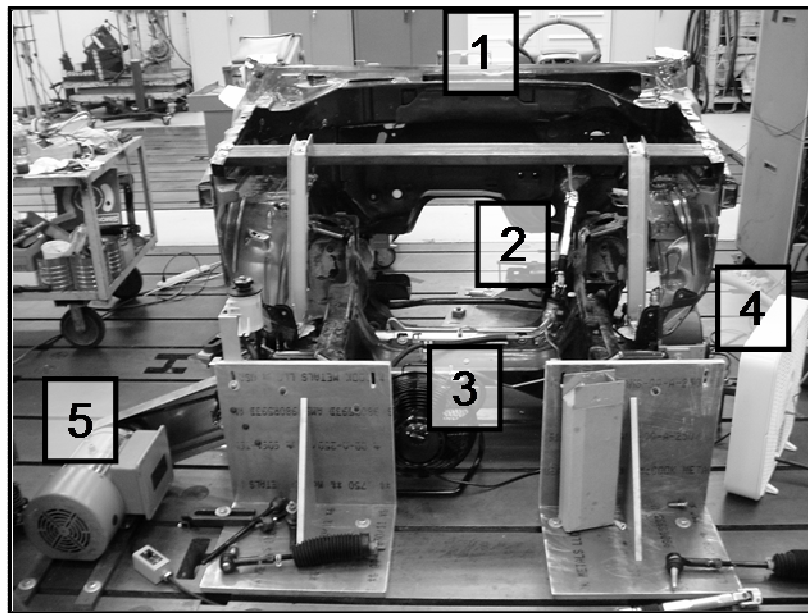


Figure 6.8 Full Steering System Test Setup

Each of the major components is labeled as follows:

Table 6.3 Labeling of Steering System Elements

Label	Steering System Component
1	Steering Wheel
2	Steering Column
3	Rack-and-Pinion Assembly
4	Electrodynamic Shaker
5	Hydraulic Pump for Power Steering

An electrodynamic shaker directly coupled to a tie-rod on one side of the rack provided a sinusoidal force input simulating the force sources on the tire discussed earlier. The entire steering system was mounted as it would be in an actual vehicle, and the hydraulic power assist was powered by an external motor and fully operational. After several modifications were made to ensure that the sub-frame structure adequately supported the steering system and did not obfuscate the vibration measurements with vibrations of its own, frequency response testing of the steering column was performed.

The procedure was to input a sinusoidal force of constant frequency using the shaker. Bruel and Kajer 4506 and PCB 356B08 accelerometers were placed on the rack and at both the 12 and 6 o'clock positions on the steering wheel. The Fourier transforms of the accelerometer responses were measured using a HP 35670A and a Siglab 20-42 Dynamic Signal Analyzer and averaged ten times. The RMS value of the averaged data for each accelerometer was recorded, and the process was repeated for the next frequency. While this took a long time, it was necessary because random or chirp signals could not be properly generated due to some problems with the electronic equipment. Using the recorded data, a frequency response of the steering system between the pinion and the steering wheel, shown in Figure 6.9, could be approximated.

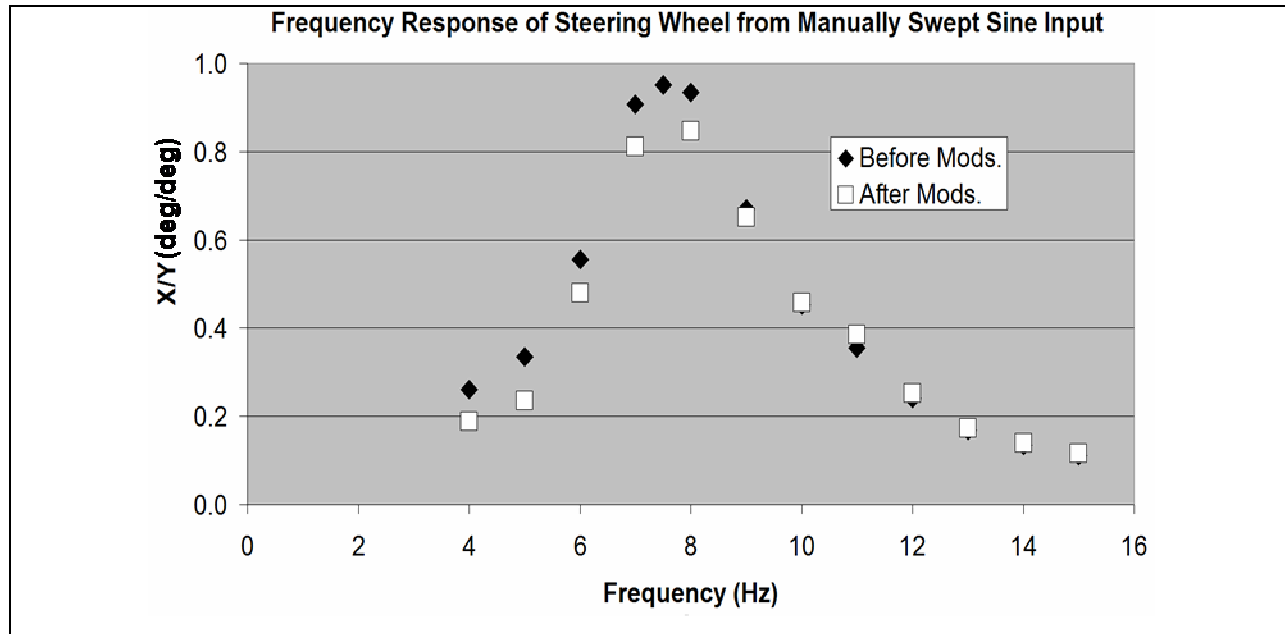


Figure 6.9 Frequency Response of Steering System Before and After Rig Modifications

The first major difference between this plot and the one in Figure 6.7 is that the resonant frequency is not the same. Here, the resonant frequency is at 7.5 Hz, not 5.7 Hz. In addition, although the shapes of the plots are similar in both figures, the magnitude of the amplitude ratios is significantly different. According to the testing results, even at resonance the amplitude ratio does not exceed one! After further investigation of the system, it was determined that this scaling difference was an effect of the hydraulic fluid being pushed into the T-bar chamber by the piston on the rack. The increased natural frequency and damping ratio, which was estimated as 0.18, in the actual system compared to the predictions was also due to the added stiffness and damping from the hydraulics. Still, the conclusions gathered from the testing are the same from the earlier analysis; the best way to reduce the nibble vibrations is to reduce the natural frequency of the system.

Parameter Selection of SAVI

Now that the SAVI has been selected as the design solution, the next step is to determine the best combination of parameter values. The two competing functional requirements that need to be balanced are the percent reduction of the nibble amplitudes and the delay introduced in the handling. The major parameters that affect these performance metrics are the small amplitude

torsional stiffness of the SAVI and the angular deflection at which the break point in the torsional stiffness occurs. An optimization study was conducted in ADAMS® to choose the values for these parameters which resulted in the best pairing of percent reduction and delay. Since the nibble performance can also be improved by adding inertia to the steering wheel, the moment of inertia of the steering wheel was also considered variable in the study. A table of the parameters and their ranges is shown below.

Table 6.4 Parameters Varied in Optimization

Parameter	Value Range
Small Amplitude Stiffness	0.6 – 5.4 Nm/deg
Stiffness Transition Point	1.0, 2.0 deg
Moment of Inertia of Steering Wheel	0.045 – 0.058 kg*m ²

Looking at the available areas to install the SAVI, it was decided that it would be easiest to test the concept if the SAVI could replace a portion of the intermediate shaft called the rag joint. Once the optimization is performed and its predictions validated via the test rig described earlier, then the performance of the SAVI anywhere else in the zone of integration may be confidently predicted from the same ADAMS® model. Moreover, the stiffness of the intermediate shaft does not need to be retested since the stiffness of the SAVI is an order of magnitude less than the other elements in the column. Hence, the intermediate shaft stiffness is dominated by the SAVI stiffness and may be approximated as equal to it.

In order to perform the optimization, two ADAMS® models were created – one to calculate the percent reduction and the other to calculate the delay. For the percent reduction, a one-DOF lumped parameter model, shown in Figure 6.10, was created in that had the same natural frequency and damping ratio as the real steering system, shown in Figure 6.9. This was accomplished by increasing the stiffness and damping of the torsion bar to account for the effects of the hydraulics. Of course, this method for predicting the response of a non-linear system is an approximation, which was validated through experimentation. A displacement input was applied to the pinion at a frequency of 13 Hz and the ratio of the displacement of the steering wheel

versus that of the pinion was calculated. Then the stiffness of the SAVI could be substituted for that of the intermediate shaft, and the ratio of displacements again calculated. The percent reduction of the nibble amplitude would then be the percent difference between the displacement ratio of the original column and the one implemented with the SAVI. However, this same process would have to be repeated for every value of the moment of inertia of the steering wheel, leading to a large number of simulations.

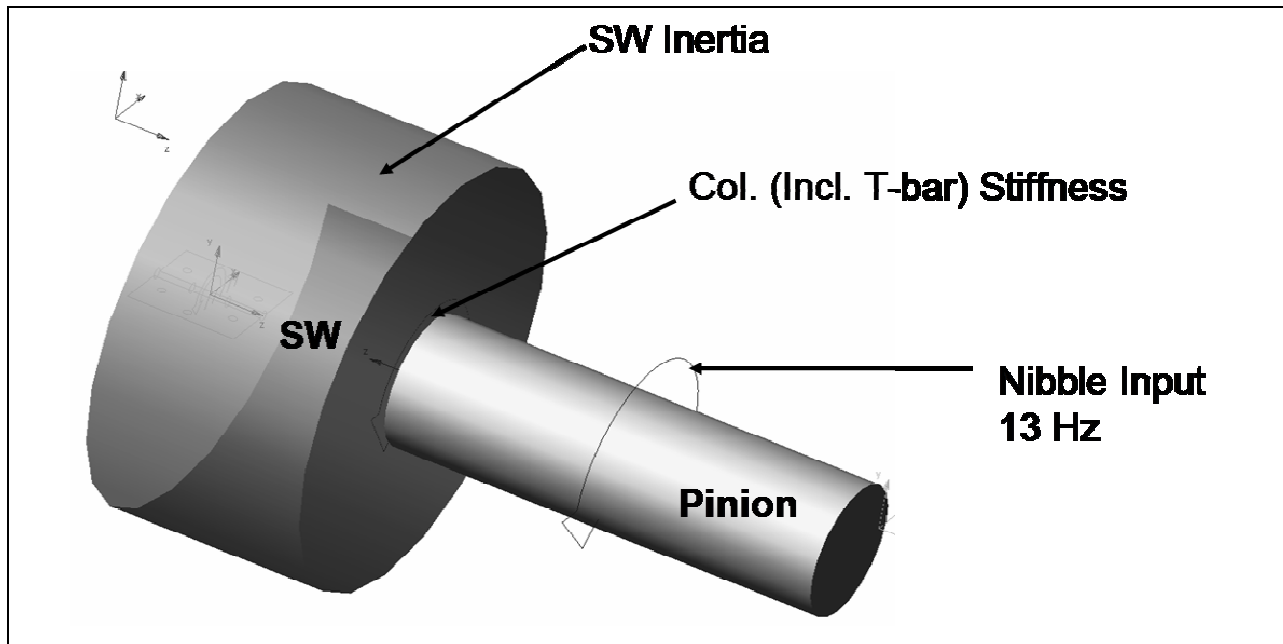


Figure 6.10 One-DOF Rotational Model in ADAMS

Instead, since the displacement ratio of the steering wheel versus the pinion is a function solely of natural frequency, bounds on the natural frequency of the steering system were calculated from the parameter ranges in Table 6.4 as follows:

$$\omega_{n,\min} = \sqrt{\frac{k_{eff,\min}}{I_{4,\max}}} = 21.4 \text{ rad/s} \quad (6.1)$$

$$\omega_{n,\max} = \sqrt{\frac{k_{eff,\max}}{I_{4,\min}}} = 48.4 \text{ rad/s} \quad (6.2)$$

By varying only the natural frequency of the ADAMS® model, a percent reduction may be calculated for any combination of SAVI stiffness and steering wheel moment of inertia through linear interpolation. It is important to note that the transition point of the SAVI stiffness was not considered in calculating the percent reduction because it was assumed that it would occur beyond the maximum deflection of the SAVI caused by the nibble vibration. A sample of the possible percent reductions is shown in Table 6.5.

Table 6.5 Percent Reduction (%) of Various Combinations of Stiffness and Inertia

Stiffness of SAVI (Nm/deg)	Inertia of SW (kg*m ²) * 10 ⁻²						
	4.5	4.6	4.7	4.8	...	5.7	5.8
1.00	78.1	78.8	79.4	79.8	...	81.8	81.9
1.50	70.0	70.7	71.3	71.9	...	76.9	77.5
1.90	64.8	65.7	66.6	67.5	...	72.8	73.3
2.40	58.2	59.4	60.6	61.8	...	69.0	69.6
2.90	52.7	54.0	55.3	56.5	...	65.5	66.2
3.40	48.3	49.7	51.0	52.3	...	62.3	63.2
3.90	44.7	46.1	47.5	48.8	...	59.1	60.1
4.40	41.0	43.0	44.6	45.9	...	56.4	57.5
4.90	37.5	39.5	41.5	43.4	...	54.2	55.2
5.40	34.4	36.5	38.5	40.5	...	52.3	53.3

For the delay calculation, a two-DOF ADAMS® model, shown in Figure 6.11, was created. However, before any calculations could be made, this delay had to be quantified. For a vehicle with power steering, it was assumed that the delay in the handling could be determined by the delay between the turning input supplied by the driver and the activation of the hydraulics. According to boost curve for the particular vehicle being tested [35], the pressure applied on the hydraulic piston connected to the rack saturates when the deflection of the T-bar reaches about 3 degrees. Assuming that the rack does not move until the hydraulics are activated, the pinion is fixed in the model, and the angular delay is calculated as the amount of rotation of the steering wheel necessary to cause a 3 degree deflection of the T-bar. It may seem important at first to also include the time delay to cause a 3 degree deflection. However, even for the lowest stiffness value of the SAVI, for velocity input of 96 °/sec, the time delay never exceeded 14 ms. Being a reasonable turning input for lane changes of a truck moving at 70 MPH, the angular delay was considered a more important indicator of consumer dissatisfaction.

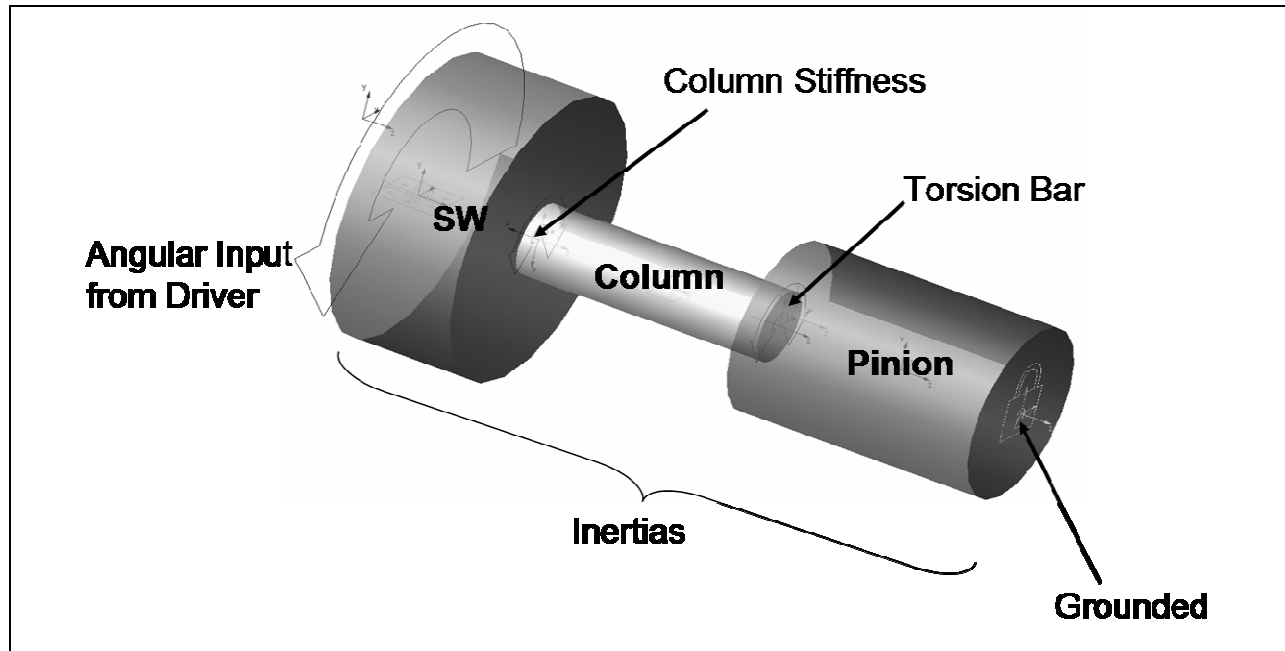


Figure 6.11 ADAMS Model for Calculating Angular Delay

To calculate the delay, an angular input is applied to the steering wheel and adjusted until the displacement of the column shown in Figure 6.11 is measured as 3 degrees. Since the displacement of the steering wheel is defined, its moment of inertia does not affect the angular delay. Therefore, only the SAVI stiffness and the angular position of the transition point were adjusted in the model. The results are shown in Figure 6.12. It should be noted that for all cases the column stiffness once the stops engage on the SAVI was, as a conservative estimate, set to the stiffness of the original, unmodified column (5.3 Nm/deg). Also, the transition between the low and high amplitude stiffness of the column always occurred within 0.5 deg.

Looking at Figure 6.12, it is clear that for values of the SAVI stiffness below 4.0 Nm/deg the position of the stiffness transition point is an important parameter for the delay of the column. Both the amount of delay in the column and the sensitivity of the delay with respect to the SAVI stiffness are affected by the angular position of engagement of the stops. Note that the delay in the original, unmodified column is 3.75 deg, which is approached as the SAVI stiffness increases. Although positioning the stops at 2 deg provides inferior delay performance, this made fabricating and assembling the prototype for proof-of-concept testing much easier. Therefore, the transition point of the SAVI stiffness was chosen to be placed at 2 deg.

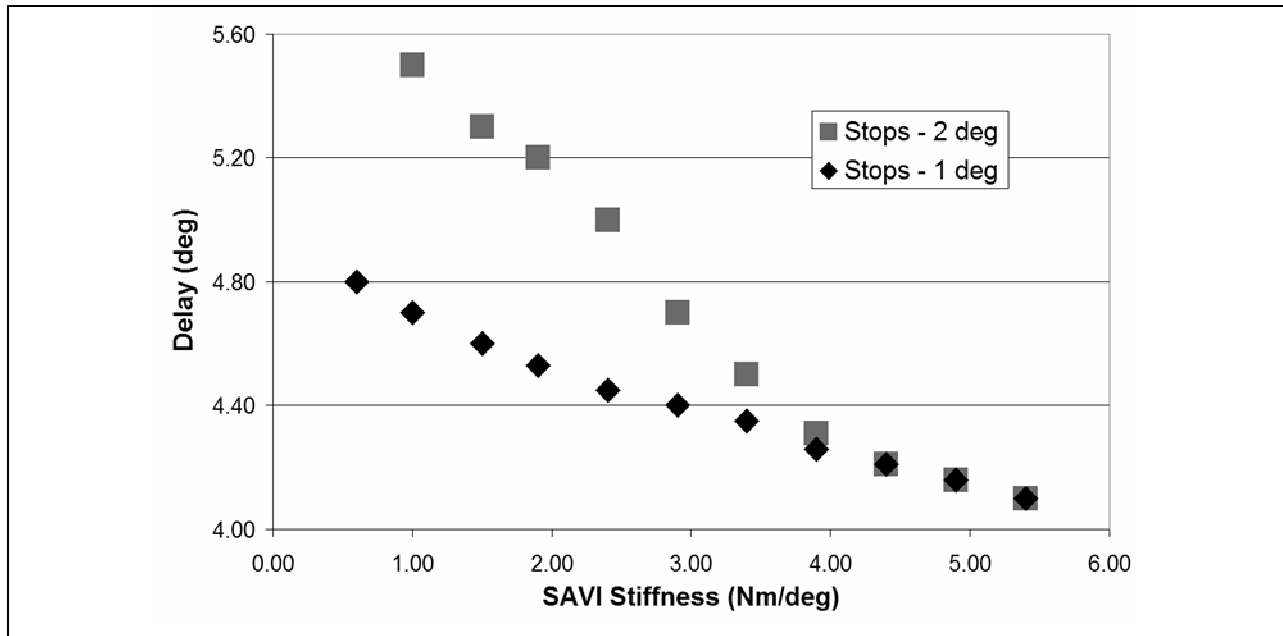


Figure 6.12 Plot of Angular Delay vs SAVI Stiffness for Transitions at 1 and 2 deg

Using Table 6.5 and Figure 6.12, a surface plot of the percent reduction of the nibble amplitude as a function of the angular delay and steering wheel inertia was generated, shown in Figure 6.13. From this plot, it is easy to visualize the relationship between the competing functional requirements of the percent reduction and angular delay. In addition, if one chooses desired values for each of these requirements, the design parameters for the steering wheel inertia and SAVI low-amplitude stiffness may be determined.

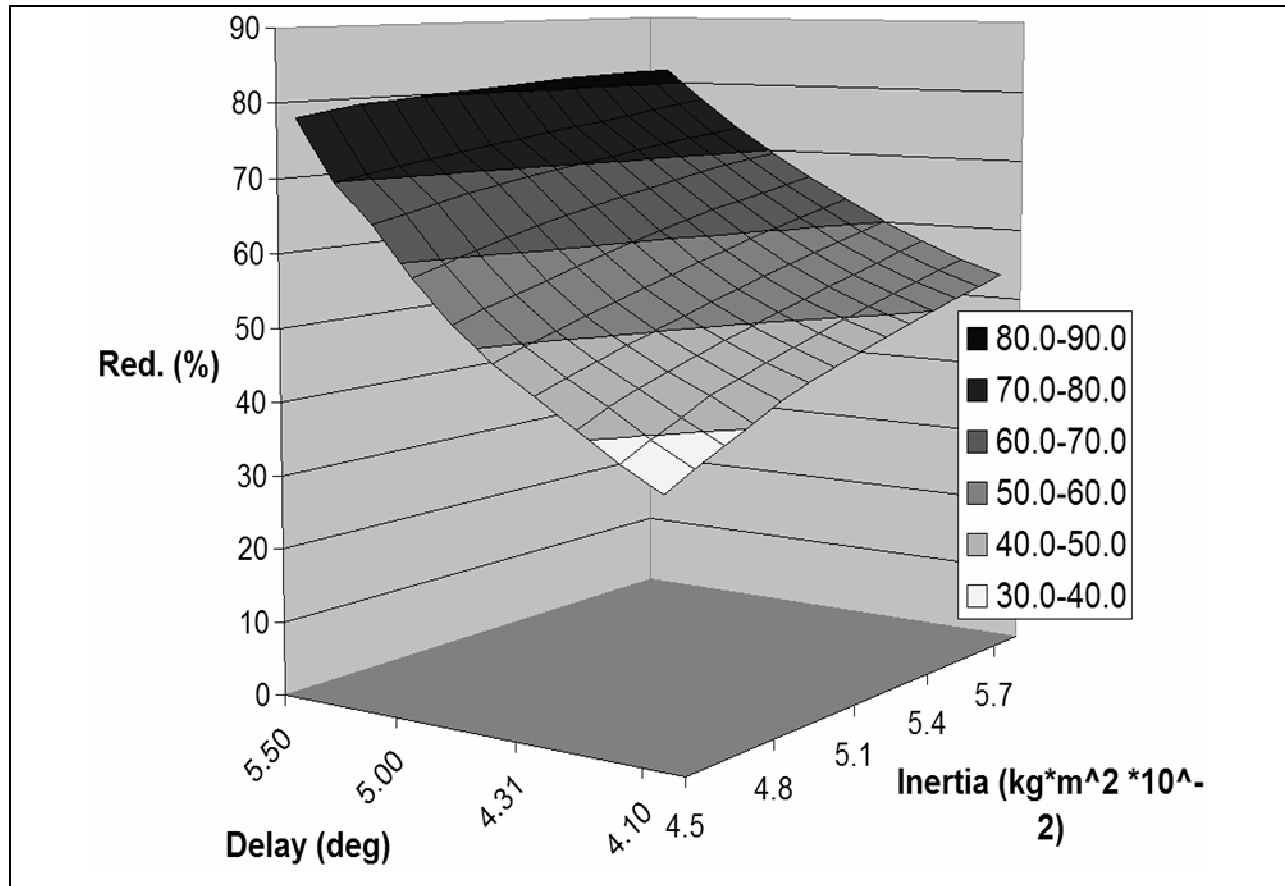


Figure 6.13 Surface Plot of Percent Reduction vs Delay and SW Inertia for Stops at 2 deg

For example, if at least 60 % reduction of the nibble amplitude is desired, looking at Figure 6.13, depending on the steering wheel inertia, the angular delay of the column may be somewhere between 4.6 and 5.2 deg. Then, either the acceptable amount of delay or steering wheel inertia may be chosen. For our purposes, it was not clear what amount of delay would be acceptable, yet for safety reasons, adding more inertia to the steering wheel was not desirable. Hence, 0.045 kg*m² was chosen as the steering wheel moment of inertia, requiring a SAVI that causes a delay of about 5.2 deg. Referring to Figure 6.12, for stops placed at 2 deg, this corresponds to a SAVI stiffness of about 1.9 Nm/deg. The selection of design parameters and their predicted effects on the performance of the column are shown in Table 6.6 and Table 6.7, respectively.

Table 6.6 Selected Values for Design Parameters of SAVI and Column

Parameter	Selected Value
Small Amplitude Stiffness	1.9 Nm/deg
Stiffness Transition Point	2.0 deg
Moment of Inertia of Steering Wheel	0.045 kg*m ²

Table 6.7 Predicted Performance of Steering System with SAVI

Performance Metric	Predicted Value
Percent Reduction of Nibble Amplitude	64.8 %
Angular Delay in Handling Response	5.2 deg

It may seem more efficient to use a surface plot of the percent reduction vs SAVI stiffness and steering wheel inertia to determine what design parameters to use. This way, in the above example, the SAVI stiffness could be found directly from Figure 6.13. In fact, the data may be represented in a multiplicity of ways, all of which may be more convenient for certain situations. In the future, once the handling performance is officially quantified, design engineers will base parameter choices on all the trade-offs inherent in the system, including percent reduction, angular delay, and necessary steering wheel inertia. Therefore, it is anticipated that Figure 6.13 as shown will be a more useful representation of the possible performance of the steering system.

Once the design parameters for the SAVI were selected, the device was designed and fabricated as discussed in Chapters 2 and 4. The next section will cover the various experiments performed to validate the performance data predicted above.

6.6 Steering System Performance Verification

6.6.1 Rig Testing

Before the prototype was tested in an actual vehicle, the percent reduction performance was measured using the steering system rig shown in Figure 6.8. The same procedure was used to test the steering system with the rag joint replaced by the SAVI as was used to test the original

column. The frequency response of the SAVI was then compared to the average measured response of the original column. One such comparison is shown in Figure 6.14.

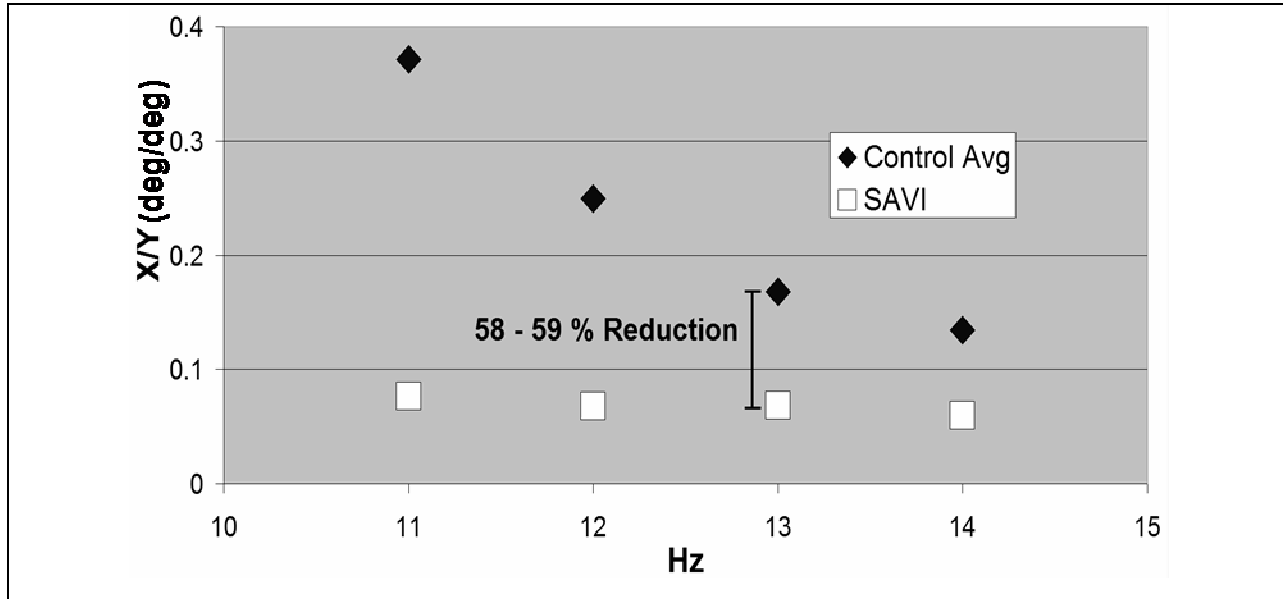


Figure 6.14 Comparison of Frequency Response between Control Average and SAVI

From two frequency response tests of the steering system with the SAVI, the average percent reduction at 13 Hz from the average control test of the original column was calculated as 58.8 percent. The average percent reduction from a frequency response within one standard deviation of the control was calculated as 57.6 percent. Therefore, it is expected that in a vehicle test the percent reduction due to the SAVI will be at least about 58 percent. Linearly interpolating the data from Table 6.5, a SAVI with a stiffness of 1.96 Nm/deg was predicted to produce a percent reduction of 59.0 percent.

6.6.2 Vehicle Testing

The prototype of the SAVI was then installed and tested in a production light-duty pickup truck. As a vehicle's sensitivity to nibble varies due to air temperature, tire pressure, road surface conditions, etc., it is necessary to perform a control test with the original steering column installed in the vehicle. Afterwards the SAVI prototype may be installed, and the same test run to find the percent reduction.

As stated earlier, wheel imbalance is typically used to study nibble and was used as the excitation force for this testing. Imbalance masses of 30 g were placed on the outer rims of each front wheel. The tire pressure for each front wheel was also purposely offset, changing the effective diameter of the tire and ensuring that the phase of rotation for each tire would slowly vary. The vehicle was then driven on a private test track straight-ahead at a constant speed and the acceleration of the steering wheel was measured by two accelerometers clamped to the 12 and 6 o'clock positions. Their outputs were averaged real-time and the peak averaged measurement was recorded for each vehicle speed. The vehicle speeds selected for testing were 60, 65, 70, and 75 MPH, which correspond to wheel angular frequencies of 11, 12, 13, and 14 Hz, respectively, for that vehicle. The results for both the control and SAVI test are shown in Figure 6.15.

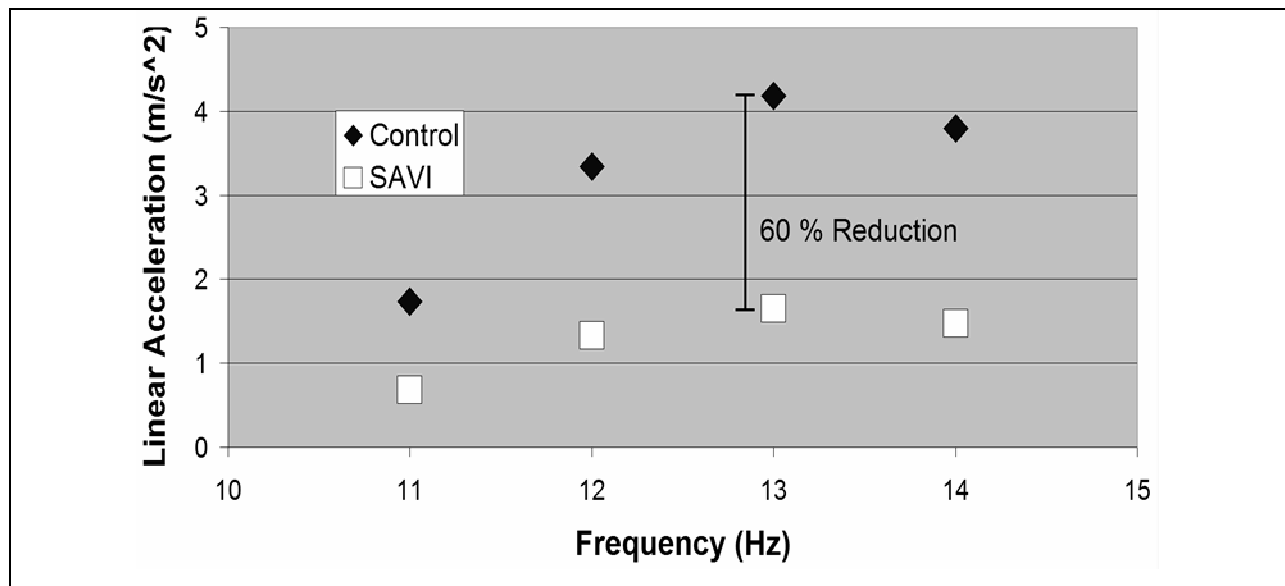


Figure 6.15 Peak Value of Linear Acceleration of SW Accels vs Measured Excitation Frequency for Imbalance Testing

For both the control and SAVI tests, each speed was tested several times and the measured steering wheel acceleration was averaged. From this data, it was observed that the SAVI prototype provided an average percent reduction of 60 percent. Extremes were estimated by comparing the steering wheel response within one standard deviation for both the control and

SAVI tests. Hence, the possible percent reductions within one standard deviation of the data are 54 – 66 percent.

After testing was completed, the SAVI was inspected and disassembled, and the torsional spring checked for any signs of yielding. Not seeing any indications to the contrary, it was concluded that the stop engagement mechanism adequately prevented the torsional spring from yielding during the vehicle testing. This indicates that the angular deflection of stop engagement occurs before the yield point of the spring, which, according to the experimentation described in Chapter 5, occurs at 2.3 degrees. Hence, this implies that it was possible to assemble the SAVI by hand with a suitable gap in the engagement mechanism providing no more than 2 degrees angular displacement.

6.7 Performance Review

Based on the testing of the proof-of-concept prototype, the results compared with the theoretical predictions are summarized below:

Table 6.8 Performance of SAVI Prototype

Performance Metric	Measured Value	Predicted Value
Percent Reduction	60 %	64 %
Handling/Angular Delay	Satisfactory	5.16 deg

From the results of the experimentation, the SAVI effectively attenuates the nibble vibration in the steering wheel. In a vehicle, the SAVI provides a 60 % reduction of the nibble amplitude over the original, unmodified column, which is also within 6.5 % of the predicted value. The angular delay in handling performance was not tested for several reasons: (1) the equipment available at Ford was not capable of making this measurement, (2) once the stiffness of each element in the column is experimentally measured, the delay may be rapidly calculated, and (3) customer satisfaction for handling performance has not yet been quantified.

Recall, that the angular delay metric for the handling performance was simply chosen as a representative functional requirement for design purposes, and is not an accepted metric by the automotive industry. Instead of a quantified performance metric, the automotive industry uses a subjective rating system to evaluate handling performance. Since any experimental validation of angular delay is, therefore, irrelevant to their performance criterion, the delay was not directly observed. While an official performance evaluation was not performed, the test driver of the vehicle used to measure the percent reduction produced by the SAVI did state that he could not detect any difference between the handling with or without the SAVI installed in the vehicle [36]. Of course, this is a preliminary evaluation, which needs to be officially confirmed.

6.8 Future Work

The primary focus for this case study was to determine the general capabilities of the CVA concept. Therefore, the following design decisions made for the proof-of-concept prototype may need to be reevaluated for the final design:

1. Replacing the rag-joint with the SAVI
2. Selection of low-amplitude stiffness design parameter
3. Selection of stiffness transition in the SAVI at 2 deg displacement
4. Topology of SAVI and assembly of device with stops
5. Fabrication process of prototype

All of these choices were made in order to simplify the design and implementation of the initial prototype so that the performance of the concept could be tested. For legacy and performance reasons, it may not be desirable to replace the rag-joint with the SAVI. Although this is the most convenient location for the device, there are other alternatives. Depending on the severity of the stiffness constraints on the steering column, the low-amplitude stiffness of 1.9 Nm/deg may not be acceptable. Positioning the transition point for the SAVI stiffness at 1 deg will provide better performance and may still be feasible and cost-effective. The overall design of the SAVI and its integration with the stops (see Chapter 4) may be improved. Furthermore, the fabrication process described in Chapter 4 is also not recommended for large-scale manufacturing.

In addition, the handling performance of the vehicle with the SAVI installed has not yet been officially evaluated. To this end, the author recommends that the handling performance be correlated to a quantifiable design metric.

Although there are still some important modifications and evaluations left to be made, this paper has set the groundwork for all these changes. In Figure 6.13, similarly to how the delay may be directly related to the SAVI stiffness, the same may be done for the total column stiffness. Therefore, the performance of the SAVI may be predicted from the total column stiffness and steering wheel inertia only, allowing for any type of device to be installed anywhere in the column. This means that as long as the final device is still essentially a non-linear spring, the modeling described above can still be used to predict the performance of the SAVI for any design. Moreover, even though the transition location of the SAVI stiffness is a critical parameter, any change will not affect the percent reduction performance as long as the stops do not engage within the nibble vibration amplitude. Given manufacturing tolerances and the size constraints within the vehicle, the minimum possible stop position is expected to be 1 deg, for which the delay has already been modeled.

Additionally, Ford may use the angular delay as a handling performance metric. If subjective ratings are correlating to this metric, then Figure 6.13 may be used directly to satisfy the functional requirements. Preliminary verifications of handling performance may be made simply by measuring all column component stiffness values and calculating the resulting angular delay. Of course, this could be followed by a subjective check of the handling. Despite these recommendations, the SAVI design seems promising because of its excellent attenuation performance and initial satisfactory subjective evaluation of handling.

CHAPTER

7 CONCLUSION

A preliminary study of two types of Compliant Vibration Attenuators (CVA) has shown that there is a potential for a large performance advantage over existing vibration reduction devices. The primary difference between a CVA and conventional modular mechanisms is that a CVA applies unidirectional vibration attenuation properties directly into the load path of rotational power transmission systems. Furthermore, since a CVA is an individual component separated from the existing components in the original system, and designed to carry the torque load of such a system, there is a minimal effect on the primary function of the system with the inclusion of the CVA. This allows for more efficient and effective vibration attenuation performance with little cost in performance.

This chapter presents the main research goals and accomplishments of the paper, followed by a discussion of the impact of CVA's in both academia and industry. The chapter will then close with concluding remarks made about what remains for the future.

7.1 Research Goals and Accomplishments

The major research contributions provided by this thesis are in the answers to the following questions:

1. What designs are well-suited to create a low-cost CVA that can transmit a desired torque input and reduce an undesirable vibration input? What are the associated trade-offs or relationships between these two functions?
2. How will the load path of the system interact with these designs, and what are the implications of the changes on the kinematics and dynamics of the system?

3. What are the practical issues regarding the design process, fabrication and implementation of these devices?
4. How will a CVA be chosen for a particular vibration problem? What modeling techniques are necessary to select a CVA design, determine its dimensions and predict its performance in a rotational system?

7.1.1 Best Design Strategies and Associated Trade-Offs

The two best strategies for reducing vibrations in a rotational system through a CVA were determined to be the use of a non-linear spring and viscoelastic damping. A non-linear spring was chosen as the principal method because of its ability to isolate the system from low-amplitude vibrations while transmitting larger amplitude torques. Vibration isolation is possibly the most effective method for reducing vibrations in a system, as long as there is some room for modification of the overall stiffness of the system.

Viscoelastic damping was chosen as a countermeasure to the non-linear spring because of its relatively good vibration reduction performance compared to its effect on the general performance of the existing system and its cost. Depending on the initial level of damping in a mechanical system, adding more damping can drastically reduce resonant vibrations. Furthermore, damping is a property wholly separate from stiffness and mass, which are typically controlled in the design of the rotational system. Therefore, adding damping to a system often has little to no effect on its primary function. Finally, viscoelastic materials and design methods are very economical and convenient ways to add damping to a system. Given the fact that most mechanical vibration problems are a result of resonances, damping is a highly useful alternative to a non-linear spring in case the constraints on a system preclude its use.

Of course, there are still fundamental trade-offs to be considered when utilizing either of these technologies in a CVA. The major concern for a non-linear spring used to isolate a system from its surroundings is determining when too much isolation becomes a negative effect. By differentiating between the intended input of the system and the undesirable vibrations through

the relative size of their amplitudes, a non-linear spring can partially avoid this issue. Besides limiting the scope of its application, this property of non-linear springs also creates a complication in determining where to place the transition point of the non-linear stiffness profile. A balance must be made to ensure that the vibrations are properly isolated and the negative effects the low-stiffness has on the primary function of the system are kept to a minimum.

The same reasons why damping is such an interesting choice for use in a CVA are also the underlying design issues for this particular technology. Viscoelastic damping is very often placed in a system as an afterthought in the form of an external CLD treatment. By placing the damping material directly in the structural load path of the system, far greater vibration attenuation performance is possible. However, a balance of damping potential and strength must be found. On one hand, if the VEM was made to absorb the full load of the system, then the strength of the system as a whole could be limited. On the other hand, if the VEM were removed from the load path then there would not be much of a difference between the device and conventional damping approaches. Furthermore, by purposely splitting the load between the VEM and traditional engineering materials, more design versatility may be achieved, allowing for greater application potential.

7.1.2 Distribution of Load Path and its Implications

The effects of distributing the load path in a CVA using damping technology have already been discussed because of their close relationship with the limitations of the design. For a CVA composed of a non-linear spring, the way in which the load path interacts with the device has many effects on the system and the device itself. As in the case of damping, there is a trade-off between strength and performance. However, this trade-off more directly affects the strength of the device and not that of the system. This is because the two paths for the load in a non-linear spring may be fully decoupled, whereas in the damping case, they cannot. Even though the load may be absorbed primarily through the elastic portion of the damped CVA, this part of the device is still coupled to the VEM material, which will absorb some of the load similar to the way a conventional damping treatment performs.

In the case of the non-linear spring, two separate components of the device may be used to absorb different levels of torque. In fact, the same component that causes the transition in stiffness may be used to protect the weaker element from larger loads. This added functionality of course also creates competing requirements between prevention of spring failure and proper dynamic performance. As long as this relationship is considered in the design of the CVA, the device should be able to accomplish both goals.

7.1.3 Practical Issues Regarding Fabrication and Implementation

Several lessons were learned about the design and capabilities of CVA's through their fabrication and implementation. A significant advantage of a CVA using a non-linear spring is that it may be very simple to build and integrate with an existing system. Due to the ability to separate the functionality of the different individual components, sections of this form of CVA may be built in parallel with one another, saving valuable design time. This saved time allows for more rapid prototyping and testing leading to more developed designs in a smaller timeframe. However, this separation can also be detrimental to the assembly of the device. Depending of the constraints on the CVA, it may be difficult to integrate the various components together. Additionally, because of the many competing requirements on components that serve multiple functions, this type of device may be fairly sensitive to the manufacturing process used for its production. Still, once a suitable assembly process is developed, and using various creative techniques to have single components effectively provide multiple functions, a CVA with a non-linear spring may be very conveniently fabricated and installed in an existing or future system.

In contrast, damping may be difficult to integrate into a CVA and makes impermanent installations complicated. Due to the coupling between the VEM and elastic substructure inherent in a damping design, the fabrication process is typically a serial task, where one component cannot be built until another is finished. This greatly increases cycle time in producing a mechanism, leading to less testing and refinement of future prototypes. Furthermore, because shear loading is the primary way in which the VEM is activated, a concentric design of a damping CVA is typically necessary for rotational systems. This may cause problems in connecting the CVA to the rotational system, again leading to less efficient

use of production time. Unless more practical methods of building these types of CVA's are developed, the difficulty in producing a CVA with damping could greatly limit their use.

7.1.4 Necessary Modeling for Design and Parameter Selection

Fortunately, the modeling for either type of CVA, a non-linear spring or damping version, is not overly limiting. It was found that a relatively simple lumped parameter model could accurately:

1. Determine the dynamic characteristics of a rotational system that could use a CVA.
2. Determine which design is the more appropriate choice for that application.
3. Determine the resulting performance benefits of either design once installed.

Furthermore, a CVA utilizing a non-linear spring may be dimensioned using FEA simulations or parametric design formulae. Statistical analysis may also be required to determine the effect of any tight tolerances on the performance of the device. Although a modeling method was not presented for a damped CVA in this paper, the theory of viscoelastic materials is very well developed. Therefore, a CVA of this type may be approximately designed by existed methods if an exact one is not at hand.

7.2 Impact of CVA's

7.2.1 Scholarly Impact

Compliant Vibration Attenuators offer a new paradigm for the design of modular vibration attenuation devices. Instead of working around an existing or future rotational system, these devices can allow designers to use the primary function of the rotational system to augment the vibration reducing capabilities of the system as a whole. While such a device is not radically different from existing technologies, it does present a novel solution methodology for applying old techniques in a new way. By presenting a preliminary investigation of the potential of load

bearing unidirectional vibration attenuators, many of the underlying performance advantages and limitations for these devices have been discovered. Two design strategies have been studied, each of which provide different operational and design benefits. By realizing these strategies into physical devices, the practical issues concerning their fabrication and implementation have been understood. Moreover, these prototypes allowed for an initial discovery of the potential of each design strategy. Finally, modeling methods were developed that show the design and a prediction of the benefits of a CVA are not difficult to achieve.

In general, CVA's may provide the following benefits over existing load bearing and non-load bearing vibration reduction devices:

1. Modular Device – As a component dedicated to reducing unwanted vibrations and separate from the rotational system, a CVA's vibration attenuation capabilities are not limited by the same functional requirements of existing system components.
2. Decoupled Performance – A CVA affects the small-amplitude vibrations only and is purposely designed to not affect the desirable large-motion torque transmission of the system.
3. Structural Element – The CVA serves as a structural element in the system rather than as an auxiliary treatment. As such, the vibration reducing function of a CVA acts directly on the system load path, thereby increasing its potential effect over damping and inertial-spring devices.

7.2.2 Engineering/Practical Impact

Two devices that act as mechanical low-pass filters, the Small Amplitude Vibration Isolator (SAVI) and the Damping Vibration Link (DVL), have been designed, modeled, fabricated and experimentally verified. Their performance was evaluated by the following four metrics:

- Frequency response of system to upstream vibration.

- Delay, either time or displacement, in response of forward input
- Simplicity
- Robustness

The SAVI is capable of reducing small amplitude upstream vibrations in resonating and non-resonating systems alike by as much as 60 % without introducing more than about a quarter of the delay that currently exists in a rotational system. For systems that cannot afford any stiffness change, an initial prototype of the DVL has been shown to provide high damping levels to attenuate vibrations in resonating systems and offer a moderate torsional stiffness and strength. Each device serves the dual purpose of attenuating upstream vibration while simultaneously transmitting torque inputs through the system.

Design guidelines have been presented for each device, and the critical issues governing their performance have been identified. Models have been developed and verified that enable engineers to appropriately dimension these mechanisms so that they can perform their required task. Furthermore, a design selection procedure has been outlined so that the appropriate device for a particular application may be identified. Finally, a case study was presented as to how the SAVI could be designed and implemented in a real-life application.

7.3 Future Work

The major work that remains for the future is to design a more versatile and effective planar torsional spring for the SAVI, and to create an analytical model for the DVL. As of now, the torsional spring used in the SAVI has some limitations on its performance. The range of stiffness values is small for a moderate packaging diameter, and the device has high stress concentrations which require the stop engagement system to be design to a tight tolerance specification. A future design of the torsional spring, which can provide better performance and even incorporates the engagement stops, is already under investigation. Other work that is required of the SAVI is to determine automated fabrication procedures for the engagement stops so that they may be more easily assembled. Furthermore, an analysis of the performance

variation due to manufacturing variations is necessary before the SAVI may be fabricated on a large scale.

The next step in developing the DVL is to generate a parametric model to predict its performance based on its dimensional values. Once this is accomplished, the device may be optimized and its true potential compared with that of existing devices. It is also important to develop other fabrication processes for the DVL than require far lower cycle times and more reliable methods. This is especially true in the assembly of the DVL with a rotational system, as current methods actually damage the device and are very difficult to perform. Finally, a full experimental evaluation of the DVL must be performed to verify its performance benefits over existing damping technologies.

REFERENCES

- [1] Mead, D. J., *Passive Vibration Control*, New York: John Wiley, 1998.
- [2] Nashif, A. D., Jones, D. I. G., Henderson, J. P., *Vibration Damping*, New York: John Wiley, 1985.
- [3] Ferry, J. D., *Viscoelastic Properties of Polymers*, 3rd Ed., New York: John Wiley, 1980.
- [4] Johnson, C. D., "Design of Passive Damping Systems", *J. of Mechanical Design*, Vol. 117, June 1995, pp. 171-176.
- [5] Rosenfeld, N. C., Wereley, N. M., "Volume-Constrained Optimization of Magnetorheological and Electrorheological Valves and Dampers", *Smart Materials and Structures*, Vol. 13, 2004, pp. 1303 – 1313.
- [6] Nakra, B. C., "Vibration Control in Machines and Structures using Viscoelastic Damping", *J. of Sound and Vibration*, Vol. 211(3), 1998, pp. 449-465.
- [7] Bamberg, E., and Slocum, A. H., "Concrete-Based Constrained Layer Damping", *Precision Engineering*, Vol. 26, 2002, pp. 430-441.
- [8] Nayfeh, S. A., and Varanasi, K. K., "Damping Torsional Vibrations of Thin-Walled Tubes with Constrained Viscoelastic Layers", *J. of Sound and Vibration*, Oct 2003.
- [9] Chandrasekharan, M.P., and Ghosh, A., "Damping Characteristics of Elastic-Viscoelastic Composite Shafts", *J. of Sound and Vibration*, Vol. 37(1), 1974, pp. 1-15.
- [10] Ramesh, T. C., "Finite element analysis of cylindrical shells with a constrained viscoelastic layer", *J. of Sound and Vibration*, Vol. 172(3), May 1994, pp. 359 – 370.
- [11] Batra, R. C., and Yu, J. H., "Analysis of Damping in Finite Shearing and Torsional Deformations", *Proceedings of SPIE Vol. 3989 (2000)*, *Smart Structures and Materials 2000: Damping and Isolation*, pp. 86 – 98.
- [12] Demoret, K. B., "The barberpole: Constrained Layer Damping for Bending and Torsion", *Proceedings of SPIE Vol. 2445 (1995)*, *Smart Structures and Materials 1995: Passive Damping*, pp. 350 – 361.
- [13] Hagood, N. W., and von Flotow, A., "Damping of Structural Vibrations with Piezoelectric Materials and Passive Electrical Networks", *J. of Sound and Vibration*, Vol. 146, 1991, pp. 243-268.
- [14] Gilbert, T. L., "A Phenomenological Theory of Damping in Ferromagnetic Materials", *IEEE Transactions on Magnetics*, Vol. 40 (6), Nov. 2004, pp. 3443 – 3449.

- [15] Varanasi, K., and Nayfeh, S. A., “Damping of Flexural Vibration by Low-Density Foams and Granular Materials”, Proceedings of ASME DETC, Sept. 2003.
- [16] Nashif, A. D., Jones, D. I. G., Henderson, J. P., Vibration Damping, New York: John Wiley, 1985.
- [17] Vinogradov, B. D., and Chernoberevskii, V. V., “Damping of Tubes by a Constrained Coating”, Soviet Physics Acoustics, Vol. 26 (4), 1980, pp. 328 – 330.
- [18] Ungar, E. E., and Kerwin, Jr., M., “Loss Factors of Viscoelastic Systems in Terms of Energy Concepts”, J. Acoustical Society of America, Vol. 34(7), July 1962, pp. 954-957.
- [19] Badre-Alam, A., Gandhi, F., and Wang, K. W., “An Improved Constrained Layer Damping Treatment Design for High Damping and Low Interlaminar Stresses”, Smart Structures and Materials 2000: Damping and Isolation, Proc. of SPIE, Vol. 3989, pp. 2-13.
- [20] Thomson, W. T., Dahleh, M. D., Theory of Vibration with Applications, 5th Ed., Upper Saddle River, NJ: Prentice Hall, 1998.
- [21] E-A-R SPECIALTY COMPOSITES. *EAR Technical Data Sheet*. 7911 Zionsville Rd. Indianapolis, IN 46268. <<http://www.earsc.com>>.
- [22] 3M INDUSTRIAL BUSINESS. *3M Technical Data Sheet*. 3M Center, Bldg. 21-1W-10, 900 Bush Ave. St. Paul, MN 55144. <<http://www.3M.com/industrial>>
- [23] Culpepper, M. L., Szczesny, S., “Design of a Compliant Revolute Mechanism for Accurate Dynamic Characterization of Automotive Steering Columns”, Proceedings of ASME DETC 2004.
- [24] Conversation with Ford employees, Summer 2004.
- [25] Neureder, U., “Investigation into Steering Wheel Nibble”, Proc. of Instn. Mech. Engrs., Vol 216, Part D: J Automobile Engineering, 2002, pp. 267-277.
- [26] Loh, W., Basch, R., Dalka, T., “Kinematic Analysis of Brake-Induced Vehicle Steering Wheel Vibration”, Proc. ASME 2003 DETC, Sept. 2003.
- [27] Jacobsson, H., “Aspects of Disc Brake Judder”, Proc. of Instn. Mech. Engrs., Vol. 217, Part D: J Automobile Engineering, 2003, pp. 419-430.
- [28] Pacejka, H. B., Tyre and Vehicle Dynamics, Boston: Butterworth Heinemann, 2002.
- [29] Hackert, P. B., “Simulation and Investigation of Shimmy on a Light Truck Independent Front Suspension”, Intl. Truck and Bus Meeting and Exposition, SAE 933043, Nov. 1993, pp. 1-8.

- [30] Filho, S. A. M., and Capser, S., “The Influence of the Steering Gear Design into the Steering Wheel Nibble”, 12th SAE Brazil Congress and Exposition, 2003.
- [31] Demers, M., “Suspension Bushing Effects on Steering Wheel Nibble”, Noise and Vibration Conference and Exhibition, SAE 2003-01-1712, May 2003.
- [32] Bosworth, R., “The Application of Taguchi Methodology to Solving Steering Wheel Niggle Vibration”, Proc. of Instn. Mech. Engrs., C382/052, 1989, pp. 346 – 360.
- [33] Equipment and Tools Inst., “Automotive Test Equipment Performance Guidelines for Wheel Balancing Equipment”, <<http://www.ertools.org/i4a/pages/index.cfm?pageid=1>>.
- [34] Eagle Equipment, <<http://www.eagleequip.com/>>.
- [35] Conversation with Ford employees, Summer 2004.
- [36] Email correspondence with Ford employees, Summer 2004.